# Approaches to the Inhibition of Class II Fructose-1,6-Bisphosphate Aldolase

by

Liangchen Wang

A thesis
presented to the University of Waterloo
in fulfilment of the
thesis requirement for the degree of
Master of Science
in
Chemistry

Waterloo, Ontario, Canada, 2009

## Author's Declaration

I hereby declare that I am the sole author of this thesis. This is a true copy of the thesis, including any required final revisions, as accepted by my examiners.

I understand that my thesis may be made electronically available to the public.

# Abstract

Fructose-1,6-bisphosphate (FBP) aldolase (E.C. 4.1.2.13) catalyzes the reversible aldol condensation of dihydroxyacetonephosphate (DHAP) and glyceraldehyde-3-phosphate (G3P) in glycolysis, gluconeogenesis and the Calvin cycle. FBP aldolases are categorized into two groups based on different catalytic mechanisms: Class I aldolases form a Schiff-base intermediate with the substrate through an active site lysine residue, whereas Class II aldolases contain a divalent metal which coordinates and stabilizes the carbanion intermediate. Notably, Class II aldolase does not exist in animals or plants, making this enzyme a potential drug target for pathogenic microbial organisms such as *Mycobacterium tuberculosis*, *Pseudomonas aeruginosa, Magnaporthe grisea*. A chromogenic substrate was synthesized as a FBP mimic from DHAP and 4-nitrobenzaldehyde catalyzed by a chiral primary-tertiary diamine-Brønsted acid catalyst that was synthesized in the optically active form. The chromogenic substrate can be applied to a direct chromogenic assay for monitoring the activity of Class II FBP aldolases and also to evaluate any good inhibitor. The catalyst was also synthesized in the racemic form that is ready for future asymmetric aldol reaction studies. In addition, our research group has found that a commercially available antidote for heavy metal poisoning, 2,3-dimercapto-1-propanesulfonic acid (DMPS) is a good competitive inhibitor of Class II FBP aldolase. In order to improve the binding affinity of this inhibitor in the enzyme active site, new molecules based on this compound, 1,1-difluoro-3,4-dimercaptobutylphosphonic acid, was rationally designed using molecular modeling. Attempts to synthesize this compound using our original synthetic plan were proven to be mostly unsuccessful. A new synthetic strategy was reasonably proposed for future reference.

## Acknowledgements

I am extremely thankful to my supervisors Guy Guillemette and Gary Dmitrienko for their encouragement and guidance on my master research project during the past two years. Special thanks to Guy for offering me the opportunity to work on this project and his help in the biochemistry aspect of the project. I am also very thankful to Gary for providing me a great personal working space and all of his knowledgeable comments in the synthetic organic chemistry aspect of the project, especially the tremendous helpful suggestions he offered to me during my thesis write-up.

I am really thankful to my committee members John Honek and Michael Palmer for their precious time on reading my thesis and being my examiner.

Many thanks to Geneviève Labbé for her help and support on the enzyme kinetic assays and all the preliminary inhibitor data that kindly provided by her.

I am also really appreciated to Anthony Krismanich and Jarrod Johnson for training me the experimental expertise of practical organic chemistry and all of their friendly suggestions on analyzing the NMR spectra. Special thank to Anthony on proofreading my thesis even when he was sick in that period of time.

Last but not least, thank all my colleagues in the Guillemette group and Dmitrienko group for creating such a professional and fun working environment for me!

# Dedication

This thesis is dedicated to my parents for their unconditional love, support, and constant encouragement during my academic career since my childhood. I am really proud and thankful to be your son. This thesis is also dedicated to my girl Christina for her support in the past few years. You are a gift from God to me. In addition, I also want to dedicate this thesis to God, for all the way he led me through and all the comfort and grace he offered to me when I was down. This thesis cannot be done without his blessing.

# Table of Contents

**List of Figures** viii
**List of Schemes** ix
**List of Abbreviations** x

**Chapter 1** 1
**Introduction** 1
1.1 Overview of aldolases 1
1.2 Catalytic roles and synthetic application of fructose-1,6-bisphosphate aldolase 1
1.3 Two mechanistic classes of FBP aldolases 3
1.4 Class I FBP aldolases 3
1.4.1 Characteristics of Class I FBP aldolases 3
1.4.2 Catalytic mechanism of Class I FBP aldolases 4
1.5 Class II FBP aldolases 6
1.5.1 Characteristics of Class II FBP aldolase 6
1.5.2 Enzyme active site in the Class II FBP aldolase of *Escherichia coli* 7
1.5.3 The catalytic mechanism of Class II FBP aldolase 9
1.6 Class II FBP aldolase as a potential drug target 12
1.7 Research Objectives 15
**Chapter 2** 16
**Development of a direct chromogenic assay for monitoring Class II FBP aldolase enzyme activity** 16
2.1 Introduction 16
2.2 Design of chromogenic substrates 18
2.3 Direct asymmetric aldol reactions catalyzed by organocatalysts 21
2.4 Simple primary amine organocatalysts 26
2.5 Chiral primary-tertiary diamine-Brønsted acid catalyst 30
2.6 Application of a phosphate ester mimic in the chromogenic assay 34
2.7 Results and Discussion 37
UV-visible spectrophotometric assay 37
Synthesis of FBP-mimicking chromogenic substrate 40
2.8 Future work 49
2.9 Experimental 50
General experimental 50
UV-visible spectrophotometric assay 50
*N*-((1*R*, 2*R*)-2-aminocyclohexyl)acetamide (2-3) 51
(1*R*, 2*R*)-*N*, *N*-dipropylcyclohexane-1,2-diamine (2-5) 53
(3*S*, 4*R*)-1,3,4-trihydroxy-4-(4-nitrophenyl)butan-2-one (2-6) 54
Attempted Phosphorylation 56
Racemic *trans*-2-aminocyclohexylacetamide 57
Racemic *N*, *N*-dipropylcyclohexane-1,2-diamine 58
Stock solution of the triflate salt of racemic *N*, *N*-dipropylcyclohexane-1,2-diamine 60
**Chapter 3** 61
**Development of novel inhibitors of Class II FBP aldolases** 61
3.1 Introduction 61

3.2 Strategies for the design of zinc protease inhibitors 62
3.3 Existing Class II FBP aldolase inhibitors 64
3.4 Development of novel Class II FBP aldolase inhibitors 68
3.5 Results and Discussion 73
3.6 Future work 89
3.7 Experimental 91
General Experimental 91
Diethyl Difluoromethylphosphonate (3-8) 91
Diethyl -1,1-difluorobut-3-enylphosphonate (3-15) 92
Diethyl-3,4-dibromo-1,1-difluorobutylphosphonate (3-16) 93
Reaction of 3-16 with thioacetate anion 94
**References** 98
**Appendix A** 106
$^{1}$H NMR spectrum (300 MHz) of racemic *N*, *N*-dipropylcyclohexane-1,2-diamine 106

# List of Figures

**Figure 1-1** Schematic representation of the structure of the dimeric *E. coli* FBP aldolase 7
**Figure 1-2** Sequence alignment of the active site region of Class II FBP aldolases 8
**Figure 2-1** Structure of *trans*-*N*,*N*-dialkylated-diaminocyclohexane 30
**Figure 2-2** Structures of *trans*-*N*,*N*-dialkylated-diaminocyclohexane derivatives 31
**Figure 2-3** Scanning of two model compounds by UV-visible spectrometry 38
**Figure 2-4** Structure of the chiral primary-tertiary diamine-Brønsted acid catalyst for preparation of FBP-mimicking chromogenic substrate. 40
**Figure 2-5** Structure of the diacetylated impurity **2-4** 41
**Figure 2-6** Schematic representation of the AA'BB' system of **2-6** 47
**Figure 3-1** Structures of PGH and its derivatives 65
**Figure 3-2** Structures of PGH, phosphoglycolosulfamate (PGS) and their phosphonate derivatives 65
**Figure 3-3** Structures of DPA and its derivatives MS 191, and commercial antidote for heavy metal poisoning 2,3-dimercapto-1-propanesulfonic acid (DMPS) 66
**Figure 3-4** Docking of a model of DMPS into the substrate binding site of *E. coli* Class II FBP aldolase 69
**Figure 3-5** Structures of 2,3-dimercaptopropane-1-sulfonic acid (DMPS) and the proposed compound 1,1-difluoro-3,4-dimercaptobutylphosphonic acid 69
**Figure 3-6** Docking of a model of 1,1-difluoro-3,4-dimercaptobutylphosphonic acid into the substrate binding site of *E. coli* Class II FBP aldolase 70
**Figure 3-7** The apparent quartet and the splitting pattern of the C-2 hydrogen on 3-20 as seen on the $^{1}$H NMR spectrum 86

# List of Schemes


**Scheme 1-1** 2
**Scheme 1-2** 5
**Scheme 1-3** 10
**Scheme 2-1** 16
**Scheme 2-2** 19
**Scheme 2-3** 21
**Scheme 2-4** 22
**Scheme 2-5** 23
**Scheme 2-6** 26
**Scheme 2-7** 28
**Scheme 2-8** 32
**Scheme 2-9** 34
**Scheme 2-10** 36
**Scheme 2-11** 37
**Scheme 2-12** 41
**Scheme 2-13** 44
**Scheme 2-14** 45
**Scheme 2-15** 46
**Scheme 2-16** 48
**Scheme 2-17** 49
**Scheme 3-1** 71
**Scheme 3-2** 73
**Scheme 3-3** 73
**Scheme 3-4** 74
**Scheme 3-5** 74
**Scheme 3-6** 79
**Scheme 3-7** 81
**Scheme 3-8** 82
**Scheme 3-9** 83
**Scheme 3-10** 84
**Scheme 3-11** 87
**Scheme 3-12** 90

# List of Abbreviations

| | |
|---|---|
| br | broad |
| CF | cystic fibrosis |
| CI | chemical ionization |
| CPA | carboxypeptidase A |
| DBU | diazabicyclo-undec-7-ene |
| ddd | doublet of doublet of doublets |
| dd | doublet of doublets |
| d | doublet |
| DHA | dihydroxyacetone |
| DHAP | dihydroxyacetonephosphate |
| DMF | dimethylformamide |
| DMPS | 2,3-dimercapto-1-propanesulfonic acid |
| DMSO | dimethyl sulfoxide |
| DPA | dipicolinic acid |
| dt | doublet of triplets |
| EI | electron impact |
| equiv | equivalent |
| ESI | electrospray ionization |
| FBP | fructose-1,6-bisphosphate |
| G3P | glyceraldehyde-3-phosphate |
| GPD | α-glycerolphosphate dehydrogenase |
| MMP | matrix metalloproteases |
| m | multiplet |
| MS | mass spectrometry |
| NMR | nuclear magnetic resonance |
| PDB | protein database bank |
| PGH | phosphoglycolohydroxamate |
| RAMA | rabbit muscle aldolase |
| s | singlet |
| TB | tuberculosis |
| td | triplet of doublets |
| TfOH | trifluoromethane sulfonic acid |
| THF | tetrahydrofuran |
| TIM | triose phosphate isomerase |
| TLC | thin layer chromatography |
| t | triplet |
| UV | ultraviolet |
| ZBG | zinc binding group |

# Chapter 1

# Introduction

## 1.1 Overview of aldolases

Historically, aldolases were first recognized near the beginning of the last century as a class of enzymes which are present in all organisms that are able to catalyze the interconversion of hexoses and their three-carbon components. Meyerhof and coworkers first described the activity of aldolases and originally named them zymohexases (*1*). Later on aldolases were found to accept a much wider range of substrates than hexoses, and were found to be capable of adding a one-, two- or three-carbon fragment stereospecifically to an aldehyde via the aldol condensation reaction. To date, aldolases have been one of the most useful classes of enzymes in the formation of monosaccharides, although only a few of them have been exploited synthetically (*2*).

## 1.2 Catalytic roles and synthetic application of fructose-1,6-bisphosphate aldolase

Fructose-1,6-bisphosphate (FBP) aldolases (E.C. 4.1.2.13) play important catalytic roles in metabolic pathways such as glycolysis, gluconeogenesis and the Calvin cycle in different organisms by catalyzing the reversible aldol condensation reaction of dihydroxyacetonephosphate (DHAP) and glyceraldehyde-3-phosphate (G3P) (Scheme 1-1) (*3*). In each of the pathways, the enzyme-catalyzed reaction involves deprotonation and protonation, formation of an enzyme-DHAP intermediate and eventually the release of G3P and DHAP molecules from the enzyme active site (*4*). The exquisite control of stereochemistry of aldol condensation reactions catalyzed by FBP aldolases renders such enzymes attractive alternatives

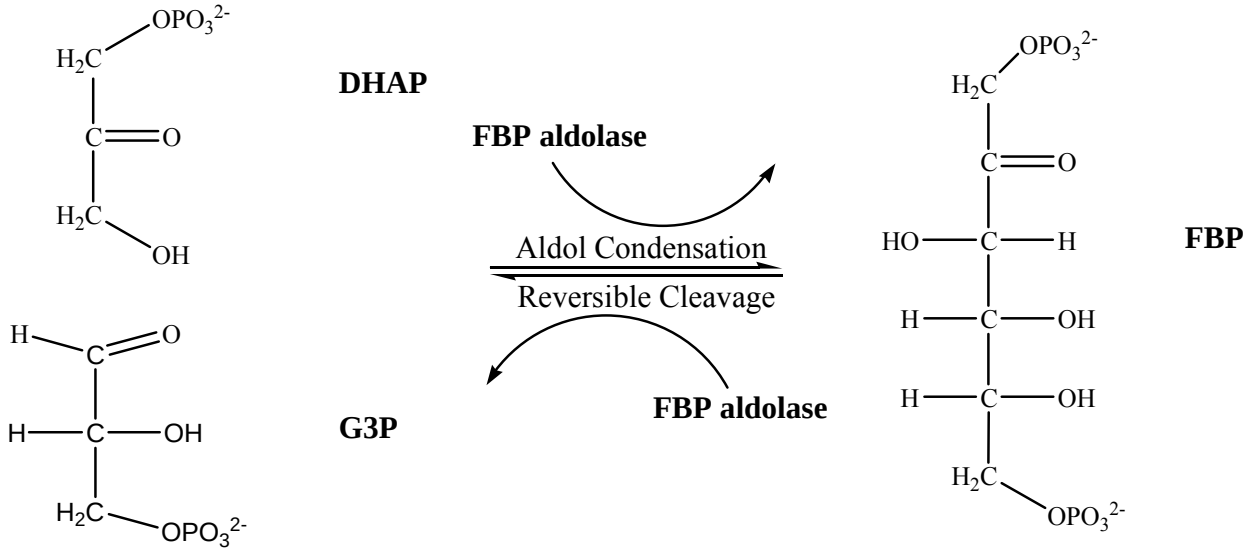


**Scheme 1-1.** The general reaction scheme of the reversible aldol condensation reaction catalyzed by FBP aldolase. DHAP and G3P combine to form into FBP in the direction of aldol condensation; conversely, FBP can be cleaved into DHAP and G3P in the reverse direction.

to the conventional chemical methods in the field of synthetic chemistry. It has already been shown to be excellent for the synthesis of compounds in the pharmaceutical industry, such as $^{13}C$-labelled, nitrogen or fluorine containing sugars, and novel high carbon sugars (*5*), as well as glycosidase inhibitors such as deoxynojirmycin and deoxymannojirmycin (*6*). FBP aldolases are highly specific for DHAP, whereas they accept a large variety of acceptor aldehydes, such as unhindered aliphatic aldehydes and α-heteroatom-substituted aldehydes (*7*). Generally, phosphorylated substrates are preferred over non-phosphorylated ones (*7, 8*). Furthermore, DHAP-dependent aldolases can create two new stereogenic centers with excellent enantioselectivity and diastereoselectivity. Principally, there are four possible stereoconfigurations at C3 and C4 of the products, while FBP aldolases are strictly specific for the 3*S*, 4*R* stereoconfiguration (*9*).

### 1.3 Two mechanistic classes of FBP aldolases

The retro-aldol cleavage by FBP aldolase is catalyzed by stabilizing the enolate intermediate through increased electron delocalization, which is contributed by the active site of the enzyme. Although all FBP aldolases adopt the $(\alpha/\beta)_8$ barrel fold structure, they are categorized into two different classes according to the reaction mechanism which they employ to stabilize the enolate intermediate in the enzyme active site, namely Class I and Class II aldolases (*3, 10*). Class I FBP aldolases use one ε-amino group of a lysine to prompt the formation of a Schiff-base intermediate, whereas Class II FBP aldolases use a $Zn^{2+}$ cation to stabilize the enolate intermediate. Class II FBP aldolases can also be activated by monovalent cations such as $Na^{+}$ (*3*).

### 1.4 Class I FBP aldolases

#### 1.4.1 Characteristics of Class I FBP aldolases

Class I aldolases are present predominantly in higher organisms such as animals, plants, green algae, certain prokaryotes and archaebacteria (*10–12*). Generally, Class I aldolases are found to be tetramers in eukaryotes, with an approximate molecular weight of 160,000 kDa; however, it has also been reported that they can exist as monomers to decamers in prokaryotes (*11, 13, 14*). The Class I enzymes have been studied extensively and a number of their three-dimensional structures have been determined by X-ray crystallography, including the FBP aldolases from rabbit muscle (*15*), *Drosophila melanogaster* (*16*), human muscle (*17*) and the dimeric *Escherichia coli* transaldolase B (*18*). Interestingly, Class I aldolases such as rabbit muscle aldolase (RAMA), possesses a broader functional pH range (pH 7-9) than Class II aldolases,

which exhibit a very sharp pH optimum. Furthermore, all the Class I FBP aldolases lose activity upon the addition of $NaBH_4$ in the presence of the substrate, whereas they are insensitive to EDTA. It has also been reported that Class I aldolases can be subdivided into 3 different organ specific isozymes in animals: isozyme A, the major form in muscles; isozyme B, found in liver and kidney, while not detected in other organs; isozyme C is present in brain tissue together with isozyme A (*10*).

### 1.4.2 Catalytic mechanism of Class I FBP aldolases

A general catalytic mechanism of a Class I FBP aldolase was proposed by Gefflaut *et al.* (*19*) based on results from crystallographic data, kinetic studies and site directed mutagenesis using RAMA (Scheme 1-2). Initially, DHAP enters the active site and binds to Arg-148 through the coordination of its phosphate group. Then Lys-146 and Glu-187 participate by aiding in the polarization of the carbonyl group of DHAP and induce the formation of the Schiff-base intermediate between the carbonyl and the ε-$NH_2$ group of Lys-229. Subsequently, a C3 proton abstraction by Tyr-363 from the imminium leads to the formation of an enamine. Hereafter, G3P binds to the active site with its phosphate group oriented by Lys-41, Arg-42 and Lys-107. The activated double bond of the enzyme-DHAP adduct attacks the electrophilic carbon of the G3P carbonyl group and a new C-C bond is formed through condensation yielding FBP.

Notably, Class I aldolases in animals share a sequence homology of amino acid residues in the enzyme active site, particularly in the region adjacent to the lysine residue (Lys-229) which favours the Schiff-base intermediate, and this conserved motif is even found in plants (*10*).

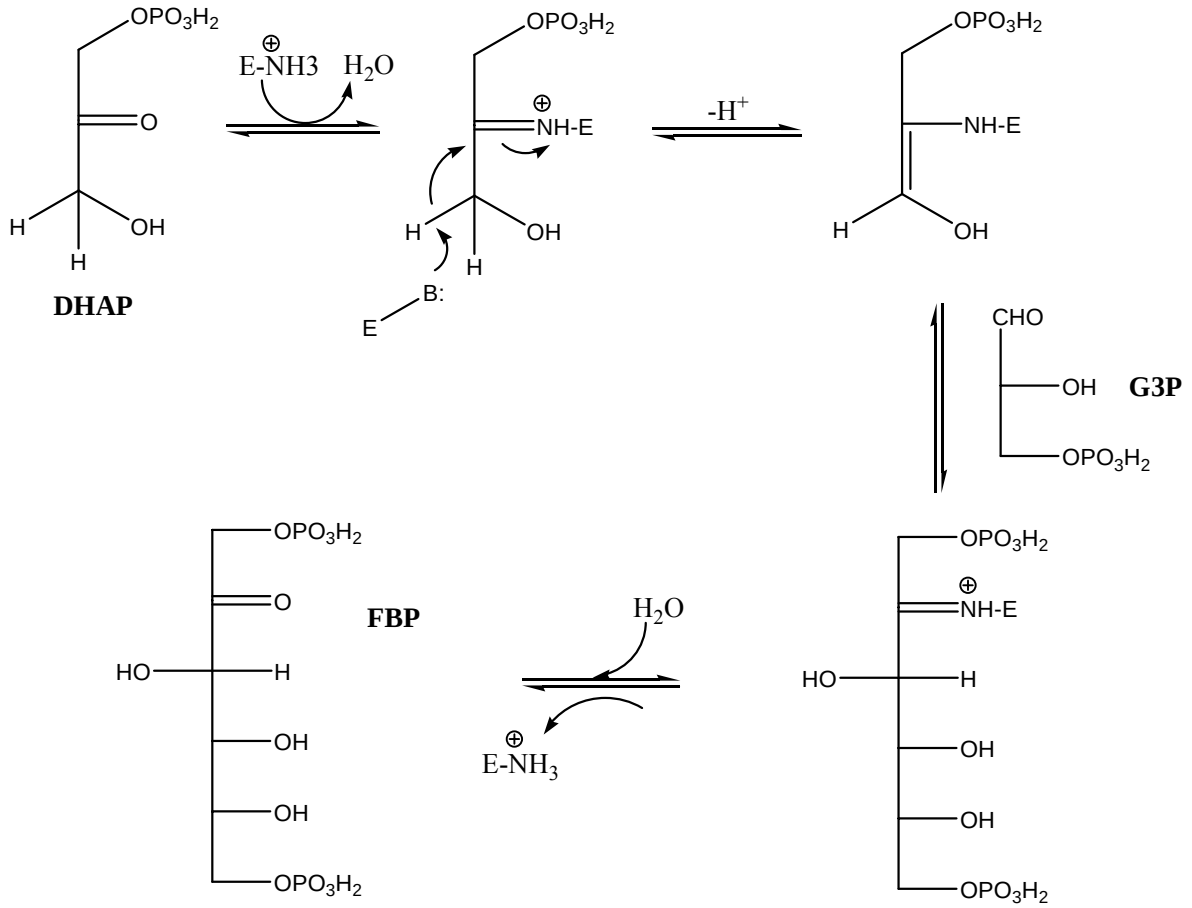


**Scheme 1-2.** Generalized catalytic mechanism of Class I FBP aldolase. The enzyme catalyzes the reaction by forming a Schiff-base intermediate with the carbonyl group of the substrate DHAP which is then ionized into an enamine. The double bond of the enamine attacks the electrophilic carbon of G3P and affords the product of FBP with the formation of a new C-C bond (*20*).

## 1.5 Class II FBP aldolases

### 1.5.1 Characteristics of Class II FBP aldolase

Unlike Class I FBP aldolases, which are found mainly in animals and higher plants, Class II FBP aldolases are present in lower organisms such as bacteria, fungi, algae and protozoa, with the co-existence of both classes in some organisms (*21, 22*). The Class II FBP aldolases are further divided into two groups according to their primary sequences: the Class IIa enzymes, which comprise the FBP aldolases and are generally characterized to be dimeric with an average molecular weight of 70,000 kDa; and the Class IIb enzymes, which consist of tagatose-1,6-bisphosphate aldolases as well as other FBP aldolases, and can be found as dimeric, tetrameric or octameric forms (*10, 23*). Members of each subclass exhibit 40% sequence similarity, with 25–30% sequence similarity among all Class II FBP aldolases (*13*).

Compared to Class I FBP aldolases, which have been extensively studied, less is known about Class II FBP aldolases. The first Class II aldolase structure obtained was fuculose-1-phosphate aldolase, and its catalytic mechanism was derived from structure-directed mutagenesis studies of the enzyme active site (*24, 25*). In addition, only a few crystal structures of Class II FBP aldolases are available, such as the dimeric *Escherichia coli* (*26*) and *Giardia lamblia* aldolases (*27*), as well as the tetrameric *Thermus aquaticus* (*28*) and *Thermus caldophilus* (*29*) aldolases. Moreover, the crystal structure of Class II FBP aldolase from *Mycobacterium tuberculosis* has just recently been reported (*30*). Although Class I and Class II FBP aldolases possess the same $(\alpha/\beta)_8$ barrel fold structure and catalyze the same overall reaction, they share only 15% sequence homology (*31*) and the locations of their active sites are different, suggesting an independent

evolutionary pattern (*32*). Recent studies based on primary structure alignments have led to the suggestion that these enzymes may have evolved independently from a common $(\alpha/\beta)_8$ barrel ancestor as is the case for other families of $(\alpha/\beta)_8$ barrel fold enzymes (*33*, *34*).

### 1.5.2 Enzyme active site in the Class II FBP aldolase of *Escherichia coli*

Little was known about the Class II FBP aldolases and the details of their enzyme active sites before the structure of the dimeric Class II FBP aldolase from *E. coli* was determined using data to 2.5 Å resolution by Cooper *et al*. (*26*). The enzyme was shown to be a homodimer (Figure 1-1), and each dimer is approximately 100 Å in length with the β-barrels positioned nearly at right

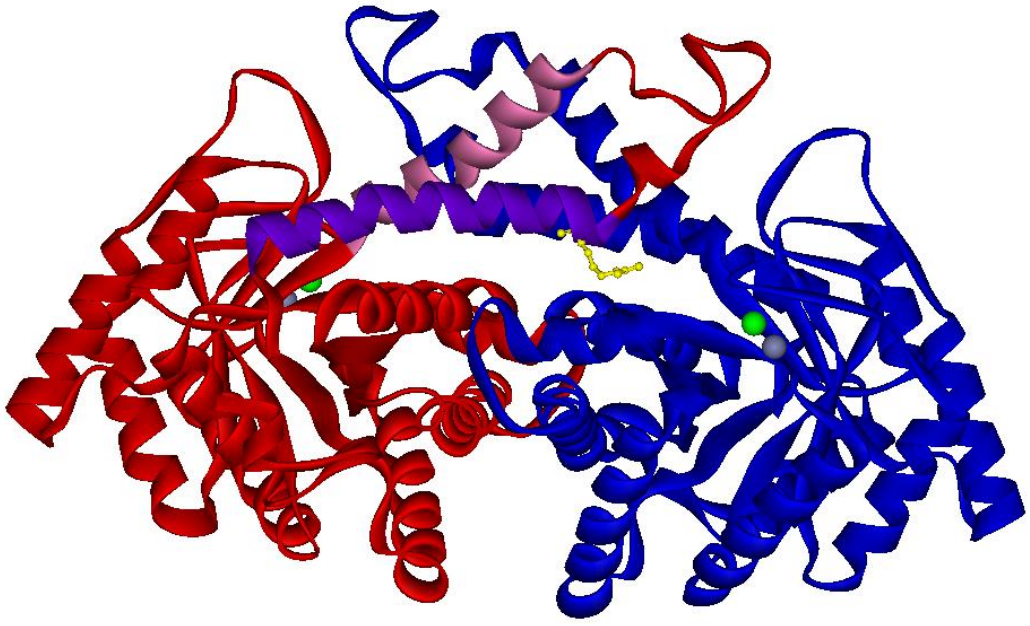

**Figure 1-1.** Schematic representation of the structure of the dimeric *E. coli* FBP aldolase. The chain A is colored in red and the chain B is colored in blue. Furthermore, the α10 and α11 helices of monomer A are colored in pink and purple, respectively. The important amino acid residue Arg-331 which is responsible for substrate recognition and binding is highlighted in yellow in a ball-and-stick fashion. M1 and M2 are displayed in CPK style and colored in grey and green, respectively. The model was derived from PDB 1B57 using Viewerlite (Acceryls) (*35*).

angles to each other. Two α-helices (α10 and α11, Figure 1-1) are antiparallel to each other, and create an association via van der Waals interactions, hydrogen bonds plus a salt bridge formed between Arg-344 and Asp-290, which are important for the dimerization. These two helices then associate with the identical structure on the other subunit through the C- and N-terminal regions, and these interactions produce a substantial hydrophobic core at the dimer interface (*26*). Furthermore, the use of site-directed mutagenesis in combination with the arginine specific reagents butanedione or phenylglyoxal by Qamar *et al.* identified Arg-331 of the helix α11 to be an important residue in terms of substrate recognition and binding (*36*). The crystal structure showed that this residue is located at the N-terminus of helix α11 within the active site and approximately 13 Å from the catalytic site of the other subunit. Subsequent sequence alignment of the eight known Class II FBP aldolases showed that Arg-331 is the only arginine residue conserved among all the known sequences (Figure 1-2), which has confirmed the critical role of this amino acid in the active site (*36*).

```
                  360         *       380         *       400
Taquaticus : ---------------NPKEFDPRKYLGPAREAVKEVVKSRMELFGSVGRA : 305
Tcaldophil : ---------------NPKEFDPRKYLGPAREAVKEVVKSRMELFGSVGRA : 305
Paeruginos : ---------------NPSEFDPRKYFSKTVEAMRDICIARYEAFGTAGNA : 328
Glamblia   : ---------------HPEKFDPRDYLGPGRDAITEMLIPKIKAFGSAGHA : 307
Bcereus    : ---------------DQEVYDPRKFIGPGRDAIKATVIGKIREFGSNGKA : 285
Ecoli      : YLQGQLGNPKGEDQPNKKYYDPRVWLRAGQTSMIARLEKAFQELNAIDVL : 359
Mgrisea    : YLNSQVGNPDGADKPNKKYYDPRVWVREGEKTMKARIQQALKVFNAENTI : 360
Mtuberculo : GVLKVDG-----EVGVKKVYDPRSYLKKAEASMSQRVVQACNDLHCAGKS : 341
```

**Figure 1-2.** Sequence alignment of the active site region of Class II FBP aldolases. The sequence alignment of the active site region from eight different microorganisms *T. aquaticus, T. caldophilus, P. aeruginosa, G. lamblia, B. cereus, E. coli, M. grisea* and *M. tuberculosis*. Arg-331 of *E. coli* is shown to be the only conserved arginine residue in the eight microorganisms. The alignment was done by using the ClustalW program and the graphic representation was done by GeneDoc program. The GenBank accession numbers are AY945938, CAF32659, AAG03944, NP_249246, NP_834997, P0AB71, XP_369021 and NP_214877, respectively.

Numerous enzymes adopt the $(\alpha/\beta)_8$ barrel structure utilizing either a single or multiple ions for catalysis. Despite the similarities with some structural features compared to other metalloenzymes, the *E. coli* Class II FBP aldolase was proposed by Cooper *et al.* to possess a bimetallic-binding active site with two metals 6.2 Å apart. One metal ion termed M1 is buried and presumed to be potassium, zinc or some other cations, possibly playing a structural or activating role; whereas the other termed M2 (a $Zn^{2+}$ ion) is positioned on the surface of the active site, participating in the catalytic reaction (see Figure 1-1). M2 presents a distorted tetrahedral geometry and it is coordinated to three histidine residues (His-110, His-226 and His-264) and Glu-174 (*26*). Further studies by Hall *et al.* confirmed that the two metals in the crystal structure obtained by Cooper *et al.* to be only one zinc ion in two mutually exclusive sites with 50% occupancy in each site (*35*). Furthermore, zinc containing enzymes can be divided into two groups based on the number of zinc ions: the mono-zinc system and the co-catalytic, or coactive sites. The latter group of enzymes contain two or more zinc atoms, bridged by an acidic residue and a water or hydroxide ion (*37-39*).

### 1.5.3 The catalytic mechanism of Class II FBP aldolase

Class II FBP aldolase uses a different catalytic mechanism as compared to Class I FBP aldolase. The crystal structure of Class II FBP aldolase of *E. coli* in complex with a transition state enediolate analogue and inhibitor phosphoglycolohydroxamate (PGH) has been determined using X-ray diffraction with a resolution of 2.0 Å (*35*). Based on the structural information and in conjunction with the results generated using site-directed mutagenesis, steady- state kinetics and Fourier transform infrared spectroscopy, a detailed mechanism involving the catalytic zinc ion in the condensation direction was proposed by Hall *et al.* (Scheme 1-3) (*35*).

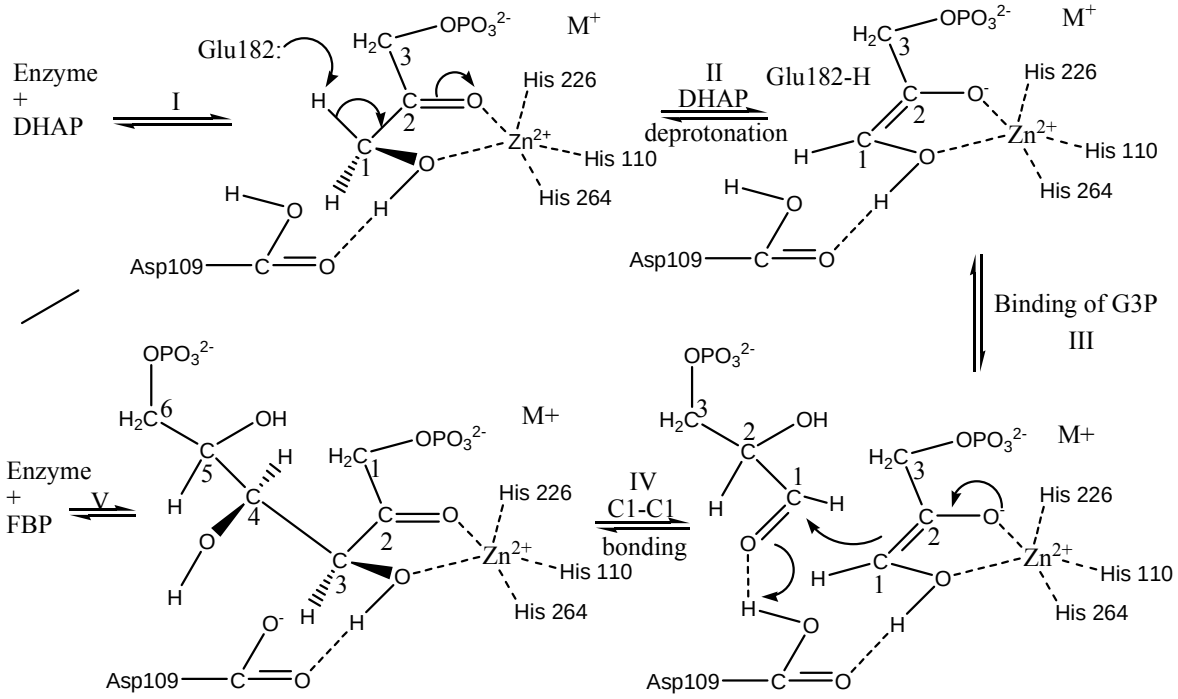


**Scheme 1-3.** The proposed mechanism of *E. coli* Class II FBP aldolase. Details of the mechanism are discussed in the text *(35)*.

In step I and step II, DHAP initially approaches and binds to the active site, which results in an active site rearrangement. DHAP then binds with the carbonyl and hydroxyl oxygens to $Zn^{2+}$ which is coordinated by His-226, His-110, and His-264, replacing the two water molecule ligands observed in the crystal structure (*36*). Then the direct coordination of DHAP to the zinc assists the precise alignment for catalysis, facilitating zinc to function as a Lewis acid and to polarize the carbonyl bond of the substrate, while increasing the acidity of the hydrogen atoms on C1. The active site residues restrict the access of the electrophilic G3P to the s*i*-face of DHAP. Subsequently, the loop carrying Glu-182 undergoes a conformational change to position the residue closer to the catalytic zinc, and Glu-182 acts as a general base to abstract the acidic proton, prompting the formation of the enediolate transition intermediate which is stabilized by the Asn-286 positioned just below it (not shown in Scheme 1-3). In step III and IV, G3P binds to

Arg-331 and is brought into the position to interact with the enediolate intermediate. Asp-109 then polarizes the C1 carbonyl group of G3P and facilitates the nucleophilic attack of the C1 carbon of the enediolate to the carbonyl acceptor, hence the formation of the FBP product. The two planes of the enediolate intermediate and the carbonyl group of G3P must be near-parallel in the initial alignment ahead of the C-C bond formation. In Step IV, Asp-109 transfers a proton to convert the C4 carbonyl group to a hydroxyl group either in concert with or right after the C-C bond formation, and finally the product will be released in step V (*35*).

### 1.6 Class II FBP aldolase as a potential drug target

Since Class II FBP aldolase is not present in higher organisms such as animals or plants, it has been suggested as a viable drug target (*31, 40*). In several pathogenic microorganisms, especially *Mycobacterium tuberculosis* and *Pseudomonas aeruginosa*, the rice blast causative agent *Magnaporthe grisea*, anthrax causative agent *Bacillus anthracis*, or bacterial meningitis causative agent, *Streptococcus pneumoniae* and *Haemophilus influenzae*, inhibitors of Class II FBP could be used as antifungal or antibacterial agents.

Tuberculosis (TB), the most common contagious pulmonary disease, is caused by infection with the human pathogen *Mycobacterium tuberculosis*. Statistics from the World Health Organization indicate that approximately 9.2 million new cases emerged in 2006, with 1.7 million *M. tuberculosis*-related deaths, and this is an increase over the 9.1 million new cases reported in 2005 (*41*). Today, TB is still the leading cause of deaths among young and middle-aged adults apart from acquired immune deficiency syndrome (AIDS). It was estimated that one-third of the world's population is currently infected with TB bacilli; meanwhile, every second there is someone in the world being infected (*42*). It has been approximately 30 years since the introduction of a novel drug for TB. Strains which are resistant to a single drug or even a particularly dangerous form, multidrug-resistant TB (MDR-TB) bacilli have emerged in the latent stage of the infection, due to inconsistent or partial treatment. Patients with MDR-TB must be treated with extensive chemotherapy (up to two years treatment), generally a combination of second-line anti-TB drugs which are not only more expensive, but also more toxic and less effective (*42*). Therefore, to shorten the duration of the treatment and the frequency of drug

administration, and to improve the effective treatment of MDR-TB and latent tuberculosis infection, there is a definite need for new drug discovery and development (*42*).

Interestingly, like *E. coli, M. tuberculosis* is one of the few organisms which contain both Class I and Class II FBP aldolases (*43, 44*). Generally, if the microorganisms possess both classes of enzymes, only one of them is constitutively expressed (*45*). In the case of *E. coli* and other prokaryotes, the gene which encodes Class II FBP aldolases is essential and constitutively expressed; nevertheless, the non-essential Class I FBP aldolase gene is induced by the presence of gluconeogenic substrates (*43, 46*). Noticeably, temperature-sensitive *E. coli* mutants of Class II FBP aldolase were unable to grow on media containing trace amounts of glucose due to the denaturation of the enzyme. Ultimately, the accumulation of FBP in the host was shown to inhibit stable rRNA synthesis when the experimental condition shifted to non-permissive temperatures (*47-49*). It was confirmed that Class II FBP aldolase is also constitutively expressed in *M. tuberculosis* since the enzyme could be purified at both high and low oxygen tension, whereas Class I FBP aldolase could only be obtained at high oxygen tension, which is consistent with studies on the *E. coli fba* gene (*43*). Further proteomic analysis on *M. tuberculosis* indicated that Class II FBP aldolase (*fda,* Rv0363c) was one of only seven proteins expressed under hypoxic conditions, supporting the idea that low oxygen tension was considered to be responsible for the emergence of latent TB (*50*). Single-gene knockout attempts of the *E. coli fba*A gene (Class II) have proven to be unsuccessful, while knockout of the *fba*B is viable (*51, 52*). Attempts to replace the wild-type *fba* gene (Class II) in *M. tuberculosis* with a deleted allele (Δ*fba*) by a two-step homologous recombination procedure have also proven to be unsuccessful

(*30*). Therefore, Class II FBP aldolase appears to be essential and is a very promising target for development of the novel drugs against TB.

Cystic fibrosis (CF) is a severe chronic respiratory and genetic disease which mainly arises from the mutation in the cystic fibrosis transmemberane conductance regulator gene, which decreases natural defence against bacterial infection, resulting in the infection of most of the patients with the microbial pathogen *Pseudomonas aeruginosa* in infancy and early childhood. Ultimately, around 80 to 95% of the CF patients succumb to the declined pulmonary function and respiratory failure due to chronic bacterial infection and concurrent airway inflammation (*53*).

The main aspect of the pathogenesis of chronic lung infection in CF is the capability of *P. aeruginosa* to develop a biofilm in the respiratory pathway, which was reported to be responsible for the increased bacterial resistance to phagocytic and antibiotic killing (*53*). The current definition of a bacterial biofilm was given by Costerton *et al. (54)* as "a structured community of bacterial cells enclosed in a self-protected polymeric matrix and adherent to an inert or living surface". Within the biofilms, sessile bacterial cells release antigens which can stimulate the host to produce antibodies; however, the antibodies produced are not effective in inhibiting the bacterial growth inside the biofilms compared to the susceptible floating bacteria. Gradually, the accumulated phagocytic enzymes which are not able to penetrate the biofilms will damage the tissues around the biofilm, resulting in further infection by the floating bacteria and accompanying symptoms (*54*). It was reported that in *P. aeruginosa* FBP aldolase is essential for the synthesis of the alginate coat, a polymer of selected acetylated D-mannuronate and L-

guluronate which is believed to be responsible for one of the independent pathways for biofilm formation (*49, 55*). Furthermore, mutants of Class II FBP aldolase in *P. aeruginosa* were found unable to grow on gluconeogenic precursors such as glutamate, succinate or lactate (*56*). Hence, drugs targeting Class II FBP aldolase in *P. aeruginosa* may be able to interrupt the formation of the biofilms and significantly increase the sensitivity of these pathogenic bacteria to antibiotics and the immune system.

### 1.7 Research Objectives

Overall, this research will focus on the development of novel small molecule compounds which will be tested and evaluated against Class II FBP aldolases in pathogenic microorganisms *M. tuberculosis* and *P. aeruginosa* as inhibitors. In addition, a direct chromogenic assay for monitoring Class II FBP aldolase enzyme activities and evaluation of lead Class II FBP aldolase inhibitors will be developed, for which chromogenic substrates mimicking FBP will be synthesized. Synthetic details of the chromogenic substrates and application of those compounds in the direct chromogenic assay are presented in chapter 2. The development and synthesis of novel Class II FBP aldolase inhibitors are summarized in chapter 3.

# Chapter 2

# Development of a direct chromogenic assay for monitoring Class II FBP aldolase enzyme activity

## 2.1 Introduction

Previously, our research group had been using a coupled NADH-linked enzymatic assay as reported in the literature (*1, 2*) to examine the activity of purified Class II FBP aldolase enzymes. The assay as depicted in Scheme 2-1 is based on the fact that DHAP can be converted to glycerol-3-phosphate by α-glycerolphosphate dehydrogenase (GPD) accompanied by the simultaneous oxidation of NADH into $NAD^+$, while rabbit muscle triose phosphate isomerase (TIM) is able to catalyze the conversion of glyceraldehyde-3-phosphate (G3P) into DHAP. NADH absorbs readily at 340 nm and the quantitative reduction of the absorbance can be monitored to determine the relative enzyme activity. This assay is simple and convenient to evaluate the inhibitory activity of potential candidate compounds towards Class II FBP aldolases. However, it is possible that non-specific inhibition by the candidate compounds being examined in this coupled assay towards the other coupled enzymes such as TIM or GPD could give false results.

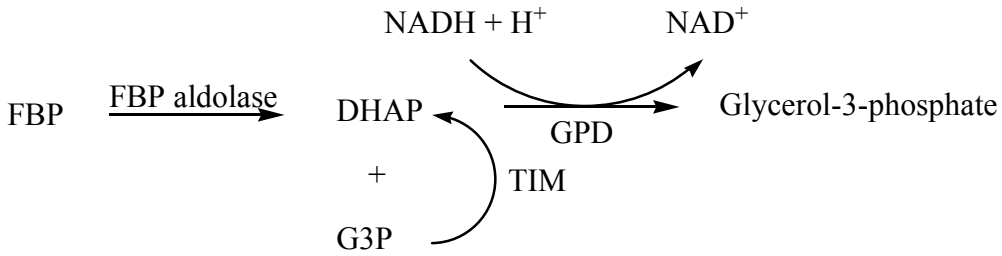


**Scheme 2-1.** Schematic representation of the NADH-linked coupled-enzymatic assay. TIM catalyzes the conversion from G3P into DHAP. GPD catalyzes the conversion from DHAP to glycerol-3-phosphate, coupled by the oxidation of NADH. NADH absorbs at 340 nm and the enzyme activity is monitored by the quantitative reduction of absorbance $A_{340}$.

Specifically in this coupled NADH-linked enzymatic assay, TIM is responsible for catalyzing the stoichiometric conversion from G3P to DHAP. Therefore, non-specific inhibition towards TIM by any candidate compound leads to less formation of DHAP, hence less conversion from DHAP to glycerol-3-phosphate. Moreover, non-specific inhibition towards GPD will also result in less formation of glycerol-3-phosphate. In this case, the assay will exhibit slower rate of NADH quantitative reduction, giving the false conclusion that the candidate compound is exhibiting specific inhibitory activity towards Class II FBP aldolases. In addition, NADH and the coupling enzymes make the assay relatively expensive, especially for practical use in large scale screening of potential inhibitors which may need to be done in future, if the rationally designed inhibitor proves to be inadequate. To circumvent these problems, a direct assay involving only Class II FBP aldolases rather than this multiple coupling enzyme system is the goal of the present research project and will be discussed in this chapter.

## 2.2 Design of chromogenic substrates

Theoretically, for a direct enzymatic assay, part of the substrate should be a chromophore that can be detected spectrophotometrically. The basic strategy is to design and chemically synthesize a series of compounds that structurally mimic FBP and incorporate a chromophore. These compounds should be capable of being cleaved by Class II FBP aldolases into the corresponding aldehyde (G3P mimicking or equivalent) and ketone (DHAP mimicking or equivalent) products leading to a distinguishable change in absorbance.

Interestingly, aldolases possess high specificity towards their respective donor substrates and generally will not accept other donors, even if they are structurally similar to the natural ones (*3*). Thus, aldolases can be classified based upon this restricted donor specificity, such as DHAP-dependent aldolases, pyruvate-dependent aldolases and acetaldehyde-dependent aldolases. FBP aldolases, together with rhamnulose 1-phosphate aldolase and tagatose 1,6-bisphosphate aldolase, all belong to the DHAP-dependent aldolases (*3*). Whitesides and coworkers (*4*) first reported that permissive variations of the DHAP moiety are highly restricted in rabbit muscle aldolases (a Class I FBP aldolase) with only two exceptions out of 11 DHAP analogues, 1,3-dihydroxy-2-butanone-3-phosphate and 1,4-dihydroxy-3-butanone-1-phosphate. Subsequently, Wong and coworkers (*5*) found that *E. coli* FBP aldolase (a Class II FBP aldolase) possessed the same donor substrate specificity as the rabbit muscle aldolase. In contrast to the strict donor substrate specificity, DHAP dependent aldolases accept a broad range of aldehyde substrates, such as unhindered aliphatic aldehydes, α-heteroatom substituted aldehydes, monosaccharides and their derivatives. Nevertheless, aromatic aldehydes, sterically hindered aldehydes and α,β-unsaturated aldehydes are generally not well accepted in the direction of aldol condensation (*6*). The DHAP

moiety is more important for immediate substrate recognition and binding from the perspective of retro-aldol direction compared to the G3P moiety of FBP aldolases. Therefore, it is crucial to retain DHAP as the donor substrate and only modify the acceptor aldehyde G3P to become chromogenic when designing a synthetic route to harvest the corresponding chromogenic substrate.

Chromogenic substrates bearing chromophores generally consist of conjugated π-systems. In this system, mostly in aromatic systems, the lowest electronic energy transition occurs when a π-electron is promoted from the highest occupied π molecular orbital to the lowest unoccupied π* molecular orbital, hence giving the absorption that can be detected spectrophotometrically (*7*). Therefore, it is reasonable to examine and screen different aromatic aldehydes as generalized in Scheme 2-2 to make the chromogenic moiety of the FBP-mimicking substrate since they can be

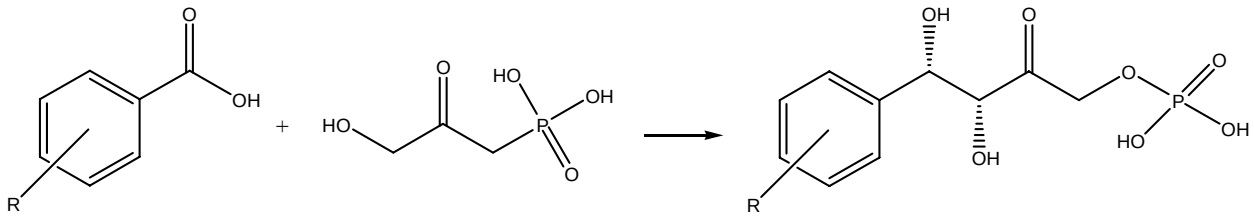


**aromatic aldehyde** **DHAP** **chromogenic substrate**

**Scheme 2-2.** The general approach to synthesize chromogenic substrates from aromatic aldehydes and DHAP. R group represents any substituent at either available *ortho, meta* or *para* position.

conveniently detected in the near ultraviolet region with UV spectroscopy. The essential theory supporting this specific chromogenic assay is based upon the bathochromic shift effect, which is

the shift of absorption of chromophores to a longer wavelength due to substitution or solvent effect. Conversely, a hypsochromic shift is the shift of absorption to a shorter wavelength due to substitution or solvent effect (*8*).

Specifically, the degree of conjugation of the substituents on the aromatic ring is different when comparing the aromatic aldehydes with FBP-mimicking chromogenic substrates. The π-bond of the carbonyl contributes to a higher degree of conjugation for the aromatic aldehyde than does the hydroxyl group in proximity to the benzene ring for the chromogenic substrate; hence producing a bathochromic shift which can be distinguished by UV spectroscopy when the chromogenic substrate is cleaved into the corresponding DHAP and aldehyde products by Class II FBP aldolases. Moreover, other substituents on aromatic aldehydes will contribute to the bathochromic shift in different degrees when various electron donating groups or electron withdrawing groups are attached to *para*, *meta* and *ortho* positions accordingly (*8*). Thus, aromatic aldehydes with different substituents should be screened to find a group of promising candidates, which would give pronounced bathochromic shift when they are applied to chromogenic assay development. Subsequently, good candidates would be further modeled as corresponding FBP mimics to examine if they would fit the active site of FBP aldolases. However, at this stage, a synthetic difficulty emerges as previously mentioned, that aromatic aldehydes are generally not well accepted by DHAP-dependent aldolases in the direction of aldol condensation. This eliminated the possibility of applying aldolases as catalysts to synthesize the chromogenic substrates, which forced us to pursue an alternative non-enzymatic organic catalyst to accomplish the synthetic goal.

## 2.3 Direct asymmetric aldol reactions catalyzed by organocatalysts

Based on excellent stereocontrol of asymmetric aldolizations catalyzed by aldolases, chemists have been pursuing simple organocatalysts that possess a similar function in formation of C-C bonds through aldol reactions. The organocatalysts were expected to act as either Class I aldolase with enamine based mechanism, or Class II aldolase with Lewis acidic metal and enolate based mechanism.

The first small molecule asymmetric Class II aldolase mimic was synthesized and reported by Nakagawa *et al.* (*9*) in the form of zinc, lanthanum and barium complexes. However, an enamine-based asymmetric Class I aldolase mimic was not described in the literature until 2000 by List *et al.* (*10*). The authors found the amino acid L-proline, which works as an aldolase mimic, to be an effective asymmetric catalyst for direct aldol reaction between unmodified acetone and a variety of aldehydes (Scheme 2-3). They demonstrated a reaction between acetone and 4- nitrobenzaldehyde catalyzed by L-proline (30 mol%) and the corresponding aldol product was produced in a good yield (68%) and enantiomeric excess (76% *ee*). As a catalyst, proline is non-toxic, inexpensive, and readily available in both enantiomeric forms. Moreover, reactions catalyzed by proline do not require inert conditions and can be performed at room temperature.

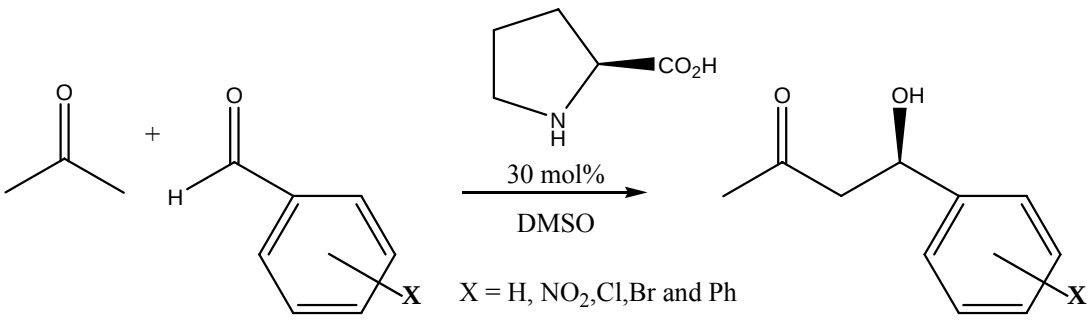


**Scheme 2-3**

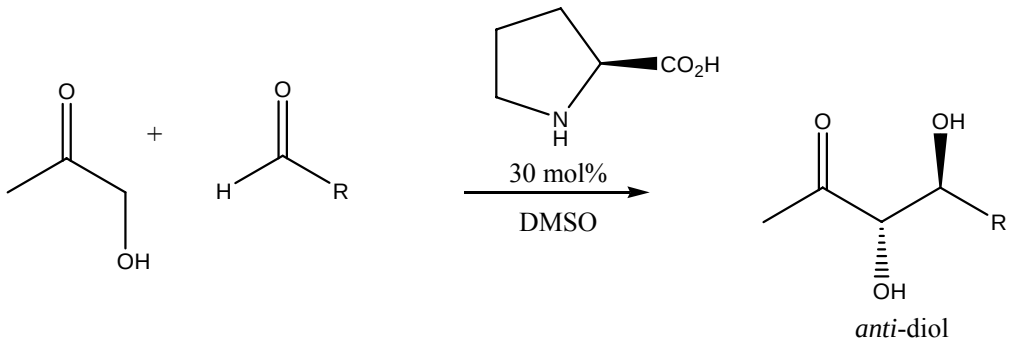


**Scheme 2-4**

Within the same year, the same research group found L-proline was also able to catalyzed the direct aldol reaction between unprotected hydroxyacetone and various aldehydes to yield *anti*-diols with excellent diastereoselectivity and enantioselectivity (Scheme 2-4) (*11*). Further research by Barbas and coworkers (*12*) proposed that the key step in the mechanism of direct asymmetric aldol reaction catalyzed by L-proline was the formation of the enamine intermediate between L-proline and the corresponding ketone donor substrate. The carbonyl group of the aldehyde acceptor was then attacked by the enamine intermediate with high enantiofacial selectivity. This was imposed by a highly organized tricyclic hydrogen bonded framework resembling a metal-free Zimmerman-Traxler type transition-state (Scheme 2-5), which is a model of the aldol reaction that describes a chair conformation of six-membered transition-states (*13*). Based on the Zimmerman-Traxler model, *E*-enolates from ketone donors give rise to *anti*-products, whereas *Z*-enolates give rise to *syn*-products (*14*). Therefore, the mechanism proposed by Barbas and coworkers could assist us in understanding the rationale of the excellent diastereoselectivity and enantioselectivity of direct asymmetric aldol reactions catalyzed by L-proline (*12*).

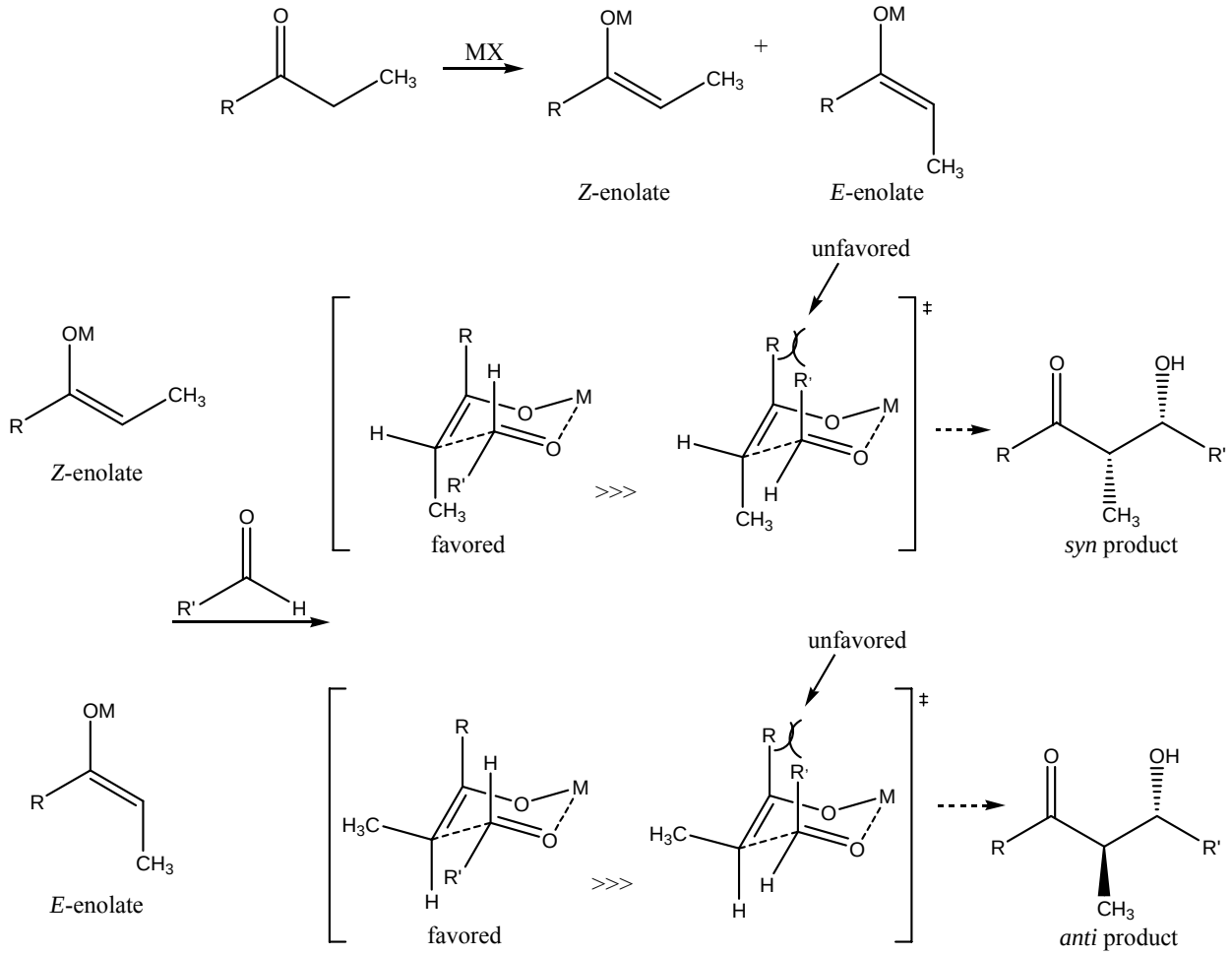


**Scheme 2-5.** Schematic representation of the Zimmerman-Traxler model. According to this model of the transition states of aldol reaction, *E*-enolates give *anti* products, whereas *Z*-enolates give *syn* products (M = metal, X = halide) (*14*).

Bearing excellent stereocontrol as a catalyst for a variety of substrates for direct asymmetric aldol reactions, proline and its derivatives have been extensively explored for organic synthesis. However, the reactivity and selectivity of certain proline-catalyzed aldol reactions still have limitations since it is relatively difficult to structurally modify proline. Furthermore, proline is known to react with electron-deficient aromatic aldehydes to form iminium salts, which then undergo decarboxylation even at room temperature, and subsequently induce significant

retardation of the aldol reactions (*15*). Moreover, direct asymmetric aldol reactions catalyzed by proline would preferentially yield *anti*-diol product; whereas the 3-hydroxyl and 4-hydroxyl groups of the FBP-mimicking chromogenic substrates that are being pursued and also FBP itself are desired to be in *syn*-3*S*,4*R* configuration. Therefore, proline as a sole catalyst cannot provide the optimal route to the aldol reactions between dihydroxyacetone (DHA) and aromatic aldehydes with the proper stereoconfigurations as demanded.

To achieve good yields and high diastereomeric and enantiomeric selectivity for catalyzed direct asymmetric aldol reactions by organocatalysts or Lewis acidic metal complexes, anhydrous organic solvents are often required. Recently, zinc complexes of proline, lysine and arginine were found to be efficient catalysts for aldol reactions of 4-nitrobenzaldehyde and acetone in aqueous media at room temperature with good yield and enantioselectivity (*16*). Furthermore, zinc-proline complex in the form of $Zn(Pro)_2$ was also reported to be able to catalyze aldol reactions between DHA and various aromatic aldehydes such as 4-nitrobenzaldehyde, 2-nitrobenzaldehyde, and 2-bromobenzaldehyde with excellent yields in water with tetrahydrofuran as co-solvent (*17*). However, in contrast to the results obtained with proline as the catalyst, moderate *syn*-selectivities were observed instead of complete *anti*-selectivities. Especially for the aldolization between DHA and 2-bromobenzaldehyde, the *syn*/*anti* ratio was found to be 3:1. Normally, a catalyst incorporating metal should act as a Lewis acid in water and in this respect $Zn(Pro)_2$ could be considered as a Class II aldolase mimic, in which the zinc ion coordinates to the carbonyl to facilitate the enolate formation, whereas the proline ligand provides the chiral environment for enantioselectivity (*17*). Interestingly, further study by Kofoed *et al.* (*18*) suggested that $Zn(Pro)_2$ complex uses both enolate and enamine

mechanisms in a substrate dependent manner. Specifically for acetone as the ketone donor, zinc ion was assumed to assist and stabilize the enamine intermediate formed between proline and acetone instead of a Lewis acid. The dual mechanism of $Zn(Pro)_2$ complex was presumably attributed to the inductive effect by the OH groups of DHA which lower the pKa of the α-CH, and also to the stabilization of enolate formation by intramolecular hydrogen bonding.

Although $Zn(Pro)_2$ complex is able to catalyze the direct asymmetric aldolization between DHA and aromatic aldehydes in preference to our desired *syn*-adduct, the only low to moderate enantiomeric excess values from the authors prompted us to search for better amine catalysts that would furnish higher enantiomeric excess values towards the *syn*-products.

## 2.4 Simple primary amine organocatalysts

In the previous section, direct asymmetric aldol reactions were demonstrated to be attainable through either metal-based catalysis, or highly enantioselective small molecule organocatalysts, such as proline and its derivatives. Noticeably, most of the presently available organocatalysts functioning via an enamine-based mechanism, such as proline and chiral pyrrolidine derivatives, are secondary amines (*19*). Therefore, it is of great interest for chemists to develop primary and tertiary amine catalysts to expand the utility of enamine-based organocatalysts.

Recently, Cordova *et al.* (*20*) have shown examples of primary amine catalysts, that several acyclic amino acids such as alanine, valine, leucine, isoleucine and threonine were able to catalyze the direct asymmetric aldol reaction between cyclohexanone and *p*-nitrobenzaldehyde with excellent enantioselectivities by 30 mol% catalyst injection in wet DMSO. Alanine was also shown by the authors to be able to catalyze the aldol reaction between cyclic protected DHA dimethyl-1,3-dioxan-5-one and *p*-nitrobenzaldehyde with promising 84% yield and greater than 99% enantiomeric excess (Scheme 2-6). Moreover, Jiang *et al.* (*21*) also found tryptophan to be able to catalyze the aldol reaction between several cyclic ketones and aromatic aldehydes

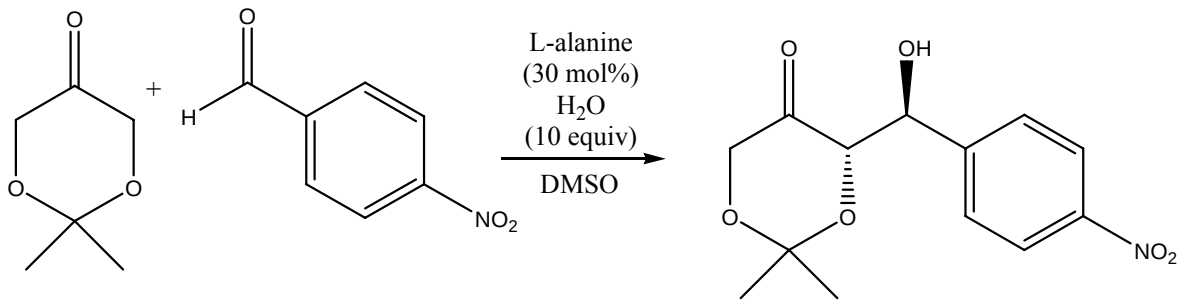


**Scheme 2-6**

enantioselectively in water. Interestingly, secondary amine catalysts such as proline and chiral pyrrolidine derivatives can only provide access to *anti*-configured 1,2-diols. These catalysts mimic the activity of D-tagatose-1,6-diphosphate and L-fuculose-1-phosphate aldolases, which only utilize *anti*-configured 1,2-diols as substrates. However, access to *syn*-configured 1,2-diols by using organocatalysts and DHA-based strategy had been not available until Ramasastry *et al.* (*22*) published the first *syn*-selective aldol reactions between unmodified hydroxyacetone and aromatic aldehydes by using several unmodified and modified acyclic amino acids such as L-tryptophan, L-threonine, O-*t*Bu-L-threonine and O-*t*Bu-L-tyrosine. Compared to the secondary amines, these primary amines functionally mimic the activity of L-rhamnulose-1-phosphate and FBP aldolases, which only utilize *syn*-configured 1,2-diols as substrates.

Ramasastry *et al.* not only demonstrated the first *syn*-selective direct asymmetric aldol reactions by using primary amine catalysts, but also elegantly explained the mechanism behind the rather different *syn*- or *anti*-selectivities when using primary amine or secondary amine catalysts, respectively (*22*). The authors reasoned that, in the reactions of hydroxyacetone with proline as a catalyst, aldol products form via reactions involving an *E*-enamine intermediate B as shown in Scheme 2-7. For pyrrolidine-derived catalysts or other secondary amines, *E*-enamine intermediates B predominate over the *Z*-enamine intermediate A, due to the steric effect between the hydroxyl group and the pyrrolidine ring in intermediate A. The *anti*-configuration of products was attributed to the transition state C in Scheme 2-7, since it is the *Si*-face of the *E*-enamine that reacts with the incoming aldehyde acceptor. Similarly, the authors suggested that *Z*-enamine intermediate F should predominate in the reaction of hydroxyacetone with primary amine catalysts, due to the intermolecular hydrogen bonding stabilization as shown in Scheme 2-7.

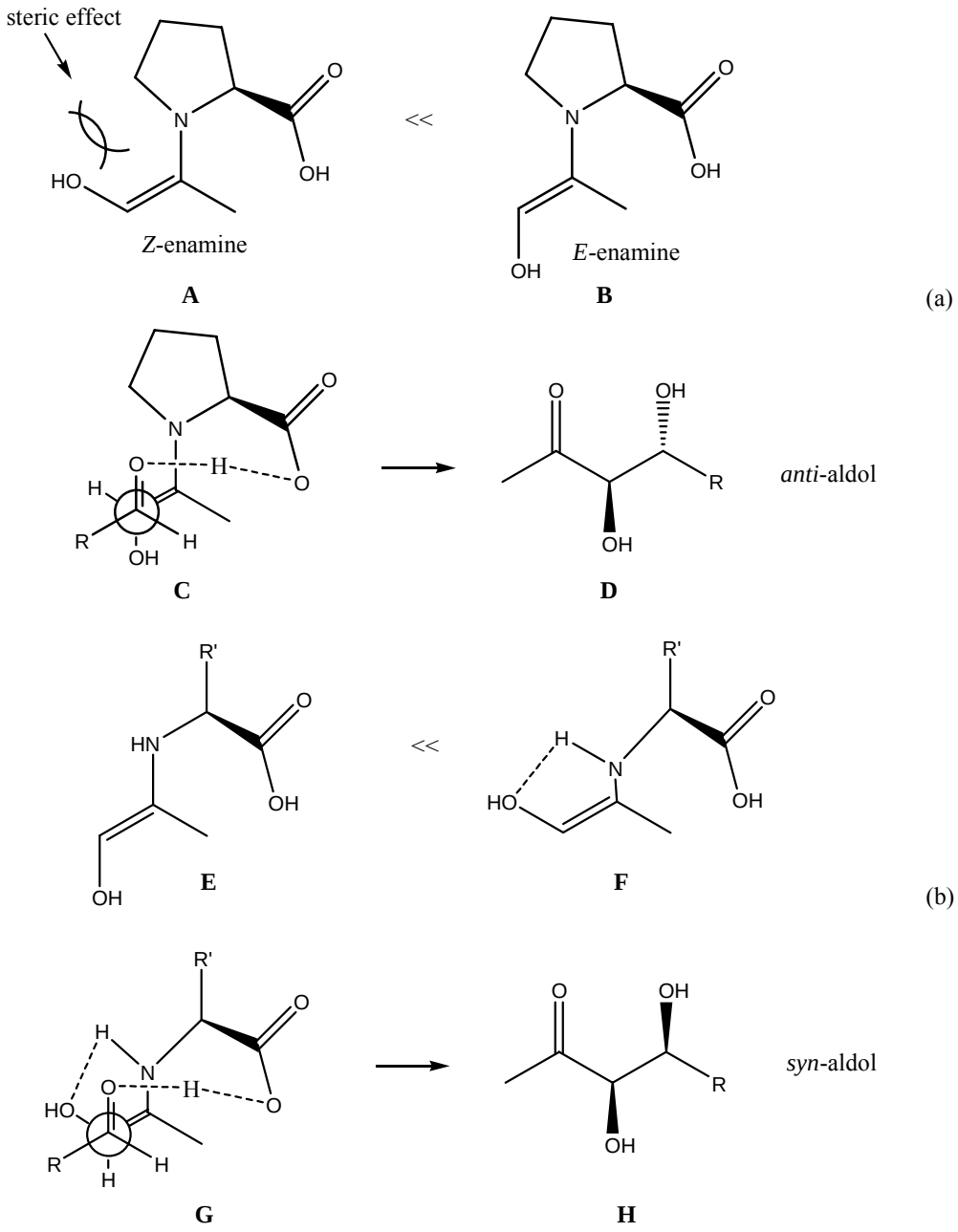


**Scheme 2-7**. Schematic representation of the mechanisms explaining *anti*- and *syn*-selectivities of secondary amine and primary amine catalysts, respectively. (a) Possible *Z*- and *E*-enamine intermediates formed between hydroxyacetone and secondary amine catalyst proline (A and B), transition state with the aldehyde acceptor (C), and the corresponding *anti*-aldol product (D). (b) Possible *E*- and *Z*-enamine intermediates formed between hydroxyacetone and primary amine catalyst (E and F), transition state with the aldehyde acceptor (G), and the corresponding *syn*-aldol product (H) (*22*).

Moreover, during their early studies of aldol reactions involving unmodified hydroxyacetone mediated by antibody catalysis, the *Z*-enamine intermediate was observed to form with the primary amine lysine side chain, the key catalytic residue in aldolases. The *syn*-configuration of products could be attributed to the transition state G in Scheme 2-7, which promotes the formation of *syn*-aldols (*22*).

Interestingly, Barbas and coworkers (*23, 24*) recently reported *syn*-selective direct asymmetric aldol reactions between unprotected and protected DHA with aromatic aldehydes catalyzed by primary amine catalysts. They successfully demonstrated that *syn*-configured aldol product can be obtained from unprotected DHA and *p*-nitrobenzaldehyde with either a 3*R*,4*S* or 3*S*,4*R* absolute configuration when catalyzed by O-*t*Bu-L-threonine, which functionally mimics L-rhamnulose-1-phosphate aldolase; or by O-*t*Bu-D-threonine, which functionally mimics FBP aldolases, respectively (*23*). The authors also showed that the same catalysts are able to catalyze *syn*-selective aldol reactions of *tert*-butyldimethylsilyl or benzyl protected DHA with corresponding aromatic or aliphatic aldehydes (*24*).

Markert *et al.* (*25*) have recently found a remarkable catalytic effect of tertiary amines in aldol reactions of unprotected DHA with certain aldehydes. They reported that 10 mol% diazabicyclo-undec-7-ene (DBU) or 30 mol% cinchonine with Dowex could mediate *syn*-selective aldol reactions just as their primary amine catalyst counterparts. However, the authors suggested that the mechanism of aldol reactions mediated by tertiary amine cannot be compared with the reactions catalyzed by primary or secondary amine catalysts, thus, further investigations are still currently underway.

## 2.5 Chiral primary-tertiary diamine-Brønsted acid catalyst

Simple primary or secondary amino acids and their derivatives were surveyed and shown to be stereoselective catalysts for direct aldol reactions in the previous sections. However, the relatively low efficiency (20-30 mol% loading) and non-broad substrate scope of these amine catalysts may preclude them from large scale and more general applications.

As mentioned previously, secondary amine catalysts such as proline and chiral pyrrolidine derivatives could only provide access to *anti*-configured 1,2-diols, and reactions are mainly limited to cyclic protected DHAs. Similarly, primary amine catalysts such as threonine and its derivatives could only catalyze *syn*-aldol reactions of hydroxyketones, or DHA and acyclic protected DHAs, respectively. Interestingly, a significant advance has been accomplished by the very recent work of Luo *et al.* (*26, 27*). The authors published the first example of chiral primary-tertiary diamine-Brønsted acid catalysts. *Trans*-*N*,*N*-dialkylated-diaminocyclohexanes (Figure 2-1) with a strong acidic additive, were reported to catalyze both *syn*- and *anti*-aldol reactions of unprotected and cyclic protected DHAs with high yields and excellent stereoselectivity. Such primary amines can functionally imitate all of the four types of DHAP-dependent aldolases, namely L-rhamnulose-1-phosphate and FBP aldolases (*syn*-aldol products), as well as D-tagatose-1,6-diphosphate and L-fuculose-1-phosphate aldolases (*anti*-aldol products).

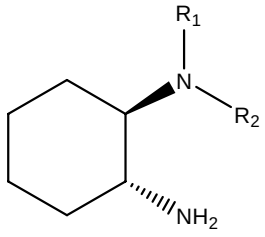


**Figure 2-1.** Structure of *trans*-*N*,*N*-dialkylated-diaminocyclohexane.

Noticeably, the authors first found the activity and stereoselectivity of chiral *trans*-*N*,*N*-dimethyldiaminocyclohexane to be superior to other primary amine catalysts when it was used to catalyze direct aldol reactions of acetone and other small aliphatic ketone donors (*26*). Further screening of the analogous catalysts of *trans*-*N*,*N*-dimethyldiaminocyclohexane bearing longer alkyl chains demonstrated improved yields and stereoselectivity, with acyclic DHA derivatives including free DHA as ketone donors (*27*). The best results were obtained with *trans*-*N*,*N*-didecanyl derivative, but *trans*-*N*,*N*-dipropyl derivative were also effective (Figure 2-2).

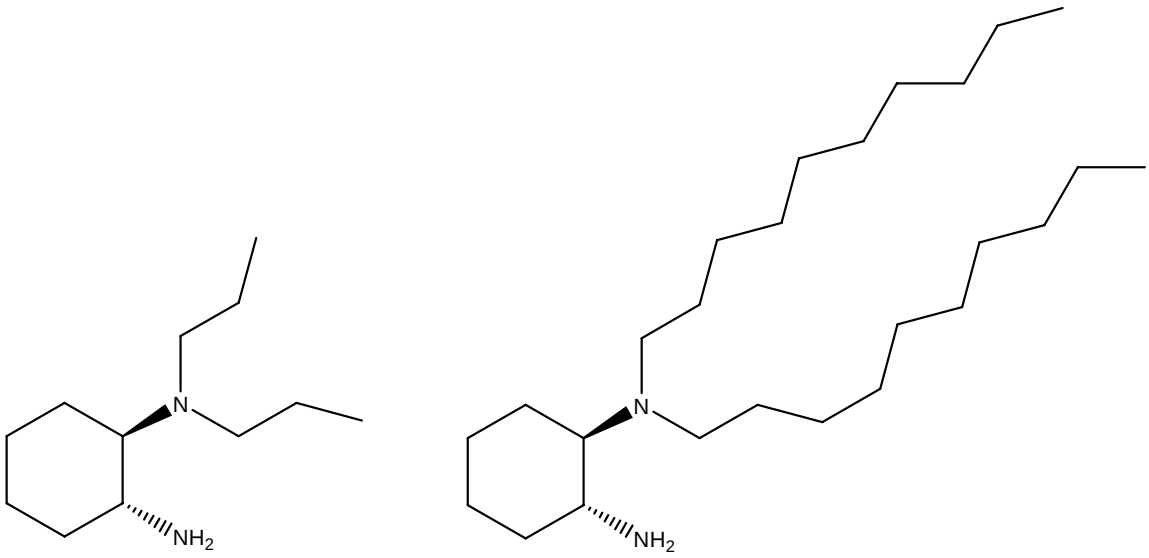


(1*R*,2*R*)-$N^1$,$N^1$-dipropylcyclohexane-1,2-diamine (1*R*,2*R*)-$N^1$,$N^1$-didecylcyclohexane-1,2-diamine

**Figure 2-2.** Structures of *trans*-*N*,*N*-dialkylated-diaminocyclohexane derivatives.

Importantly, the strong Brønsted acid trifluoromethane sulfonic acid (TfOH) was demonstrated to be essential for the catalysis, as the reaction in absence of TfOH was observed to give less than 10% yield and poor stereoselectivity. The authors suggested that protonation on the tertiary amine moiety of the catalyst by TfOH rendered it a direct hydrogen bonding donor as shown in Scheme 2-8. Furthermore, the *syn* stereoselectivity towards acyclic DHA derivatives could be

explained by a *Z*-enamine transition state **a** as the model proposed in Scheme 2-8, which is consistent with the model presented by Ramasastry *et al*. in the previous section (*22*). In contrast, the reactions of cyclic DHA derivatives, which are only capable of forming *E*-enamine intermediates (**b** in Scheme 2-8), would afford *anti*-aldol products instead.

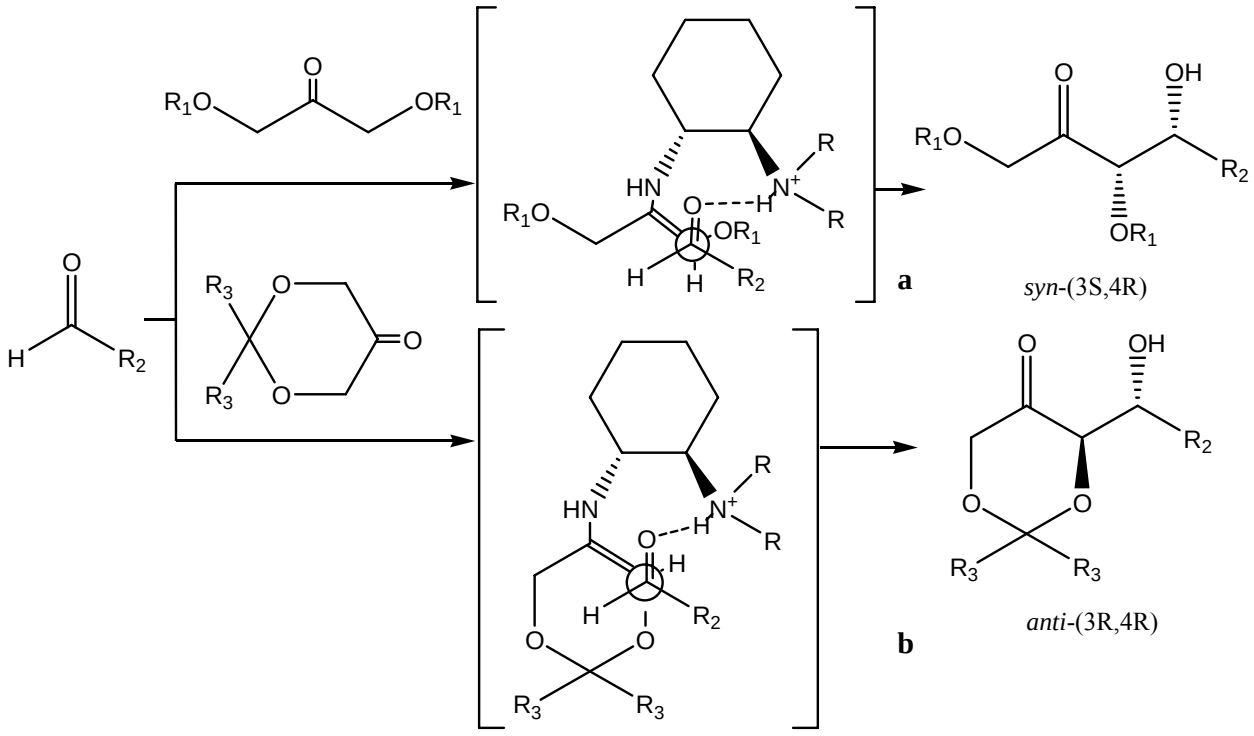


**Scheme 2-8**. Proposed transition states and corresponding products of aldol reactions of acyclic and cyclic DHA derivatives catalyzed by primary-tertiary diamine-Brønsted acid catalysts. This scheme was adapted from Luo *et al.* (*27*).

Furthermore, the authors also reported that addition of a second weak Brønsted acid such as *m*-nitrobenzoic acid did further improve the yield. Moreover, in their early experiments, it was found that the loading of the catalyst could be reduced to as low as 2 mol% in certain conditions, while still maintaining good enantioselectivity and significant activity by adding this weak acid.

This weak Brønsted acid was proposed to facilitate the enamine catalytic cycle and to increase the yield of products, but the detailed mechanism is still unknown (*26, 28*).

In summary, under optimal experimental conditions, the best results as reported by the authors were up to 97% yield, 99:1 *syn*:*anti* ratio and 99% enantiomeric excess by using these chiral primary-tertiary diamine-Brønsted acid catalysts from DHA and its derivatives. Therefore, this was viewed as the best strategy for us to follow in synthesis of the unphosphorylated version of the desired chromogenic substrates.

## 2.6 Application of a phosphate ester mimic in the chromogenic assay

The desired chromogenic substrates can be synthesized from DHA and aromatic aldehydes through direct asymmetric aldol reactions catalyzed by the chiral primary-tertiary diamine-Brønsted acid catalysts presented in the previous section; however, the problem of phosphorylation on the DHA moiety still remains unsolved. Recall the fact that DHAP-dependent Class II FBP aldolases possess strict donor substrate specificity towards DHAP. Since the phosphate moiety of DHAP is responsible of forming hydrogen bonds with four residues in the enzymatic active site, this factor has become the major determinant for binding affinity between Class II FBP aldolases and DHAP (*29*). Therefore, it is crucial to develop a proper strategy of phosphorylation on the DHA moiety to create the chromogenic substrates which will be subjected to the actual chromogenic assay.

In their publication, Ma *et al.* (*30*) described an experimental method to chemically phosphorylate the primary hydroxyl group of aromatic ketal alcohols, by simply mixing diethyl or diphenyl phosphoryl chloride with the ketal alcohols in solution in pyridine (Scheme 2-9).

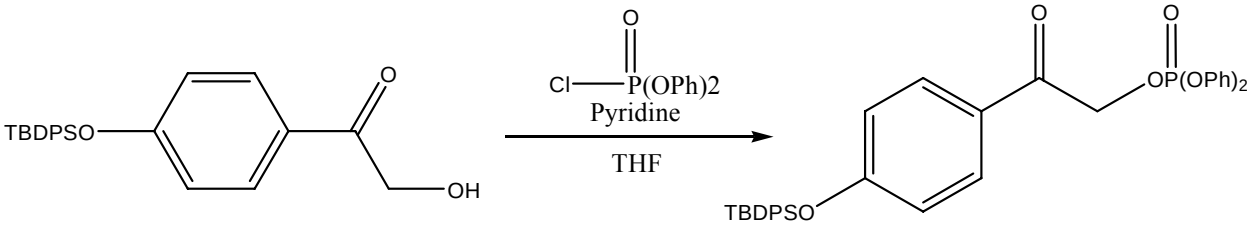


**Scheme 2-9**

Free phosphates can be obtained by subsequent hydrolysis of the phosphate esters. However, it is possible for the phosphorylating agent to perform non-selective phosphorylation on the secondary 3- or 4-hydroxyl groups on the chromogenic substrate. Furthermore, the secondary hydroxyl groups may also nucleophilically attack the phosphate ester and lead to formation of ring structured compound even if the phosphorylating agent could selectively phosphorylate the primary hydroxyl group on the chromogenic substrate.

Interestingly, it has been reported that inorganic arsenate and vanadate are able to form arsenate and vanadate esters with free DHA *in situ*, which act as phosphate ester mimics in practical enzymatic aldol reactions (*31, 32*). Wong and cowokers (*31*) first demonstrated that DHA in the presence of a catalytic amount of arsenate and vanadate was an effective substrate for FBP aldolases. Unlike phosphate esters, the arsenate and vanadate esters were formed spontaneously and reversibly in aqueous solution. This makes it feasible to perform enzymatic reactions with a mixture of inorganic arsenate or vanadate and the unphosphorylated organic alcohol products to replace the corresponding organic phosphate, which is naturally the substrate. Nevertheless, the high toxicity of arsenate could be problematic from a practical point of view. Although vanadate can be utilized even at lower concentration, its redox activity, instability and its high cost would limit its practical application.

To circumvent the drawback of arsenate and vanadate, Wong and coworkers (*29*) found that inorganic borate also allows DHA to be accepted as a substrate by rhamnulose 1-phosphate aldolase (RhaD), presumably by reversibly forming a borate ester with DHA *in situ* (Scheme 2-10). Compared to arsenate and vanadate, borate is safe and inexpensive, while still retaining the

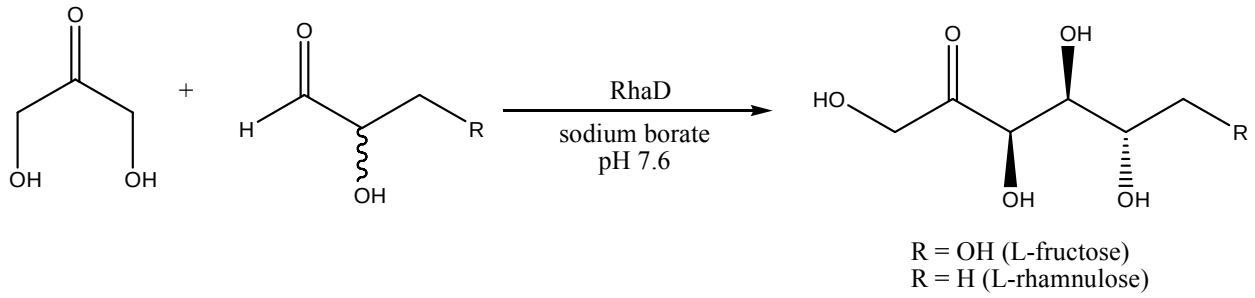


**Scheme 2-10**

utility to be used as a phosphate ester mimic. Noticeably, when the borate concentration was in 4-fold excess of the DHA concentration, the maximum yield of aldol product was obtained by the authors. It was proposed that excess borate may play a role in trapping the aldol product and preventing the reverse reaction.

Therefore, inorganic borate can be utilized to form a borate ester with our chromogenic substrate once it has been synthesized, acting as a phosphate ester mimic, which presumably will be accepted by Class II FBP aldolases in the chromogenic assay as we have planned. The borate concentration will also be controlled to facilitate the retro-aldol cleavage of the FBP mimicking chromogenic substrates.

## 2.7 Results and Discussion

### UV-visible spectrophotometric assay

Two aromatic model compounds, 5-nitro-furaldehyde (represents the aromatic aldehyde) and 5-nitro-furfuryl alcohol (represents the chromophore moiety of the FBP-mimicking chromogenic substrate) were examined by UV-visible spectrometry to determine if there was an adequate spectrophotometric difference between the alcohol and the aldehyde which would be the product

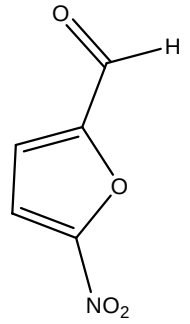


5-nitro-furaldehyde

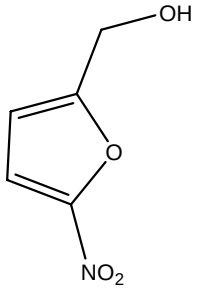


5-nitro-furfuryl alcohol

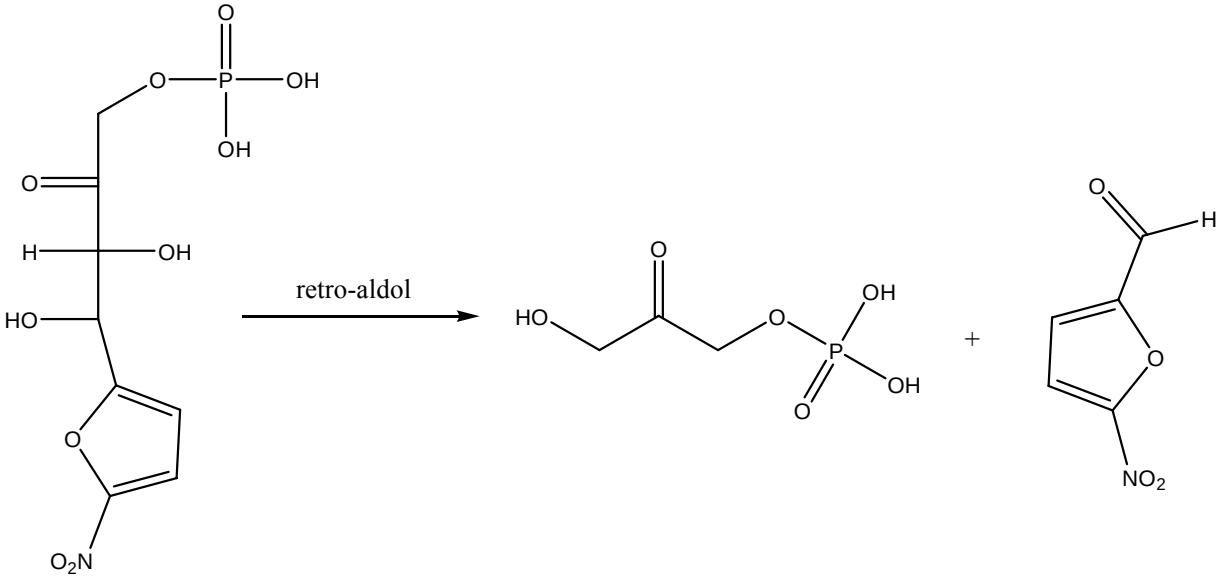


**Scheme 2-11**

of the retro-aldol reaction, in order to ensure the feasibility of the direct chromogenic assay (Scheme 2-11). This was done by screening the maximum absorbance and the corresponding 5-nitro-furaldehyde was found to be 0.794 O.D. at 313 nm, and the maximum absorbance of 5-nitro-furfuryl alcohol was found to be 0.551 O.D. at 322 nm, with a final concentration of 50 μM in the assay mixture (Figure 2-3). The difference of the extinction coefficients Δε of this two

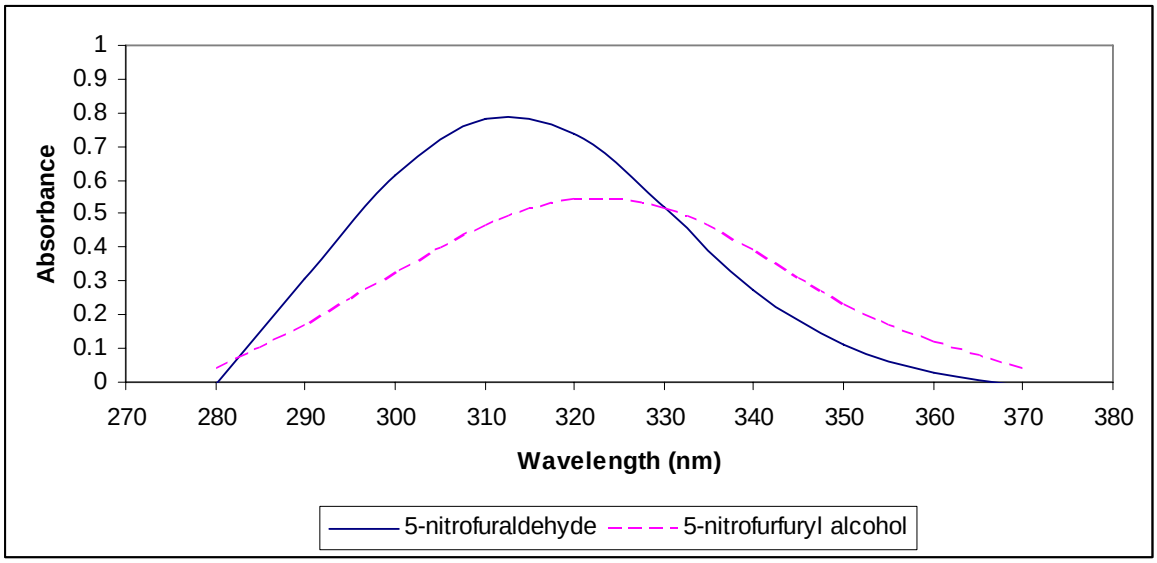


**Figure 2-3.** Scanning of two model compounds by UV-visible spectrometry**.** Solutions of two model compounds 5-nitrofuraldehyde and 5-nitro-furfuryl alcohol in DMSO and $KH_2PO_4$ buffer, were scanned from 200 nm up to 600 nm by UV-visible spectrometry to determine the maximum absorbance and corresponding wavelength. Only the region from 270 nm to 380 nm and selective data points were shown in the figure.

compounds were calculated to be 6440 $cm^{-1}M^{-1}$ at 307 nm, apparently can be distinguished by UV-visible spectrometry. However, different aromatic aldehydes and corresponding chromogenic substrates would produce different Δε values, which could be potentially higher or lower compared to the value obtained by the aforementioned model compounds. Further screening of compounds by UV-visible spectrometry will be demanded to confirm this.

Although the data look promising, the feasibility of direct chromogenic assay in examining the enzyme activity of Class II FBP aldolases still demands further testing. Since it is still unknown if the chromogenic substrates would be accepted by Class II FBP aldolases until the synthesis of those compounds are completed, which will be subjected to kinetic assay subsequently. Compared to the $\Delta\varepsilon$ value between $NAD^+$ and NADH (10680 $cm^{-1}M^{-1}$) used in the coupled-enzymatic assay (*33*), $\Delta\varepsilon$ of the two model compounds is approximately 2 times smaller, indicating the sensitivity of the direct chromogenic assay could be lower. Noticeably, in the coupled-enzymatic assay, the presence of the coupled enzyme TIM prompts the conversion from one G3P to one DHAP, hence doubles the apparent concentration of DHAP, which will then increase the sensitivity of this coupled assay.

**Synthesis of FBP-mimicking chromogenic substrate**

The method chosen for synthesis of the potential chromogenic substrates for FBP aldolases is based on the work published recently by Luo and coworkers (*27*). It has been reported that the asymmetric aldol condensation of dihydroxyacetone (DHA) with various aromatic aldehydes can be accomplished at room temperature employing a catalyst derived from optically pure trans-1,2-diaminocyclohexane as described earlier (see page 35). The version of the catalyst that is appropriate for preparation of a FBP mimic is shown below (Figure 2-4).

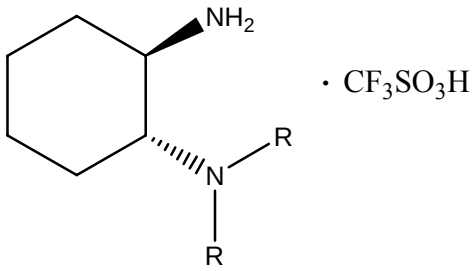


**Figure 2-4.** Structure of the chiral primary-tertiary diamine-Brønsted acid catalyst for preparation of FBP-mimicking chromogenic substrate.

The synthesis of this catalyst is based on a procedure developed earlier by the same group (*26*). The method involves the mono-*N*-acetylated version of the $C_2$-symmetric diamine by reaction with the hydrochloride salt of ethyl acetimidate as originally described by Mitchell and Finney (*34*). The acetylation process is thought to first yield the imidazoline **2-2** which is then hydrolyzed to the mono-*N*-acetylated product **2-3** (Scheme 2-12). In the published experimental procedure, the ethyl acetimidate salt was first generated *in situ* by reaction of two equivalents of acetonitrile with HCl gas in dry ethanol, followed by addition of one equivalent of the diamine compound. In the present study, it was found that the acetimidate salt was commercially available and thus the diamine was added to 2.8 equivalents of the commercial material in dry ethanol.

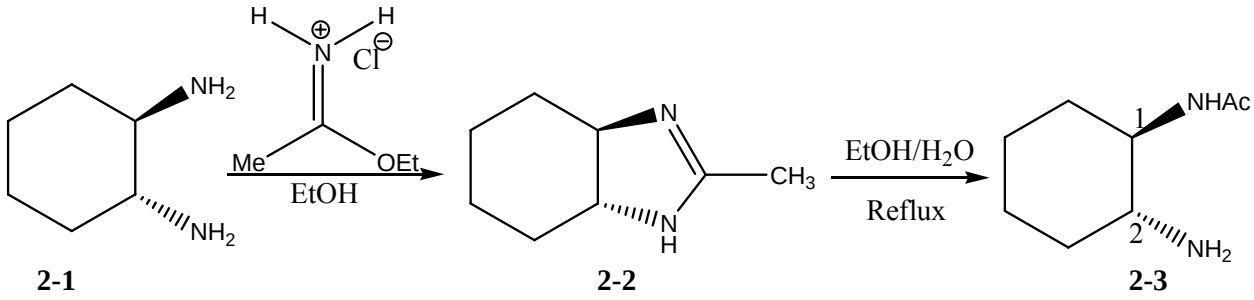


**Scheme 2-12**

However, the product obtained in this reaction was found to contain an impurity. The $^{1}$H NMR spectrum of the crude product exhibited two singlets assignable as *N*-acetyl groups at δ = 2.14 and 2.11 ppm. $^{1}$H-$^{1}$H homonuclear correlation spectroscopy (COSY) NMR analysis revealed a correlation between two complex multiplets of equal intensity at δ = 3.35 and 2.32 ppm that were reasonably assigned to C1-H and C2-H signals of the desired product. In addition, there is a simpler multiplet at δ = 3.57 ppm which seemed to be consistent with a signal expected for the *N*,*N*-diacetyl derivative **2-4** which has a $C_2$ symmetry (Figure 2-5). ESI-MS analysis of the mixture also provided support for the suggestion that the impurity was the diacetylated material by exhibiting a peak at m/z = 199, consistent with the ($M+H^+$) fragment for the diacetylated material.

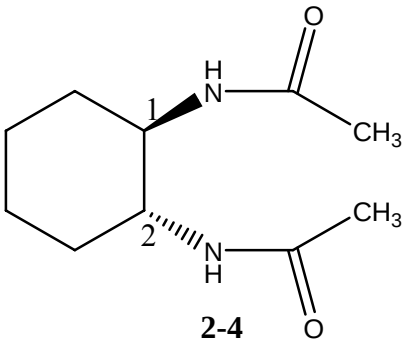


**Figure 2-5.** Structure of the diacetylated impurity **2-4**.

Furthermore, a peak found at m/z = 157 is consistent with the ($M+H^+$) fragment for the desired monoacetylated compound. Also, the $^{13}C$ JMOD NMR spectrum offered further evidence to support this conclusion. The asymmetrical monoacetylated product was expected to provide 8 signals (5 phased up and 3 down), whereas the $C_2$-symmetric diacetylated product would give rise to 5 signals (3 phased up and 2 down). Observation from the full JMOD spectrum provided 13 signals in total (8 phased up and 5 down), which is consistent with expected distribution pattern of a mixture of these two compounds.

Once the nature of the impurity was recognized, it was decided that separation of the desired monoacetylated product **2-3** from the diacetylated byproduct **2-4** might be accomplished by taking advantage of the basicity of the former compound. Thus, the mixture was treated with excess amount of commercial solution of 1.25 M HCl in ethanol followed by evaporation of solvent to provide a mixture of the diacetylated compound and the solid hydrochloride salt of the monoacetylated compound. The solid mixture was then triturated successfully with multiple portions of diethyl ether, acetonitrile and ethyl acetate, with the progress of the separation being monitored by NMR analysis of the solid residue. In the 500 MHz $^1H$ NMR spectrum of the solid hydrochloride salt of **2-3**, the $NH_3^+$ protons appear as a singlet at $\delta$ = 7.88 ppm partially overlapped with a one hydrogen doublet ($\delta$ = 7.93 ppm, $J$ = 8.5 Hz) corresponding to the amide proton of the protonated target molecule. The signal assignable to the amide NH of the impurity is at 7.55 ppm and the relative intensity suggests that the catalyst precursor contained approximately 15% of the impurity. This separation process reduced the quantity of the diacetylated byproduct sufficiently so that the material could be used at later stage in attempts at the catalytic asymmetric aldol condensation reaction between DHA and aromatic aldehydes.

The free base form of **2-3** was produced form the salt using sodium hydroxide solution. The use of this material in asymmetric aldol reactions is described later. While asymmetric aldol reaction were explored with this small amount of catalyst precursor, additional work was carried towards improving the preparation of the catalyst but using the much less expensive racemic form of *trans*-1,2-diaminocyclohexane. The primary concern was to work out the conditions that would avoid the formation of the diacetylated byproduct which was not obtained in the original literature report. Compared to the conditions used in the present study with those used in the original literature report, it was noted that our study employed 2.8 equivalents of preformed ethyl acetimidate salt with the diamine precursor; whereas the literature method involved generation of the acetimidate *in situ* from two equivalents of acetonitrile. Thus it was reasoned that in the previously reported method the formation of the acetimidate may have been incomplete when the reaction with the diamine was done, so that only approximately one equivalent of the acetimidate salt might have been present; whereas in our work, we employed two full equivalents of the preformed salt. With only one equivalent of acetimidate, the initial product cyclizes to the imidizolium salt that yields a monoacetylation product upon hydrolysis. In our work it appears that there is a considerable competition between cyclization of the initial product and reaction of the second amino group with a second molecule of the aceimidate, leading eventually to the substantial diacetylated byproduct **2-4** (Scheme 2-13).

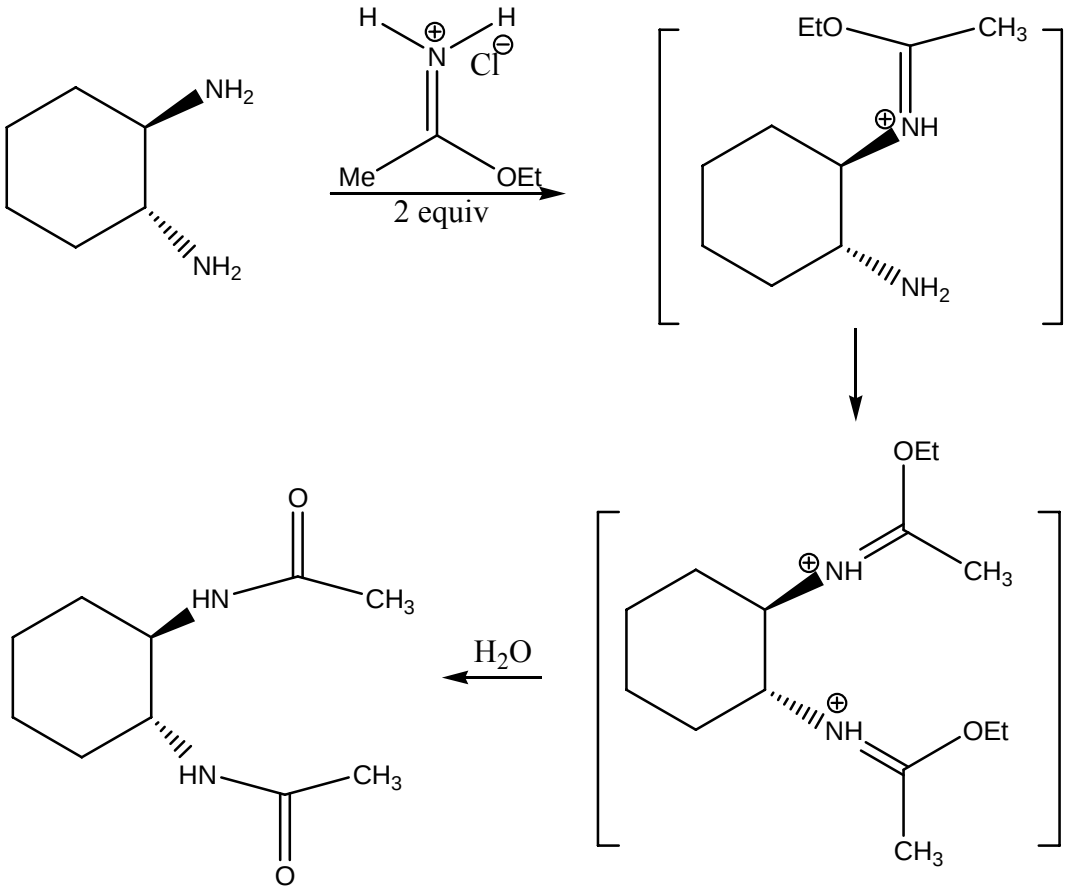


**Scheme 2-13**

With the racemic diamine, and with only one equivalent of the acetimidate salt, it proved to be possible to get a good yield of the monoacetylated diamine. The reductive amination of the free amino group in the monoacetylated diamine was found to proceed well in both the chiral system on a small scale, and in the racemic series on a substantially larger scale (Scheme 2-14). After hydrolysis of the amide, *N*,*N*-di-*n*-propyl-*trans*-1,2-diaminocyclohexane (**2-5**) was afforded that would be used in catalyst preparation. In the case of the racemic material, it was possible to obtain the product in a very high state of purity by vacuum distillation, which was not feasible in the enantio-pure series because of the small scale of that preparation. Comparison of the proton NMR spectrum of the highly purified racemic catalyst precursor with the published scanned

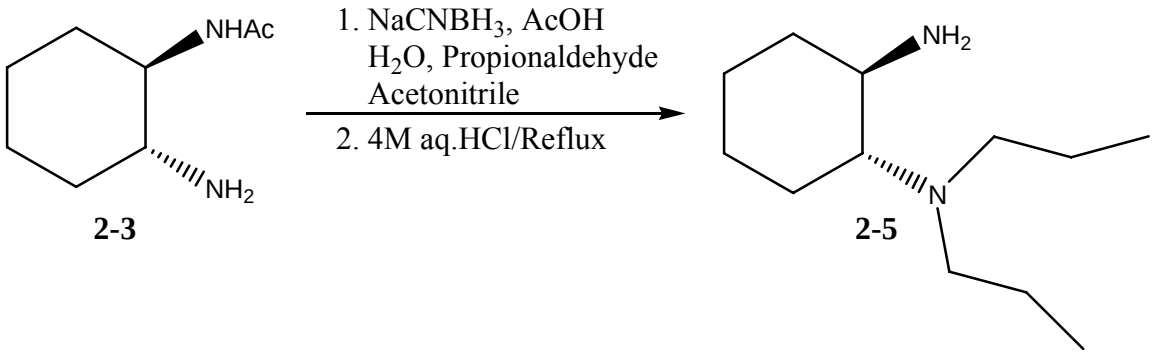


**Scheme 2-14**

spectrum of the same material as reported in the literature reveals that a number of the signals in the reported spectrum actually arise from impurities that were not identified nor even recognized as being present. The catalyst system is prepared by reaction of **2-5** with trifluoromethane sulfonic acid to form the triflate salt of this compound. The *N*-protonated system plays a key role in the asymmetric induction seen in the aldol condensation as described earlier.

Our first experiments with the catalyst system involved the chiral version of **2-5** which was produced only in very small amount, thus reactions were done on a relatively small scale. Since trifluoromethane sulfonic acid is moderately expensive and highly reactive and corrosive, we were reluctant to make the triflate salt of the small amount of the chiral catalyst. This is because it would lead to loss of much of the triflic acid once the seal on the glass ampule in which it is sold was broken since triflic acid reacts violently with even traces of moisture. Therefore, it was decided that the chiral material would be reacted instead with methane sulfonic acid which is much more readily handled. Thus a solution of the methane sulfonic acid salt of the chiral catalyst was generated and then used in preliminary attempts at the aldol condensation of DHA with *p*-nitrobenzaldehyde.

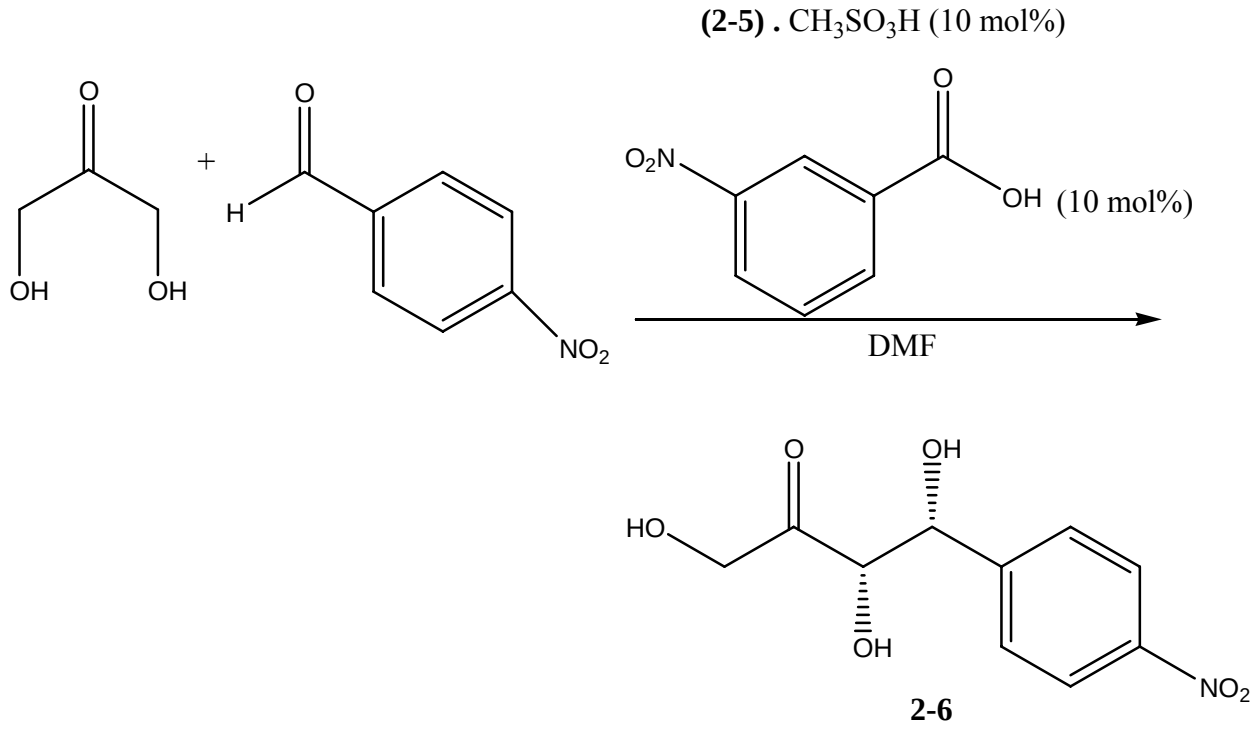


**Scheme 2-15**

Following the literature procedure (Scheme 2-15), except for use of the methane sulfonic acid salt (10 mol%) form of the catalyst rather that the triflic acid salt, including the use of *m*-nitrobenzoic acid as an additive, a crude DMF solution containing the product was obtained and which was passed through a silica gel column to remove much of the DMF and some unreacted starting materials. $^1$H NMR analysis of the product at this stage revealed the presence of the desired product as indicated by signals at $\delta$ = 5.22, 4.55 and 4.30 ppm as reported in the literature but also a comparable amount of unreacted *p*-nitrobenzaldehyde. A relatively pure sample of the target compound **2-6** was then obtained by trituration with dichloromethane which removed the unreacted aldehyde and residual DMF. The $^1$H NMR spectrum in methanol-$d_4$ solution of the purified product **2-6** showed the expected AA'BB' system (Figure 2-6) as an apparent set of two doublets and signals from the two C-H and the $CH_2$ group. The two C-H groups appear to be

mutually coupled but with a surprisingly small coupling constant of about 2 Hz. The $CH_2$ group appears, deceptively, to be a doublet with a coupling constant of 0.6 Hz. In reality it is likely that this signal corresponds to a collapsed AB system with very weak outer lines and the line separation indicated above is not actually a coupling constant. Also, an impurity that gives rise to a singlet at $\delta = 4.28$ ppm is also present, but the structure of the impurity is as yet unknown. In addition, the JMOD $^{13}C$ NMR spectrum of this material exhibited signals that were very similar to those reported by Luo *et al.* (*27*).

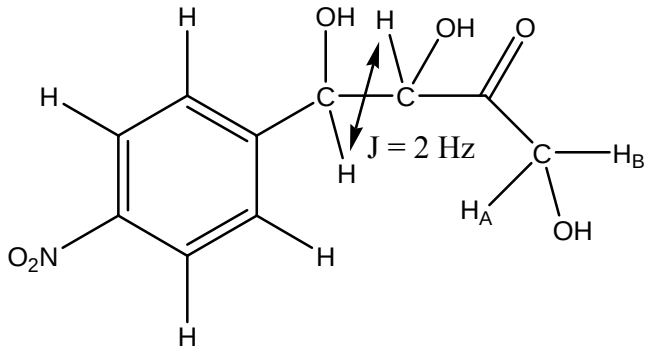


**Figure 2-6.** Schematic representation of the AA'BB' system of **2-6**.

This product **2-6** was available in sufficient amount to allow for just one attempt at the introduction of the phosphate group. Reaction of this compound with diphenyl chlorophosphate provided a crude product which appeared to contain only one phenyl group as indicated by the ratio of the intensity of signals from the phenyl group and those from the *p*-nitroaryl group. One possibility is that the initially formed phosphate derivative has undergone an intramolecular reaction to form a cyclic phosphate derivative **2-7** with the expulsion of a molecule of phenol (Scheme 2-16). If this is the case, then it is unlikely that this approach will allow us to prepare the desired monophosphate compound by this approach.

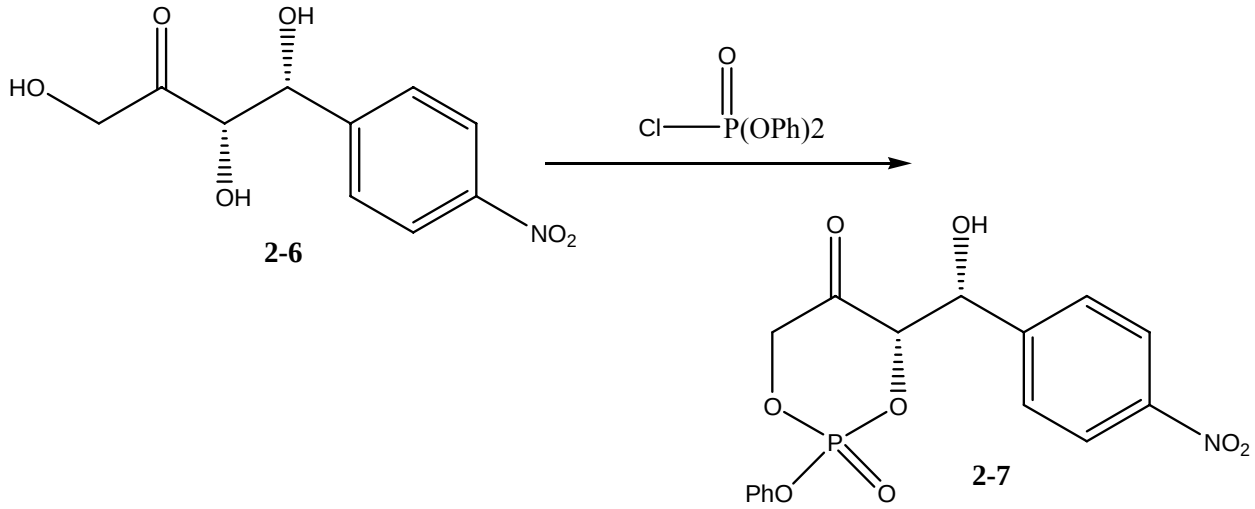


**Scheme 2-16**

In the racemic catalyst preparation, the amount of material which was prepared was large enough that it was reasonable to make the triflic acid salt form of the catalyst. Noticeably, the dispensing of the triflic acid was accompanied by extreme fuming, thus it is much less convenient than forming the methane sulfonic acid salt. Since there is no report of the spectroscopic characteristics of this triflic acid salt of the catalyst, the $^{1}H$ NMR spectrum is provided as an appendix for future reference.

## 2.8 Future work

Since a substantial quantity of the racemic form of the triflic acid salt of the catalyst is now available, it is recommended that this to be used to make the racemic version of the aldol adducts with a variety of aromatic aldehydes including 5-nitrofuraldehyde. Since the monophosphorylation strategy appears to be problematic, it is suggested that the introduction of a phosphate group onto **2-6** should be avoided and that the alcohol form of the aldol products be used in the presence of borate to form the boric acid adducts, as mimics of the phosphate *in situ* in the chromogenic assay mixture (Scheme 2-17). Additionally, it is suggested that the racemic aldol products to be evaluated in the assay and that the most promising one of these compounds would be then prepared in an optically pure form for further chromogenic studies.

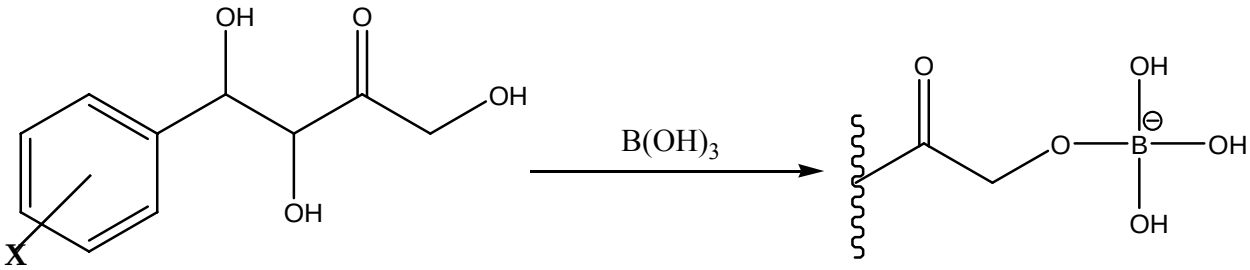


**Scheme 2-17**

## 2.9 Experimental

### General experimental

All the reagents used were purchased from Sigma-Aldrich or from Lancaster Synthesis unless otherwise stated. All reactions were performed either under an argon or nitrogen atmosphere and monitored by thin layer chromatography (TLC) using aluminum-backed sheets precoated with silica gel (0.2 mm) (EMD Chemical Inc.). TLC plates were analyzed by an ultraviolet lamp (254 nm). Anhydrous solvents were obtained from the Manual Solvent Purification System (M. Braun Inc.). Flash column chromatography was performed using silica gel (230-400 mesh). The UV-visible assay was performed with Cary 100 UV-visible spectrometer (Version 8.01, Varian). The low resolution electron impact (EI), chemical ionization (CI) and electrospray (ESI) mass spectra were obtained by Dr. Richard Smith at the University of Waterloo. $^{1}$H NMR and $^{13}$C NMR (J-MOD) spectra were obtained on a Bruker Avance-300 (300 MHz) or Avance-500 (500 MHz) NMR spectrometer with d-chloroform, $d_4$-methanol or $d_6$-dimethyl sulfoxide as the solvent.

### UV-visible spectrophotometric assay

Each of 5-nitro-furaldehyde (0.10 mmol) and 5-nitro-furfuryl alcohol (0.10 mmol) was dissolved in 0.10 mL of DMSO to make 1.0 M stock solution of the compound, respectively. To make one standard UV-visible assay mixture, 1.0 μL of the compound solution was transferred into 199 mL of DMSO to prepare a 1/200 diluted sample. Then 10 mL of the diluted sample was transferred as an aliquot into 990 mL of 50 mM prepared $KH_2PO_4$ buffer to make a 1 mL assay mixture with final concentration of 50 μM and 1% v/v DMSO. The 1 mL assay mixture was then completely transferred into a UV-compatible cuvette (VMR, 1 cm path length) and scanned with

Cary 100 spectrometer (Varian) from 600 nm down to 200 nm with a 1 nm interval at room temperature for each model compound.

***N*-((1*R*, 2*R*)-2-aminocyclohexyl)acetamide (2-3)**

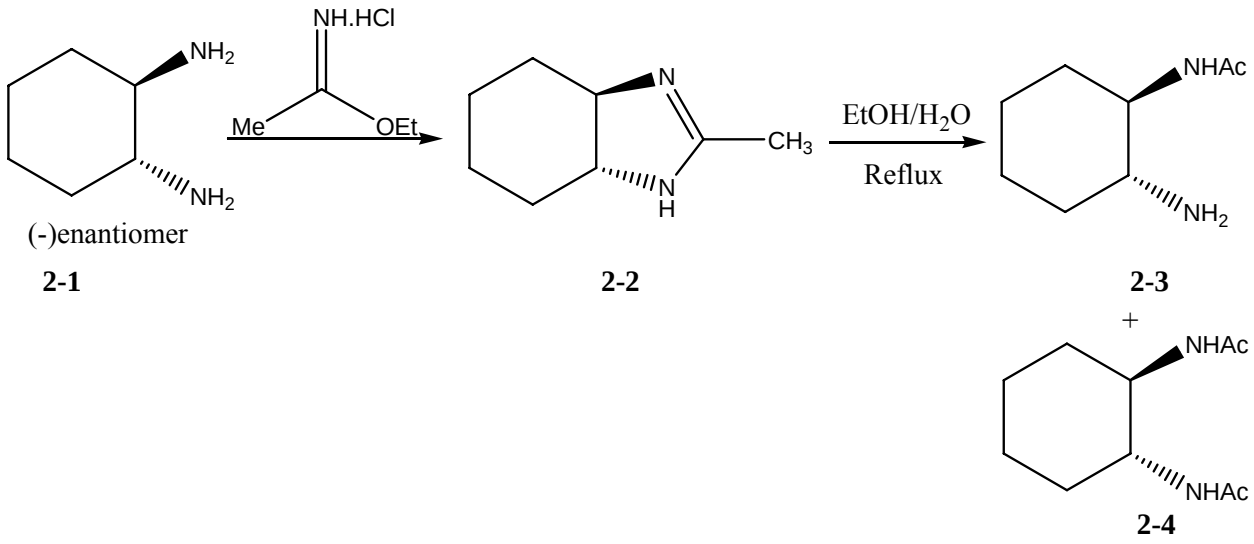


This experimental procedure was adapted from Mitchell and Finney (*34*). The reaction was first performed with optically active (-)-enantiomer of **2-1**. In a 25 mL round-bottomed flask, ethyl acetimidate hydrochloride (1.09 g, 8.81 mmol, 2.8 equiv) was dissolved in 5 mL of dry ethanol, and the reaction flask was then transferred to 0 °C bath under an $N_2$ atmosphere. Then the optical active enantiomer of **2-1** (0.35 g, 3.02 mmol, 1.0 equiv) was added to the flask and the reaction mixture was allowed to stir overnight at room temperature. The reaction mixture was then quenched with 40 mL of 1.0 M NaOH and extracted three times with 50 mL of 5% MeOH/$CH_2Cl_2$. The combined organic layers where dried over anhydrous $Na_2SO_4$ and concentrated in vacuo to afford 0.43 g of crude product **2-2**. The crude product was refluxed in 30 mL of ethanol/$H_2O$ (1:1 v/v) overnight, then concentrated to afford 0.24 g of crude product

containing both the monoacetylated (**2-3**) and diacetylated compounds (**2-4**). To separate **2-3** from **2-4**, a solution of 1.25 M anhydrous HCl/ethanol (1.2 mL, 1.25 equiv) was added to this crude product and it was allowed to stir for 30 minutes at room temperature to convert **2-3** to its salt. The solvent in the solution was blown off under $N_2$ to afford the solid and it was then triturated four times with 5.0 mL of diethyl ether, followed by 5.0 mL of acetonitrile, then three times with 5.0 mL of ethyl acetate to afford the salt of **2-3** (0.16 g). $^1$H NMR δ = 7.93 ppm (1H, d, *J*= 8.5 Hz, N**H**Ac), 7.88 (3H, s, N**H**$_3^+$), 3.60 (1H, m; C**H**NHAc), 2.77 (1H, m, C**H**NH$_3^+$) 1.95-1.98 (1H, m), 1,83 (3H, s, NHC(=O)C**H**$_3$), 1.5-1.7 (approx. 3H, m), 1.10-1.34 (approx. 4H, m). The spectrum also shows signals from the N, N'-diacetyl impurity (approx. 15%) δ = 7.51 (br s, N**H**Ac), 3.27 (m, C**H**NHAc), 1.72 (s, NHC(=O)C**H**$_3$). Then **2-3** was liberated from its salt by adding 40 mL of 1.0 M NaOH, followed by extracting three times with 20 mL of 5% MeOH/$CH_2Cl_2$. The organic layers were combined and dried over anhydrous $Na_2SO_4$ and concentrated in vacuo to afford relatively pure **2-3** (0.08 g). $^1$H NMR (300 MHz) δ = 6.14 (1H, br s, N**H**Ac), 3.49 (1H, br, C**H**NHAc), 2.40 (1H, br), 2.02 (3H, s, NHC**H**$_3$), 1.15-1.73 (approx. 8H, m). Signals from the N, N'-diacetylated product are also present (approx. 12%). $^{13}$C J-MOD δ = 170.3 (up), 56.0 (down), 55.2 (up), 53.6 (down), 35.3 (up), 25.0 (up), 23.4 (down). Signals from the N, N'-diacetylated impurity are also present at δ = 170.1 (up), 55.2 (down), 32.1 (up), 24.6 (up), 23.2 (down).

**(1*R*, 2*R*)-*N*, *N*-dipropylcyclohexane-1,2-diamine** (**2-5)**

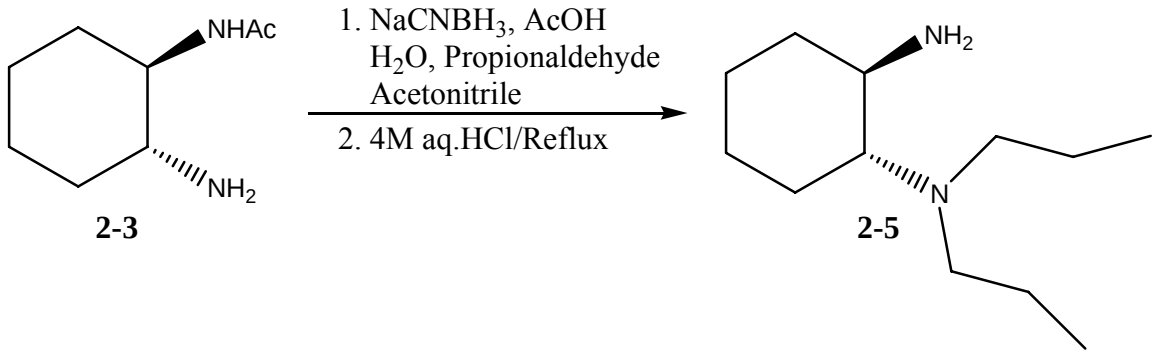


**2-3** **2-5**

This experimental procedure was adapted from Luo *et al. (26)*. In a 25 mL round-bottomed flask, **2-3 (**0.08 g, 0.46 mmol, 1.0 equiv) was dissolved with 5.0 mL of acetonitrile, followed by 0.2 mL of distilled water and 0.2 mL of propionaldehyde (2.28 mmol, 5.0 equiv) and stirred for 15 min under an $N_2$ atmosphere at room temperature. Then an aliquot of 1.0 M $NaCNBH_3$ solution in THF (0.96 mL, 0.96 mmol, 2.1 equiv) were delivered into the reaction mixture slowly via syringe and it was allowed to stir for 15 min under $N_2$ at room temperature. Then 0.2 mL of glacial acetic acid was added to the flask and the reaction was allowed to proceed for 2 hours under $N_2$ at room temperature. The volatiles were removed in vacuo and the crude product was taken up in 20 mL of ethyl acetate and 5.0 mL of 1.0 M NaOH, then washed three times with 5.0 mL of 1.0 M NaOH and 5.0 mL of brine. The organic layer was dried over anhydrous $Na_2SO_4$ and concentrated in vacuo. The crude product was then taken up in 15 mL of 4.0 M aqueous HCl and refluxed overnight under $N_2$. The reaction mixture was cooled to room temperature and the pH was adjusted to approximately 13 with 20 mL of 4.0 M NaOH. The aqueous solution was extracted three times with 40 mL of and $CH_2Cl_2$, dried over anhydrous $Na_2SO_4$ and concentrated in vacuo to afford 0.04 g of the crude product **2-5**. $^1$H NMR $\delta$ = 0.89 ppm (6H, t, $J$ = 7 Hz), 2.48-2.53 (1H, m), 2.25-2.45 (4H, m), 1.0-2.2 (complex overlapping multiplets).

**(3*S*, 4*R*)-1,3,4-trihydroxy-4-(4-nitrophenyl)butan-2-one (2-6)**

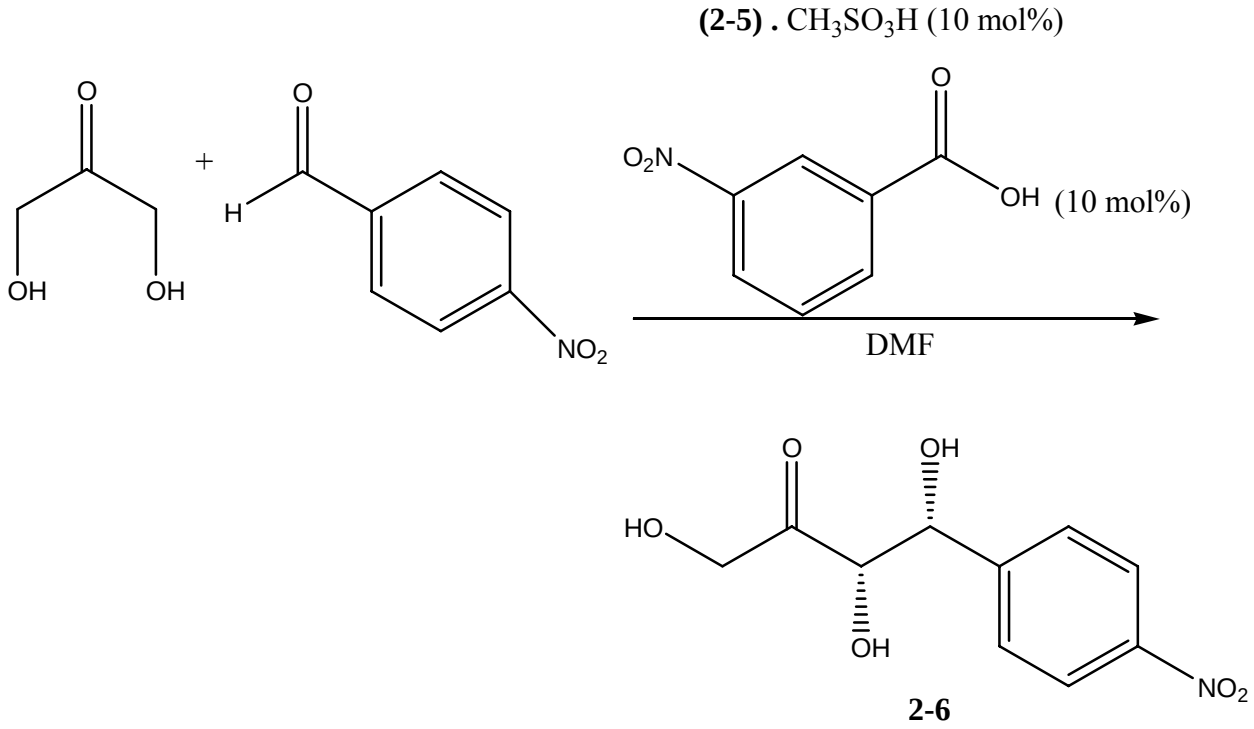


**2-6**

This experimental procedure was adapted from Luo *et al*. (*27*). To make the catalyst stock solution (0.036 M), **2-5** (0.38 g, 0.19 mmol, 1.0 equiv) was dissolved with 2.0 mL of HPLC grade $CH_2Cl_2$ and transferred to a 5.0 mL volumetric flask. Due to the small scale of this reaction and the hygroscopic nature of trifluoromethanesulfonic acid, methanesulfonic acid (0.012 mL, 0.18 mmol, 1.0 equiv) was used instead and transferred to the flask via a 100 mL-syringe. Then HPLC grade $CH_2Cl_2$ was added to fill up the rest volume and the solution was gently mixed. Then an aliquot of solution from the catalyst stock (1.2 mL, 0.043 mmol, 10 mol%) was transferred to a 5 mL round-bottomed flask and the catalyst was concentrated by blowing off the solvent under $N_2$. DMF (400 mL) was added to the reaction flask followed by *m*-nitrobenzoic acid (8.0 mg, 0.043 mmol, 10 mol%), dihydroxyacetone (0.041 g, 0.23 mmol, 1.0 equiv, added as dimer) and 4-nitrobenzaldehyde (0.070 g, 0.46 mmol, 1.0 equiv). The reaction mixture was allowed to stir overnight under $N_2$ at room temperature. The reaction was monitored by TLC

with isopropanol/hexane (3:7) and the spots of starting material were observed. The crude product was just then purified by silica gel flash chromatography using the same solvent system as TLC and the fractions containing the desired product were combined, dried over anhydrous $Na_2SO_4$ and concentrated in vacuo to afford 0.012 g of the product. Results from $^1H$ NMR indicated the presence of residual DMF in the product. Three portions of ethyl acetate (2.0 mL) were used to triturate the product and 0.010 g of the product **2-6** containing minor impurities were afforded. $^1H$ NMR (methanol-$d_4$) $\delta$ = 8.19 (2H) and 7.69 ppm (AA'XX', apparent doublets), 5.22 (1H, d, $J$ = 2 Hz), 4.55 (2H, likely collapsed AB system), 4.34 (1H, d, $J$ = 2 Hz). $^{13}C$ NMR J-MOD $\delta$ = 212.8 (up), 151.1 (up), 149.0 (up), 129.0 (down), 128.7 (up), 80.9 (down), 74.9 (down), 68.5 (up).

To examine the influence of the total amount of catalyst present in the reaction, 20 mol% injection and two times longer reaction time was used to repeat this reaction. An aliquot of solution from the catalyst stock (1.5 mL, 0.054 mmol, 20 mol%) was transferred to a 5 mL round-bottomed flask. The catalyst was concentrated by blowing off the solvent under $N_2$. DMF (400 mL) was added to the reaction flask followed by *m*-nitrobenzoic acid (9.0 mg, 0.054 mmol, 20 mol%), dihydroxyacetone (0.024 g, 0.14 mmol, 1.0 equiv, added as dimer) and 4-nitrobenzaldehyde (0.041g, 0.27 mmol, 1.0 equiv). The reaction mixture was allowed to stir overnight under $N_2$ at room temperature. The reaction was monitored by TLC with isopropanol/hexane (3:7) and the spots of starting material were observed. Results from $^1H$ NMR did not indicate any significant improvement compared to the first trial of this reaction. The crude product was thus not purified further.

**Attempted Phosphorylation**

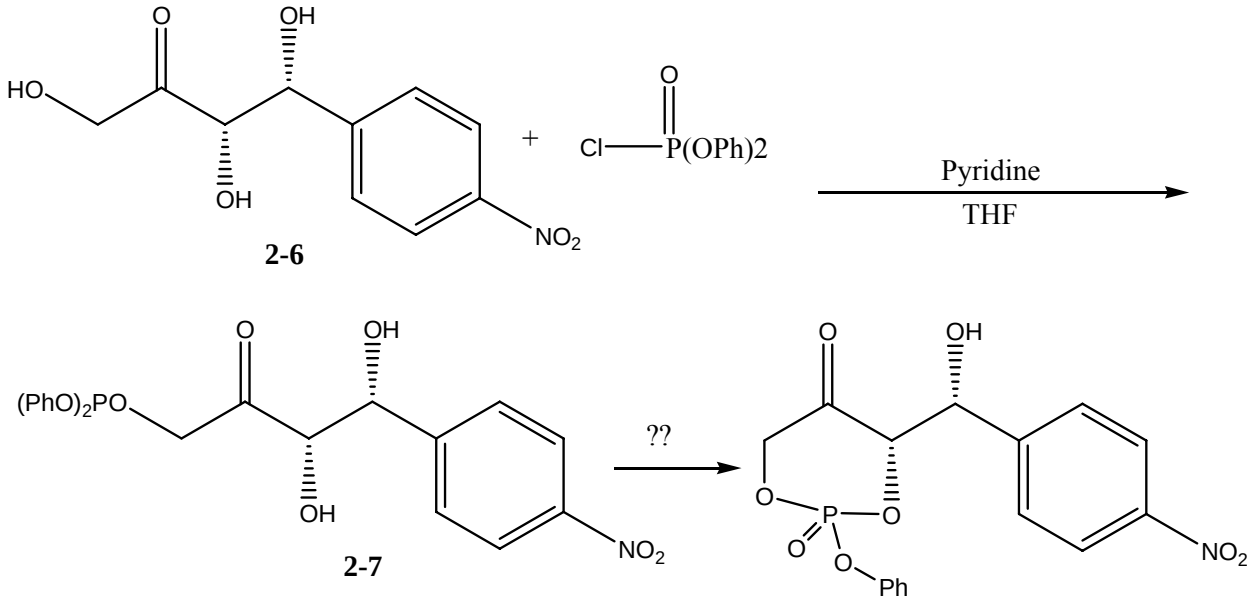


This experimental procedure was adapted from Ma *et al.* (*30*). To make a 2.0 mL of the stock solution of the starting materials diphenylchlorophosphate (0.42 M), 0.17 mL of this compound (0.22 g, 0.84 mmol) was diluted in 1.83 mL of THF. To make a 5.0 mL of the stock solution of pyridine (0.63 M), 0.26 mL of pyridine (0.25g, 3.16 mmol) was diluted in 4.74 mL of THF. In a 10 mL round-bottomed flask, 600 mL of dry THF was added to dissolve **2-6** (0.01 g, 0.042 mmol, 1.0 equiv). An aliquot from the stock solution of pyridine (100 mL, 0.063 mmol, 1.5 equiv) was then transferred to the flask and the reaction mixture was brought down to −5 °C by using ice/salt bath. Then an aliquot from the stock solution of diphenylchlorophosphate (100 mL, 0.042 mmol, 1 equiv) was added slowly to the flask and the reaction mixture was then brought up to room temperature. The reaction was then allowed to stir overnight under $N_2$ at room temperature. The reaction was monitored by TLC (69% hexane, 30% isopropanol, 1% acetic acid) and then 2 mL of distilled water and 5 mL of ethyl acetate was added to the reaction mixture. The aqueous

layer was separated and washed twice with 5 mL of ethyl acetate. The organic layers were combined, and washed with 5mL 1.0 M HCl, 5 mL saturated $NaHCO_3$ and 5 mL $H_2O$ in sequence, then dried over anhydrous $Na_2SO_4$ and concentrated in vacuo to afford the crude product (0.088g). The crude was then purified by silica gel flash column chromatography with a solvent system of hexane/ethyl acetate (4:1) and the fractions containing the desired product were combined, dried over anhydrous $Na_2SO_4$ and concentrated in vacuo to afford 0.048 g of the product with impurities. $^1$H NMR (methanol-$d_4$) δ = 8.2 (2H) and 7.71 ppm (AA'XX', apparent doublets), 7.24-7.30 (4H, m), 7.05 (1H, t, *J* = 7.2 Hz), 5.23 (1H, d, 2 Hz), 4.56 (2H, s), 4.37 (1H, d, *J* = 2 Hz).

**Racemic *trans*-2-aminocyclohexylacetamide**

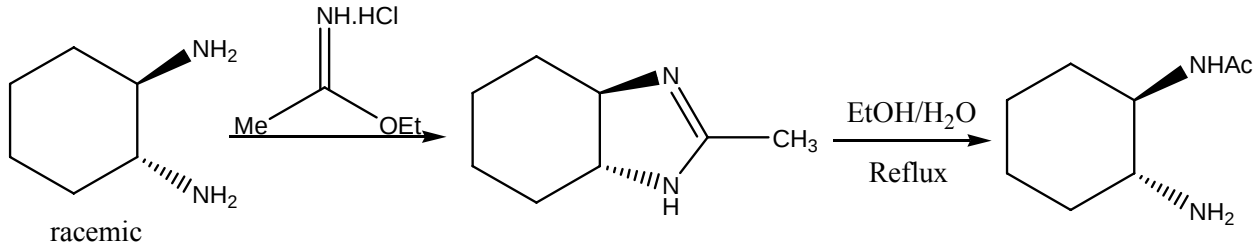


This experimental procedure was adapted from Mitchell and Finney (*34*). This reaction was repeated in a large scale with a racemic mixture of *trans*-1,2-diaminocyclohexane. In a 100 mL round-bottomed flask, ethyl acetimidate hydrochloride (8.75g, 0.071 mol, 1.0 equiv) was dissolved in 90 mL of ethanol at room temperature, and the reaction flask was then transferred to 0 °C bath under an $N_2$ atmosphere. Via syringe, an aliquot of *trans*-1,2-diaminocyclohexane (8.50 mL, 0.071 mol, 1.0 equiv, racemic mixture) was added to the reaction flask and it was then brought up to room temperature. The reaction was allowed to proceed overnight, and was then

quenched with 150 mL of 1.0 M NaOH. The solution was then extracted three times with 100 mL of 5% MeOH/$CH_2Cl_2$, and the organic layers were combined, dried over $Na_2SO_4$ and concentrated in vacuo to afford 9.99 g of crude product. The crude product was then dissolved in 260 mL of ethanol/$H_2O$ (1:1 v/v) and refluxed overnight. The reaction solution was then concentrated, dried over anhydrous $Na_2SO_4$ and concentrated again in vacuo to afford the crude product (10.5 g). The crude product was checked against the starting material on TLC (85% MeOH, 14% $CH_2Cl_2$ and 1% $NH_4OH$ v/v/v) and residual starting material was still observed. Then 9.29 g of the crude product was purified though silica gel flash column chromatography with the same solvent system as used in TLC. The combined fractions containing the desired compound were then concentrated in vacuo to afford 7.58 g of the product (racemic mixture) with an overall yield of 68.3%.

**Racemic *N, N*-dipropylcyclohexane-1,2-diamine**

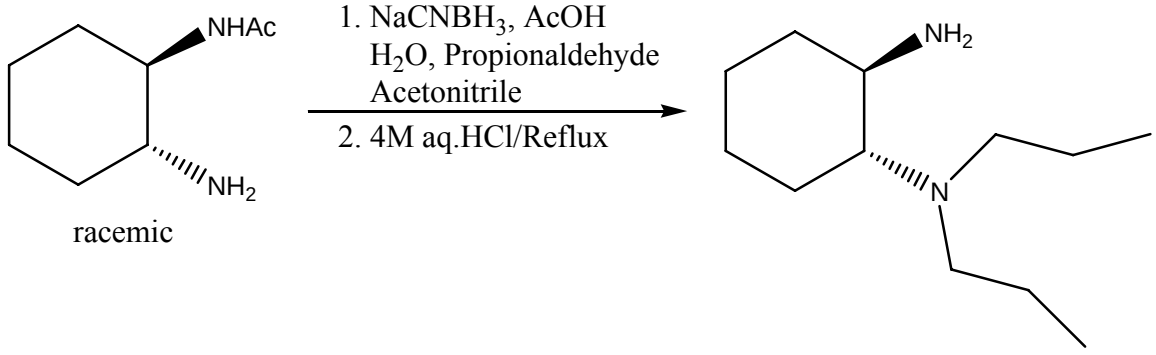


This experimental procedure was adapted from Luo *et al. (26)*. The large scale reaction was continued from the racemic mixture of *trans*-2-aminocyclohexylacetamide. In a 250 mL round-bottomed flask, the racemic mixture of *trans*-2-aminocyclohexylacetamide (7.47 g, 0.048 mol, 1.0 equiv) was dissolved in100 mL of acetonitrile, followed by addition of 13 mL of distilled

$H_2O$. Then propionaldehyde (17.2 mL, 0.24 mol, 5.0 equiv) was delivered into the reaction flask via syringe and the mixture was allowed to stir for 20 min at room temperature under an $N_2$ atmosphere. Then a solution of 1.0 M $NaCNBH_3$ in THF (96 mL, 0.096 mol, 2.0 equiv) was transferred into the flask via syringe and the mixture was stirred for 20 min at room temperature under $N_2$. At this stage, 15 mL of glacial acetic acid was added to the flask and the mixture was stirred for 2 hours at room temperature under $N_2$ atmosphere. The solvents were then removed in vacuo and the reaction mixture was taken up in 200 mL of ethyl acetate and washed three times with 100 mL of 1 M NaOH and 100 mL of brine. The organic layer was dried over anhydrous $Na_2SO_4$ and concentrated in vacuo. The crude mixture was taken up in 200 mL of 4.0 M aqueous HCl and refluxed overnight under an $N_2$ atmosphere. The reaction mixture was cooled to room temperature and then the pH of the solution was adjusted to approximately 13 using 250 mL of 4.0 M NaOH. The aqueous layer was then extracted three times with 200 mL of $CH_2Cl_2$ and the organic layers were combined, dried over anhydrous $Na_2SO_4$ and concentrated in vacuo to afford 8.14 g of crude product. The crude product was purified by vacuum distillation (boiling point is 75–77 °C at 0.5 torr) and two fractions were collected. The second fraction was found to contain impurities by $^1H$ NMR and only the first fraction was saved and identified to contain 4.61 g of the pure product. The proton and carbon NMR spectra agreed very well with the data provided in the literature. EI-MS m/z = 198.25 ($M^+$), 169.22, 140.18, 114.16, 98.14.

**Stock solution of the triflate salt of racemic *N*, *N*-dipropylcyclohexane-1,2-diamine**

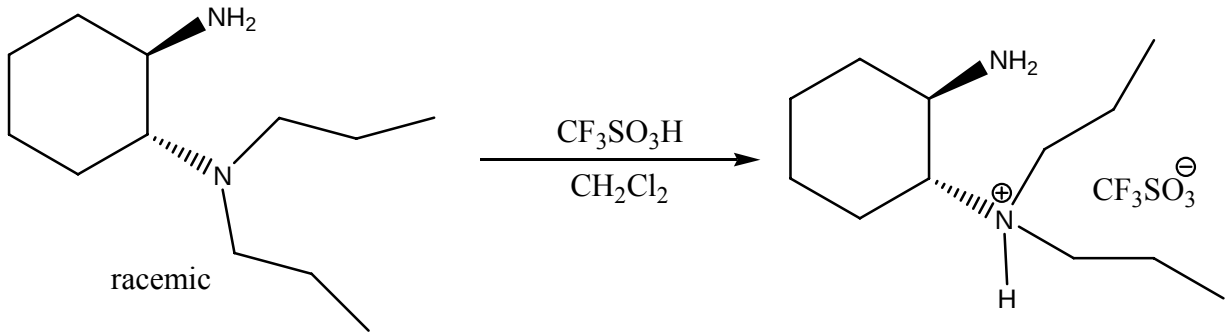


The racemic mixture of *N*, *N*-dipropylcyclohexane-1,2-diamine (4.43 g, 0.022 mol, 1 equiv) was diluted with 5.0 mL of dry $CH_2Cl_2$ in a 10 mL volumetric flask under an $N_2$ atmosphere. The glass ampule containing triflic acid was opened carefully under an $N_2$ bath where the $N_2$ was blowing from an inverted glass funnel. Then the triflic acid (1.97 mL, 0.022 mol, 1 equiv) was carefully transferred from the ampule to the flask very slowly via syringe. Then dry $CH_2Cl_2$ was added to the flask to fill up the volume under $N_2$ and the solution was carefully mixed to afford the stock solution of the triflate salt of racemic *N*, *N*-dipropylcyclohexane-1,2-diamine (0.89 M).

# Chapter 3

# Development of novel inhibitors of Class II FBP aldolases

## 3.1 Introduction

Class II FBP aldolases have been proposed to be potential drug targets since they are not present in higher organisms such as animals and plants (*1, 2*). Ideally, selective inhibition of microbial Class II FBP aldolases would affect a major metabolic pathway of pathogens by disrupting glycolysis, thereby hindering their survival and persistence within the host. To date, there are only limited numbers of publications associated with the development of Class II FBP aldolase inhibitors (*1, 3-5*), and the inhibitors have largely been found to be either non-selective or of low potency. Our research group is interested in developing a selective and more effective inhibitor towards Class II FBP aldolases, and has already obtained some preliminary results. This chapter of the thesis focuses on the design and synthesis of small compounds which will be tested against Class II FBP aldolases. Furthermore, Class II FBP aldolases belong to the zinc protease family by possessing a catalytic zinc ion in the enzyme active sites. Numerous zinc protease inhibitor designing strategies have been described and they are quite valuable to this project, which will be surveyed in the next section.

### 3.2 Strategies for the design of zinc protease inhibitors

Zinc proteases such as the angiotensin converting enzymes and the matrix metalloproteases (MMP) are part of a major family of enzymes characterized by having a catalytically essential zinc ion at their active sites (*6, 7*). Among all the zinc proteases, carboxypeptidase A (CPA) is the most extensively investigated enzyme. CPA has been used as a model for developing inhibitor design strategies which can be applied to other enzymes such as MMPs (*6-8*).

MMPs are important endopeptidases functioning in tissue remodelling, organ development, ovulation, embryogenesis and angiogenesis, and in addition, are implicated in numerous pathological conditions including cancer growth, tumor angiogenesis, arthritis, cardiovascular and autoimmune diseases. Therefore, due to the significant association between the pathological conditions with the disregulation of MMP activity, inhibitors targeting this type of enzyme have drawn great attention for drug development (*7, 9, 10*).

Notably, almost all the zinc protease inhibitors are designed with at least 2 pharmacophores, a zinc binding group (ZBG) and a peptide-like group. The ZBG will coordinate with the zinc atom and the peptide-like group is able to fit into one or more substrate recognition sites (*11*). Generally, ZBGs are metal-binding groups such as hydroxamate, carboxylates, thiols, or sulfamides, which are capable of binding to the zinc ion in the enzyme active site. The hydroxamate ZBG is thought to be the most common and powerful one due to its strong metal binding ability (*11, 12*). Giavazzi and Taraboletti (*13*) discussed the extensive application of hydroxamate-based inhibitors of MMPs in different clinical trials as potential cancer therapies. Although such compounds are effective, most of the candidates failed due to observed adverse

effects or major toxicity that emerged at high doses. As a result of the undesirable side effects and the high non-specific transition-metal binding ability, the hydroxamate-based inhibitors are no longer being used; while other types of inhibitors with ZBGs such as carboxylate, phosphonate, and thiol groups are sought instead. Nonetheless, a loss of activity when compared to the hydroxamate counterpart due to the structural change was observed (*11*). Moreover, sulfamide-based and sulfamide-derivative inhibitors were synthesized as transition state analogues and proved to be effective novel inhibitors of CPA (*6, 8*). Lee and Kim (*7*) also found that thiol groups form stronger coordination with the active site zinc ion than carboxylate groups when they evaluated a mono-thiol substituted compound instead of a dicarboxylate substituted compound against CPA.

Importantly, inhibitor design should not only be focused on the specificity of the ZBGs, but also on the other core peptide-like structure which is capable of interacting with the specific binding pocket of the enzyme active site. Generally, inhibitor discovery can be accomplished through natural product screening, substrate-derived analogue-based drug design, mechanism-based drug design, with incorporation of computer-based design or a combination of them all (*14*).

### 3.3 Existing Class II FBP aldolase inhibitors

The inhibitor design strategies from the previous work on the zinc proteases directed us on the design of inhibitor for Class II FBP aldolase, since the enzyme also requires an essential divalent metal to participate in catalysis. In the case of *E. coli* and *M. tuberculosis,* a zinc ion is found in the enzyme active site (*15, 16*). Surprisingly, while numerous inhibitors of Class I FBP aldolase have been synthesized and tested (*17*), only a few inhibitors of Class II FBP aldolase have been reported. The first potent inhibitor was synthesized and reported by Lewis and Lowe (*1*). Phosphoglycolohydroxamic acid (PGH), a remarkable competitive inhibitor of yeast class II FBP aldolase with a $K_i$ of 0.01 μM, is less active while still potent towards rabbit muscle Class I FBP aldolase with a $K_i$ of 1 μM. The selectivity of PGH for Class II FBP aldolases is determined to be 100 by comparing the $K_i$ values (*18*). The reported crystal structure of *E. coli* Class II FBP aldolase by Hall *et al.* in the presence of PGH revealed that this compound is not only a powerful zinc chelator, but also a stable analogue of the enediolate intermediate (as the T.S.I. in Figure 3-1) (*19*). However, the high potency of PGH towards Class I FBP aldolase prevents its application as a drug. Recently, based on the phosphoglycolate skeleton of PGH, Fonvielle *et al.* (*3*) synthesized two PGH derivatives (Figure 3-2) in which the hydroxamate was replaced either by an amidoxime or by a hydrazide moiety instead of the hydroxamate, and found these inhibitors to be more selective towards yeast Class II FBP aldolases, although less potent than PGH ($K_i$ of PGA is 2.3 μM and $K_i$ of PGHz is 0.34 μM). Based on these results, Gavalda *et al.* (*4*) prepared a new family of inhibitors possessing the phosphoglycolate skeleton bound to a sulfamate group (Figure 3-2). They suggested that compounds with an NH moiety between the carbonyl and sulfonyl groups are very acidic; thus the negative charge at this position of PGS would improve the interaction with the active site zinc ion.

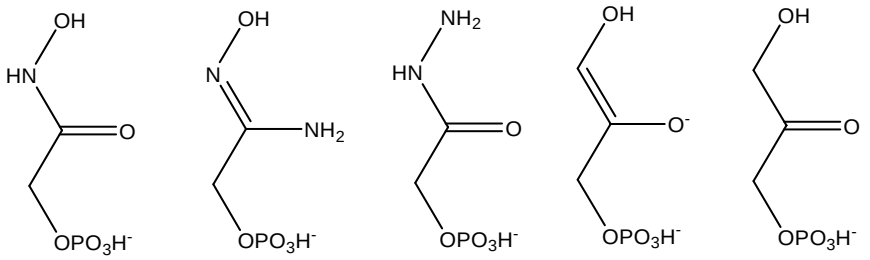


**Figure 3-1.** Structures of PGH and its derivatives. The compounds in the figure are PGA (amidoxime), PGHz (hydrazide), T.S.I. (Transition state intermediate formed by protonation of DHAP) and DHAP (*3*).

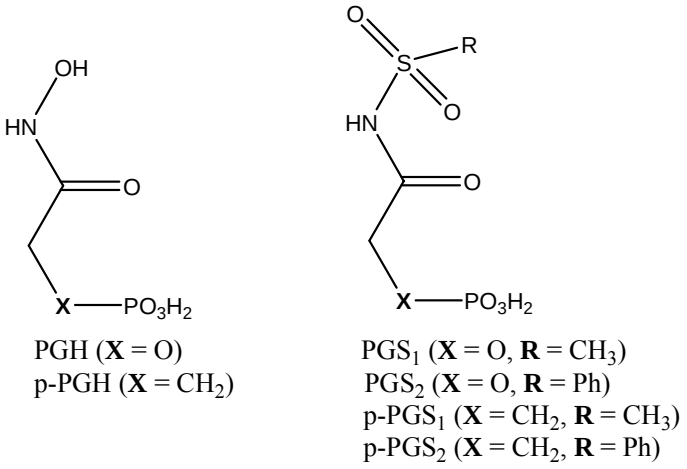


**Figure 3-2.** Structures of PGH, phosphoglycolosulfamate (PGS) and their phosphonate derivatives (*4*).

In addition, $PGS_1$ and $PGS_2$ were both found to be competitive inhibitors of *E. coli* Class II FBP aldolase ($K_i$ values are 350 and 100 μM, respectively), indicating the active site binding affinity is dependent on the chemical group bound to the sulfamate moiety. Nevertheless, the structural modification of converting phosphate into phosphonate weakened the inhibitor binding significantly ($K_i$ values are greater than 10 mM for p-$PGS_1$ and p-$PGS_2$); the phosphonate derivatives were designed due to their exceptional stability towards phosphatases compared to

the phosphates under physiological conditions. From these results it was deduced that the ester oxygen of the phosphate moiety is critical for the inhibitor binding and stable interaction with the enzyme active site (*4*).

Preliminary results from our research group obtained by the screening of metal binding agents revealed that dipicolinic acid (DPA) (Figure 3-3) was a moderately effective inhibitor towards

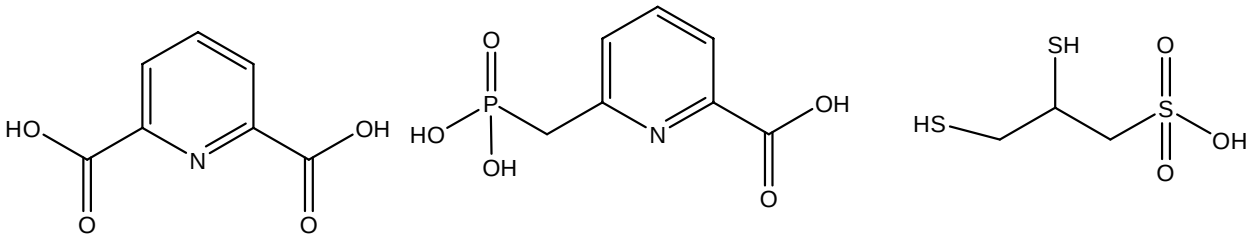


DPA MS191 DMPS

**Figure 3-3.** Structures of DPA and its derivatives MS 191, and commercial antidote for heavy metal poisoning 2,3-dimercapto-1-propanesulfonic acid (DMPS).

Class II FBP aldolases ($IC_{50}$ = 40 μM for *M. tuberculosis* and $IC_{50}$ = 75 μM for *P. aeruginosa*), whereas no measurable inhibitory activity towards Class I FBP aldolase from rabbit muscle was observed (Geneviève Labbé, unpublished results). Although DPA is a well known metal chelating agent, kinetic studies of DPA as an inhibitor of yeast Class II FBP aldolase are consistent with active site binding without metal ion removal. Molecular modelling led M.D.R. Brown in our group to construct a phosphonate DPA derivative (MS191) (Figure 3-3) and it was found to be a good inhibitor with an $IC_{50}$ of 90 μM towards yeast Class II FBP aldolase while not inhibiting the Class I counterpart. In order to screen for a better inhibitor, compounds with modifications on the pyridine ring were prepared by Timothy Rasmusson and Dr. Muhong Shang

to introduce appropriate functional groups. Unfortunately, none was found as effective as DPA or MS 191. Furthermore, in our recent studies, a commercial antidote for heavy metal poisoning, 2,3-dimercapto-1-propanesulfonic acid (DMPS) (Figure 3-3) was found to be a good inhibitor with an $IC_{50}$ of 5 μM for *M. tuberculosis* enzyme and $IC_{50}$ of 40 μM for *M. grisea* enzyme. Meanwhile, no inhibitory activity was observed toward Class I FBP aldolase from rabbit muscle, and the inhibition was shown to be reversible without metal ion removal. Moreover, DMPS had been previously found in our group to be a moderately effective inhibitor of metallo-β-lactamases by Siemann *et al. (20)*.

### 3.4 Development of novel Class II FBP aldolase inhibitors

The observation that DMPS is not inhibitory towards the Class I FBP aldolase from rabbit muscle indicates that rationally designed structural variants of DMPS may exhibit selectivity and specificity towards Class II FBP aldolases. Furthermore, the failure of this compound to inhibit Class I FBP aldolase also proved DMPS is not inhibitory towards triose phosphate isomerase (TIM), an essential mammalian enzyme as well as an integral part of the coupled-enzyme assay which is used to evaluate the inhibitory activity of compounds towards the Class II enzymes as discussed in chapter 2. Interestingly, one drawback of the aforementioned powerful inhibitor PGH is that it inhibits both Class I FBP aldolases and TIM significantly (*18*).

A molecular modeling study was recently performed by T. Ramadhar and G. Labbé involving the docking of a model of DMPS into the x-ray crystal structure of *E. coli* Class II FBP aldolase (PDB code 1B57) followed by energy minimization. The study revealed that this compound should be capable of binding to the active site of Class II FBP aldolases. However, when the sulfonate moiety is located in the phosphate binding pocket, only the terminal SH group can coordinate with the zinc ion in the active site whereas the secondary SH group is too far from the zinc ion to allow strong interaction (Figure 3-4). The number of atoms separating the sulfonate group and the zinc binding thiols in DMPS are different by one to the phosphate group and the zinc binding hydroxyl oxygen in PGH. We then proposed a new compound, 1,1-difluoro-3,4-dimercaptobutylphosphonic acid (**3-2** in Figure 3-5) which contains an extended carbon skeleton with a phosphonate group instead of a sulfonate group based on the structure of DMPS (**3-1** in Figure 3-5) and the enediolate intermediate. This compound is expected to be a somewhat better inhibitor since the spatial relationship between the thiol groups

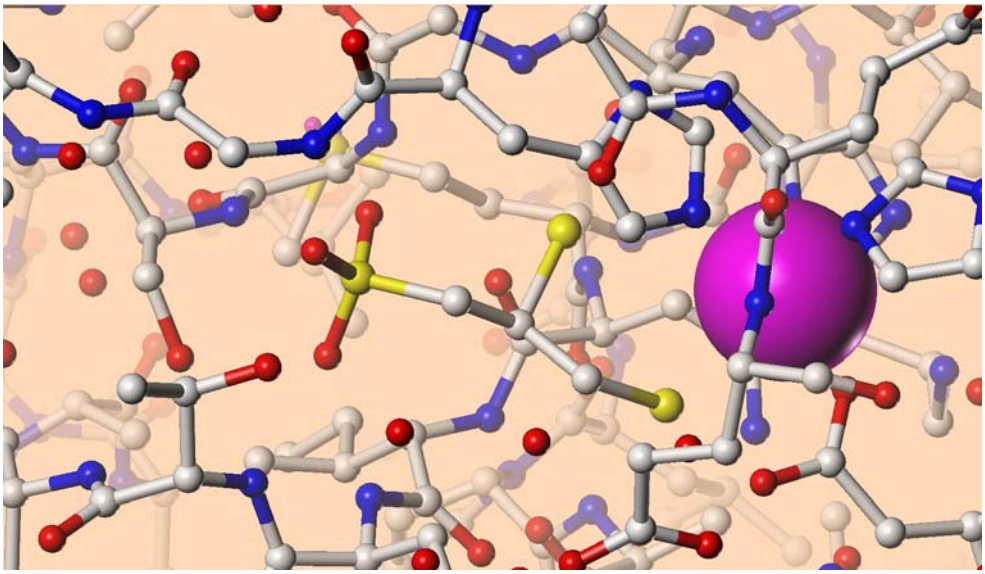

**Figure 3-4.** Docking of a model of DMPS into the substrate binding site of *E. coli* Class II FBP aldolase. The crystal structure was adapted from PDB 1B57. In the figure, the atoms are zinc (magenta), sulphur (yellow), carbon (white), oxygen (red), nitrogen (blue), respectively.

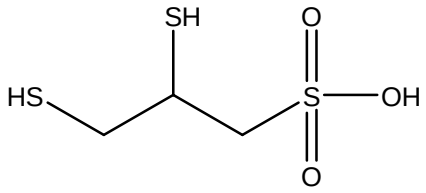


**3-1**

2,3-dimercaptopropane-1-sulfonic acid
(DMPS)

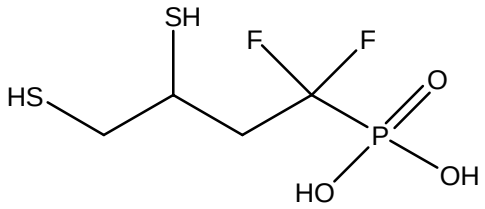


**3-2**

1,1-difluoro-3,4-dimercaptobutylphosphonic acid

**Figure 3-5.** Structures of 2,3-dimercaptopropane-1-sulfonic acid (DMPS) and the proposed compound 1,1-difluoro-3,4-dimercaptobutylphosphonic acid.

and the phosphonate groups might allow for a better interaction of both thiol groups with the active site zinc ion than appeared to be the case in modelling studies with DMPS. In the structure **3-2** in Figure 3-5, the two fluorine atoms are expected to allow for favourable H-bonding interactions with the functional groups in the active site which normally H-bond to the phosphate oxygen atom attached to C-1 of DHAP.

The proposal of compound **3-2** was then further supported by the molecular modeling studies performed by T. Ramadhar and G. Labbé (Figure 3-6). They docked the model of compound **3-2** into the *E. coli* Class II FBP aldolase (PDB code 1B57) active site, and a comparison was done between this model and the previous DMPS model. The result reveals that the extension of the

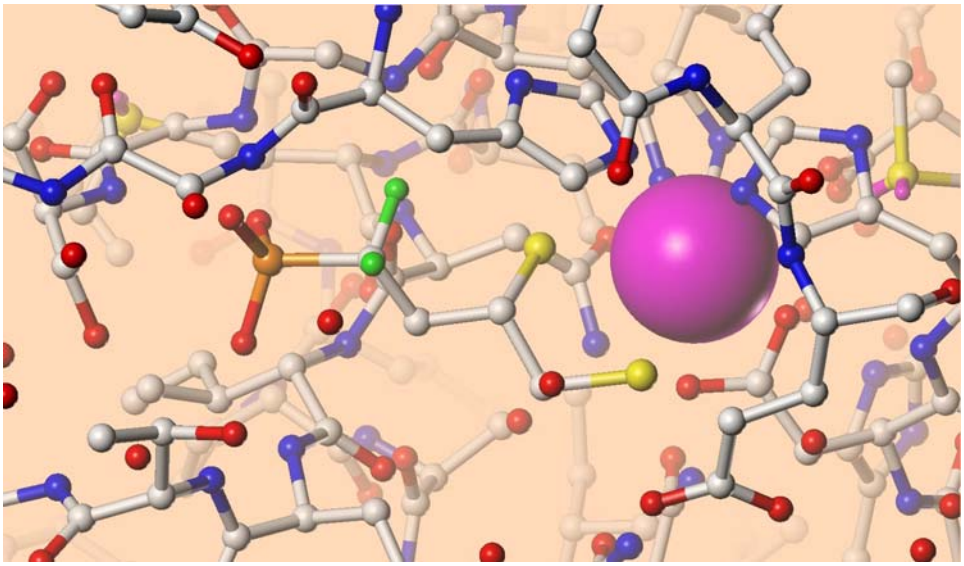

**Figure 3-6.** Docking of a model of 1,1-difluoro-3,4-dimercaptobutylphosphonic acid into the substrate binding site of *E. coli* Class II FBP aldolase. The modeling was done with SYBYL 7.3 (Tripos) using the MMFF94 force field and the Anneal function. The crystal structure of the *E. coli* Class II FBP aldolase is adapted from PDB 1B57. In the figure, the atoms are zinc (magenta), sulphur (yellow), phosphorus (brown), carbon (white), oxygen (red), nitrogen (blue), respectively.

carbon skeleton by one methylene group of DMPS allows the secondary thiol group in compound **3-2** to bind to the zinc ion with a stronger interaction. The terminal thiol and the secondary thiol groups were found to be 3.35 Å and 2.82 Å from the zinc ion, respectively, suggesting a strong interaction among them. The *pro-R* fluorine was found to be 2.78 Å from a water molecule which is H-bonding with Thr-289 and Glu-182 and in van der Waals interaction with the imidazole ring of His-226. Furthermore, the *pro-S* fluorine was found to be in van der Waals interaction with the amide nitrogen which is between His-264 and Gly-265. Therefore, the goal of the present study was the synthesis of compound **3-2** as a potential inhibitor for Class II FBP aldolases. A reasoned retrosynthetic analysis is provided below (Scheme 3-1).

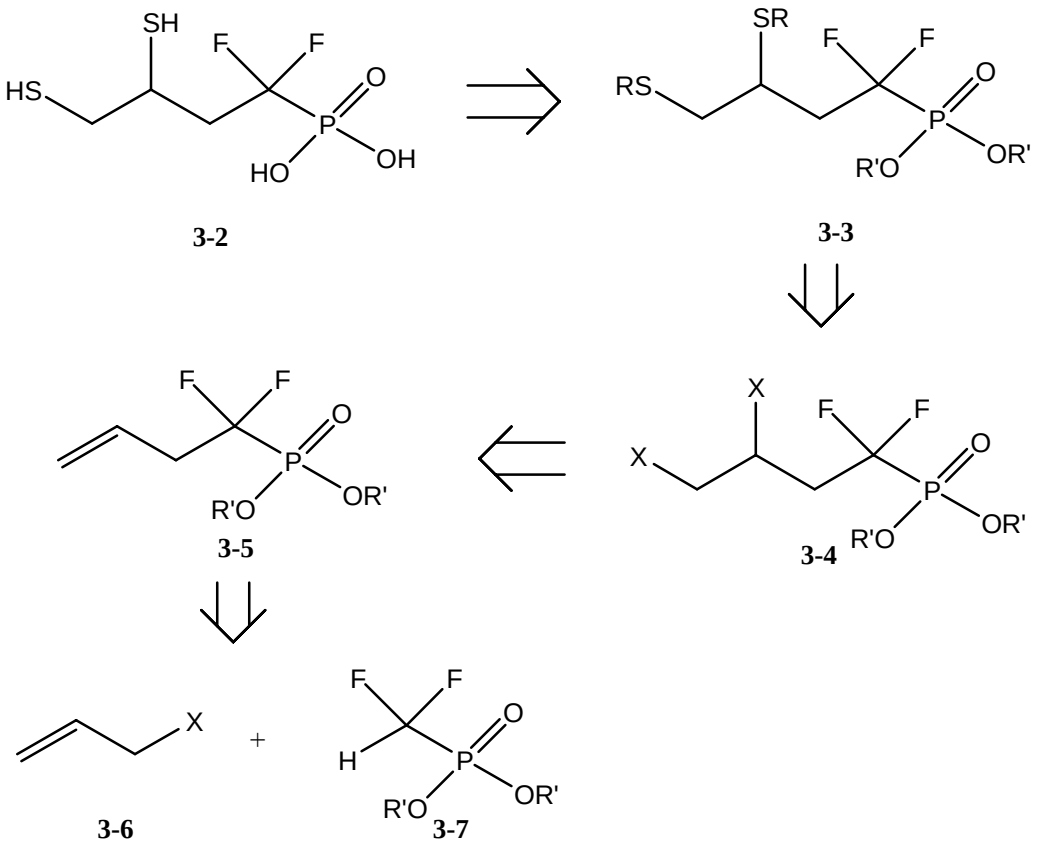


**3-2** **3-3** **3-4** **3-5** **3-6** **3-7**

**Scheme 3-1**

It was proposed that the dithiolphosphonate **3-2** might be formed from a precursor **3-3** in which the thiol and phosphonate groups are appropriately protected. It was further imagined that nucleophilic displacement of proper leaving groups (e.g. X = Br) by a suitable sulfur nucleophile on a precursor such as **3-4** could lead to formation of **3-3**. The alkene **3-5** was thought to be a suitable precursor for **3-4** and the formation of **3-5** was considered to be possible using an allyl system **3-6** with a suitable leaving group as an electrophile in an $S_N2$ reaction with a difluorophosphonate anion. The difluorophosphonate anion could be formed by deprotonation of the precursor **3-7** by a suitable strong base as the nucleophile.

### 3.5 Results and Discussion

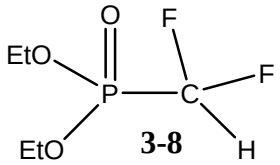


**3-8**

The starting material **3-8**, which was used as the precursor of the alkylation compound, has been previously reported in the literature. This compound can be prepared via a Michaelis-Arbuzov reaction between triethylphosphite and bromodifluoromethane (Scheme 3-2) (*21*). Alternatively, **3-8** can be obtained via $S_N2$ reaction of chlorodifluoromethane with the anion generated by deprotonation of diethylphosphite by reaction with sodium metal (Scheme 3-3).

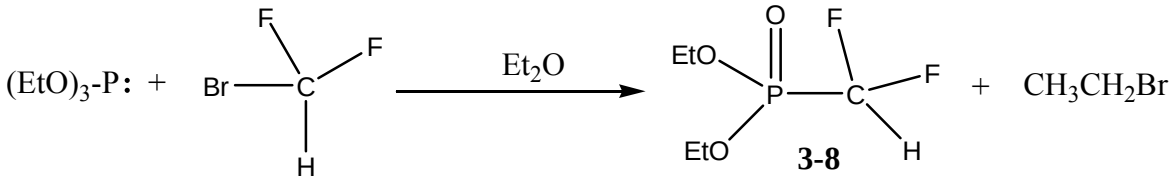


**Scheme 3-2**

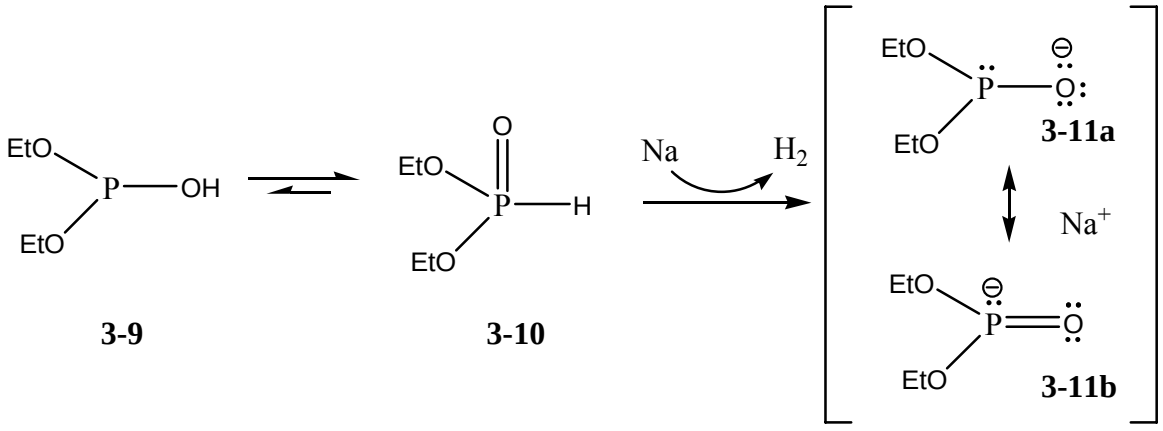


**Scheme 3-3**

Interestingly, diethyl phosphite **3-9** exists in equilibrium with its tautomer diethyl phosphonate **3-10**, with **3-10** being more stable by approximately 6 kcal/mol through Density Function Transform (DFT) calculation as recently reported by Rai and Namboothiri (*22*). Both **3-9** and **3-10** can form the same conjugate base **3-11** which is a resonance hybrid of the contributors **3-11a** and **3-11b**. It is generally described that the phosphorus atom in the anion is the most nucleophilic site and reacts with various electrophiles to provide the phosphonate derivative **3-13** rather than the phosphite derivative **3-12** (Scheme 3-4).

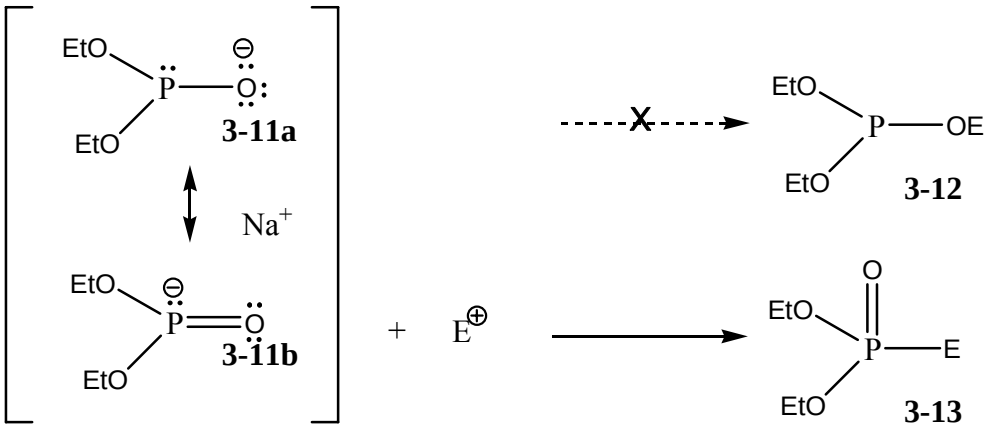


e.g. E⊕ = alkylhalide

**Scheme 3-4**

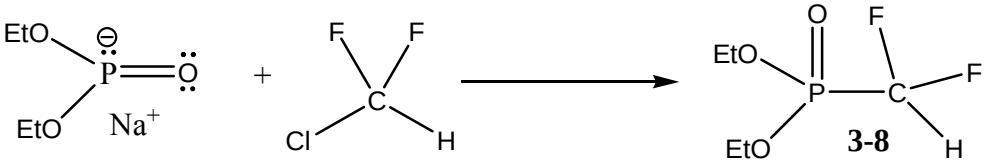


**Scheme 3-5**

In this research group, Dr. Christopher Lanthier has previously prepared a sample of compound **3-8** using the method involving alkylation of the anion **3-11** by chlorodifluoromethane (Scheme 3-5), followed by purification by distillation. This sample was

hence made available as the starting material for the present study. Since the description of the spectroscopic characteristics of **3-8** in the literature is not very detailed, the $^{1}H$ NMR of **3-8** was analyzed and interesting features were revealed.

Due to the fact that both $^{19}F$ and $^{31}P$ nuclei are NMR active with spin ½, the C-H signal in **3-8** consists of a triplet of doublets with a $J$ ($^{1}H$-$^{19}F$) = 48 Hz and a $J$ ($^{1}H$-$^{31}P$) = 27 Hz. In addition, the hydrogens within each ethoxy $CH_2$ group are diastereotopic so that each ethyl ($-CH_2CH_3$) group is actually an $AA'X_3$ system in the Pople nomenclature. Therefore the hydrogens within each $-CH_2$ group are expected to couple with one another. Because the chemical shift difference between $H_A$ and $H_{A'}$ is very small, the spin system is non-first order and the splitting pattern is not predictable by simple first order analyses, which applies only when $\Delta\nu/J$ ratio is large. Additionally, there appears to be a contaminant that contains an [$^{31}P$-X-CH-$^{19}F$] system as indicated in the $^{1}H$ NMR by the small signals beside each of the lines in the triplet of doublets of the major product. The nature of the impurity is not clear, however, it may represent compound **3-14**, the product of "O" alkylation of the anion **3-11**. In any event, the phosphonate compound **3-8**, along with its contaminant, was used as the starting material in the present study. The deprotonation of **3-8** followed by reaction with various electrophiles including allyl bromide was reported previously in a communication by Obayashi *et al. (23)*. Unfortunately, very little information was provided by the authors in regard of the experimental conditions and no spectroscopic characterization data of the product was made available in the study.

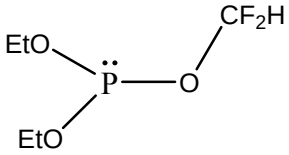


**3-14**

In the present study, the anion form of **3-8** was generated using lithium diisopropylamide (LDA) prepared by reaction of dry diisopropylamine with n-butyllithium in anhydrous THF. Once the anion had been prepared, allyl bromide was added and the reaction mixture was allowed to stir at 0 °C. It was proved to be difficult to monitor the progress of the reaction by TLC in the usual way; hence an arbitrary reaction time of 2 hours was used. The reaction was quenched by saturated $NH_4Cl$ solution and worked up with ethyl acetate to afford the crude product, which contained signals arising from the starting material **3-8** as well as from the desired allylation product **3-15**. The terminal vinyl hydrogens at C-4 in compound **3-15** give rise to a multiplet at δ

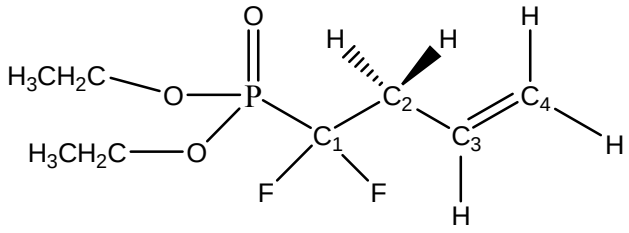


**3-15**

= 5.25 to δ = 5.31 ppm in the $^{1}H$ NMR spectrum. The single vinyl hydrogen attached to C-3 appears as a multiplet overlapping with the triplet of doublets from the C-H of the starting material **3-8**. The crude allylation product also contained a minor impurity (approximately 10%) that exhibited multiplets in the vinyl hydrogen region. This impurity may have arisen from the impurity present in the starting material **3-8**, but there is insufficient evidence to establish the structure of this compound. The two hydrogens at C-2 give rise to a complex but symmetrical multiplet from δ = 2.74 to δ = 2.94 ppm. This is consistent with two hydrogens coupled to two $^{19}F$ nuclei and one $^{31}P$ nucleus on an adjacent carbon atom in addition to the coupling to a vicinal

hydrogen (-C(H)=C-), and possibly the weak allylic coupling to the terminal hydrogens (-C=$CH_2$).

Attempts to find a solvent system that might allow separation of the allylated product **3-15** from the starting material **3-8** by silica gel flash chromatography were unsuccessful. Thus the crude reaction product was reacted further with molecular bromine in order to synthesize the next product.

The reaction was continued by mixing the crude allylation product with a solution of molecular bromine (1 equivalent) in dichloromethane followed by purification with silica gel flash chromatography, giving a combined fraction that containing the desired product **3-16** as well as a minor impurity. The presence of the desired dibromide product was suggested by the $^1$H NMR

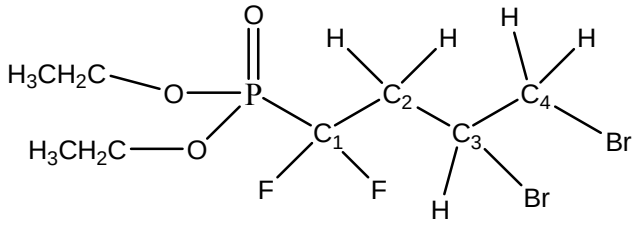


**3-16**

spectrum. The presence of the two ethoxy groups was indicated by a multiplet (apparent "quintet"). The diastereotopic hydrogens of the two $CH_2$ groups were found at δ = 4.20 and δ = 4.35 ppm and a triplet of six protons was found at δ = 1.39 ppm ($J$ = 7.1 Hz). Two very complex but symmetrical multiplets at δ = 2.96 to δ = 3.19 and δ = 2.55 to δ = 2.79 ppm can be assigned to the two hydrogens attached to C-2 near the -$CF_2$ group and the phosphorus atom. Two doublets of doublets at δ = 3.72 ($J$ = 7.6, $J$ = 10.9 Hz) and δ = 3.90 ppm ($J$ = 4.5, $J$ = 10.9 Hz)

are assigned to the two diastereotopic hydrogens at C-4, which coupled to one another and to the hydrogen at C-3. The C-3 hydrogen gives rise to a symmetrical multiplet at δ = 4.53 ppm, which includes coupling to the non-equivalent hydrogens at C-2 and C-4, and perhaps some long range coupling to $^{19}F$ and $^{31}P$.

The $^{13}C$ NMR spectrum of this fraction was also helpful in confirming the presence of the dibromide compound **3-16**. In the J-MOD spectrum, where $CH_3$ and CH carbons are phased downwards while $CH_2$ and quaternary carbons are phased upwards, the singlet at δ = 16 ppm (downwards) is assigned to the $–CH_3$ of the ethoxy groups. The singlet (upwards) at δ = 64.5 ppm is assigned to the $-CH_2$ of the ethoxy groups. The signal (downwards) at δ = 42 ppm is assigned to the (C-3)-HBr group, and upon scale expansion at high digital resolution, it was found to be a six line symmetrical multiplet as a result of long range coupling to the two $^{19}F$ nuclei and the $^{31}P$ nucleus. Then the (C-4)-$H_2Br$ group is assigned to the singlet (upwards) at δ = 37.2 ppm. The more complex multiplets at δ = 40.6 ppm and δ = 119.2 ppm clearly must represent carbons that are coupled to $^{19}F$ or $^{31}P$ or both since the spectrum is decoupled from $^{1}H$ nuclei. The most downfield signal is a doublet of triplets with a $J_{C\text{-}F}$ = 261 Hz and $J_{C\text{-}F}$ = 215 Hz and is assigned to the $^{31}P$-**C**$^{19}F_2$ (C-1) group. The multiplet at δ = 40.6 ppm ($J$ =15.5 Hz, $J$ = 20.1 Hz) is also in a six line pattern (doublet of triplets) with smaller $^{13}C$ to $^{19}F$ and $^{31}P$ coupling constants; thus, it is assigned to C-2 atom.

The presence of the dibromide compound **3-16** is further confirmed by the mass spectrum of the purified bromination product obtained by chemical ionization (CI) with ammonia as the bath gas shows a three peak pattern at m/z = 404, 406, and 408 in a 1:2:1 ratio, respectively. This is a

result of the presence of ($M+NH_4^+$) ions of $^{79}Br^{79}Br$, $^{81}Br^{79}Br$ ($^{79}Br^{81}Br$) and $^{81}Br^{81}Br$ isotopomer combinations of the dibromide product **3-16**. A weaker set of three signals at m/z = 387, 389, 391 corresponding to the ($M+H^+$) ions for the isotopomeric dibromides was also observed.

Interestingly, an additional set of three signals at m/z = 384, 386 and 388 is consistent with the presence of ions derived from a molecule that retains the two bromine atoms but has somehow lost a HF fragment [i.e. ($M–HF+NH_4^+$)]. This observation proved to be of some significance in the context of helping to analyze the nature of the major impurity present in the purified dibromide product.

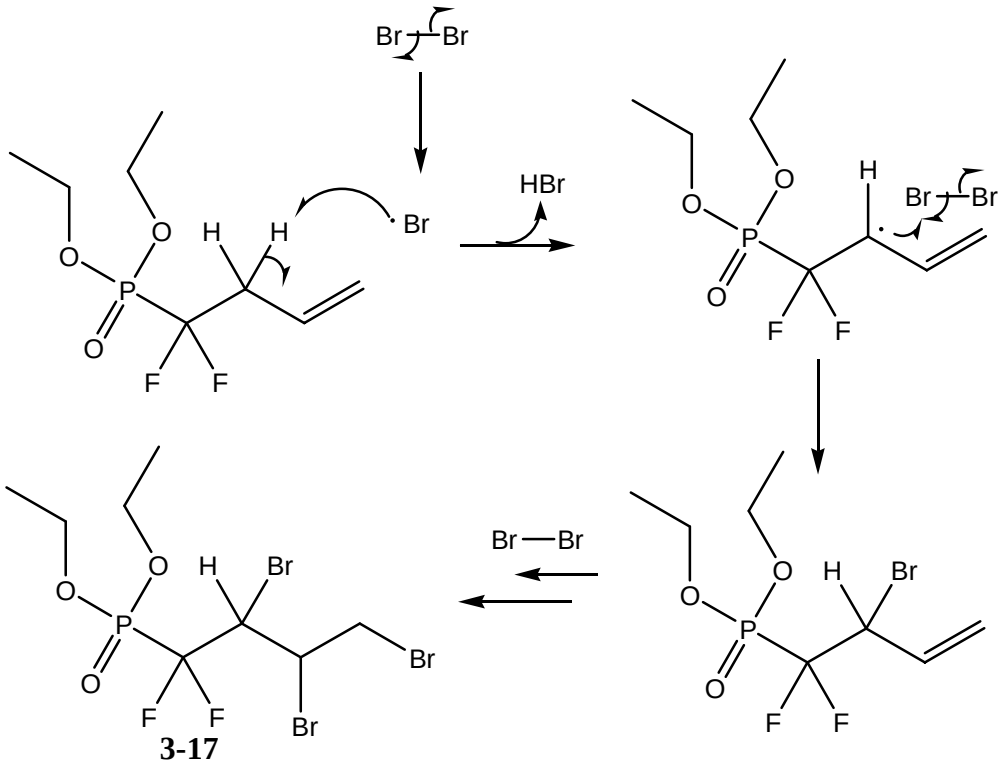


**Scheme 3-6**

Initially, it was proposed that the impurity that gives rise to the sets of complex symmetrical mutiplets in the $^1$H NMR spectrum of the dibromide product might be the tribromide compound **3-17** as shown above (Scheme 3-6). This tribromide compound might arise by some competing free radical chain bromination preceding the ionic addition of $Br_2$ to the C=C bond. However, signals in the mass spectrum corresponding to the tribromide compound were not found. Furthermore, the chemical shifts from the impurity of the $^1$H NMR agree poorly with those for the tribromide product, thus leading us to consider other possible structures corresponding to the impurity instead. The presence of a multiplet at $\delta$ = 6.11 ppm in the $^1$H NMR with large coupling constant is suggestive of a vinyl proton in proximity to the fluorine atoms and the phosphorus atom. This suggested the possibility of a structure derived by loss of a HF fragment as detected in the mass spectrum described above should be considered. In particular, it was proposed that the major impurity in the dibromide sample (approximately 13%) is the unsaturated dibromide **3-18** shown below with the chemical shifts and coupling constants indicated for specific hydrogens (Scheme 3-7).

As indicated in Scheme 3-7, the chemical shifts predicated by application of the incremental additivity rules for substituents as implemented in ChemDraw Ultra 8 for the hydrogens in the tribromide structure agree poorly with those obtained experimentally for the impurity from the dibromide product. In particular, the hydrogen at C-2 which is expected to be coupled to the two fluorine atoms and the phosphorus atom in the tribromide structure **3-17** is predicted to have a chemical shift of 4.4 ppm, whereas this hydrogen was found at 6.11 ppm experimentally. For the vinylfluoride-dibromide structure **3-18** of the impurity, the predicted chemical shift for the vinyl hydrogen is in better agreement ($\delta$ = 5.85 ppm). Moreover, the observed coupling constant $J_{H\text{-}F}$

(34.4 Hz) is in the range expected for a *trans* relationship between a fluorine and hydrogen atom on a C=C bond.

Observed $^{1}$H NMR

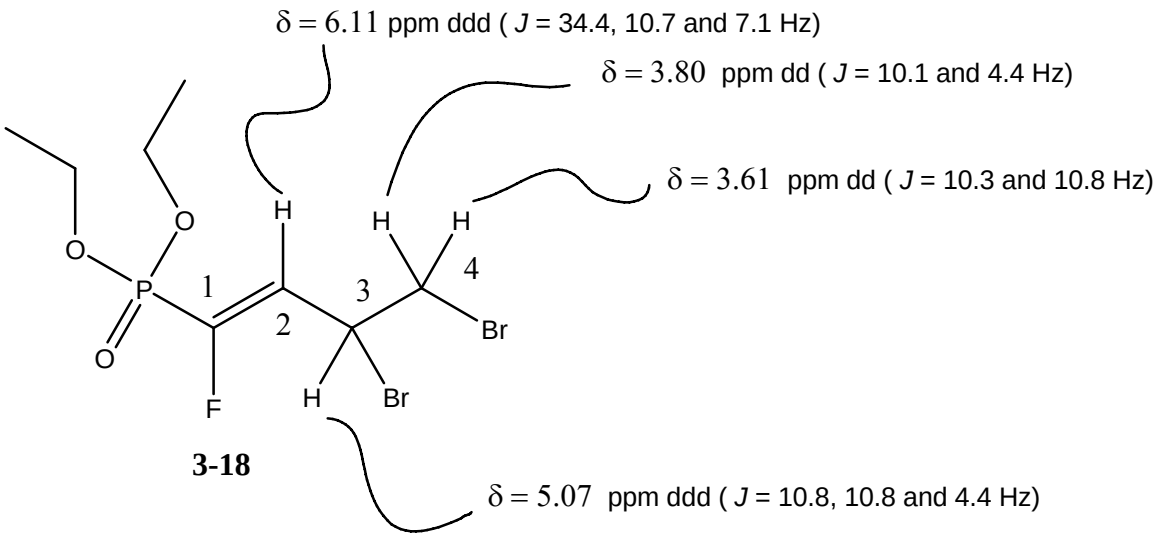


**3-18**

Calculated chemical shifts

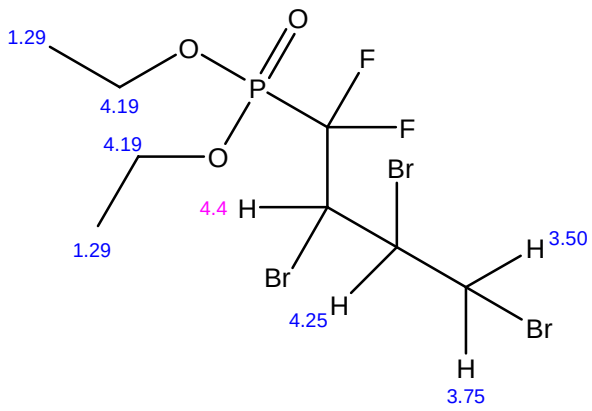


**3-17**

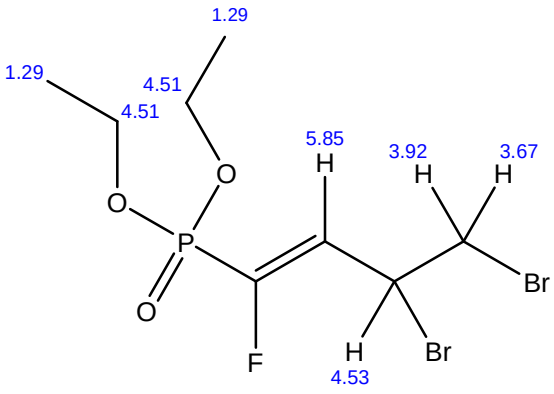


**3-18**

**Scheme 3-7**

Further evidence to support the presence of **3-18** is from the $^{13}C$ NMR spectrum of the dibromide/impurity mixture. It shows a downfield signal at δ = 153.0 ppm that is a double of doublets with *J* = 286 and 228 Hz that is consistent with a carbon with one fluorine and one phosphorus atom attached. The J-MOD spectrum also includes a doublet of doublets at δ = 123.4 ppm with *J* =29 and 4 Hz which is phased downwards. This signal matches with a vinyl carbon with one hydrogen attached and one fluorine plus one phosphorus atoms at the adjacent vinyl carbon atom.

Noticeably, examination of the literature shows that there have been some recent efforts to synthesize α-fluorinated phosphonates. For example, Prestwich and coworkers have reported that Wadsworth-Emmons reaction of α-fluorovinylphosphonates with various aldehydes provides mixtures of *E* (major) and *Z* (minor) α-fluorinated phosphonates as shown below (Scheme 3-8) (*24*).

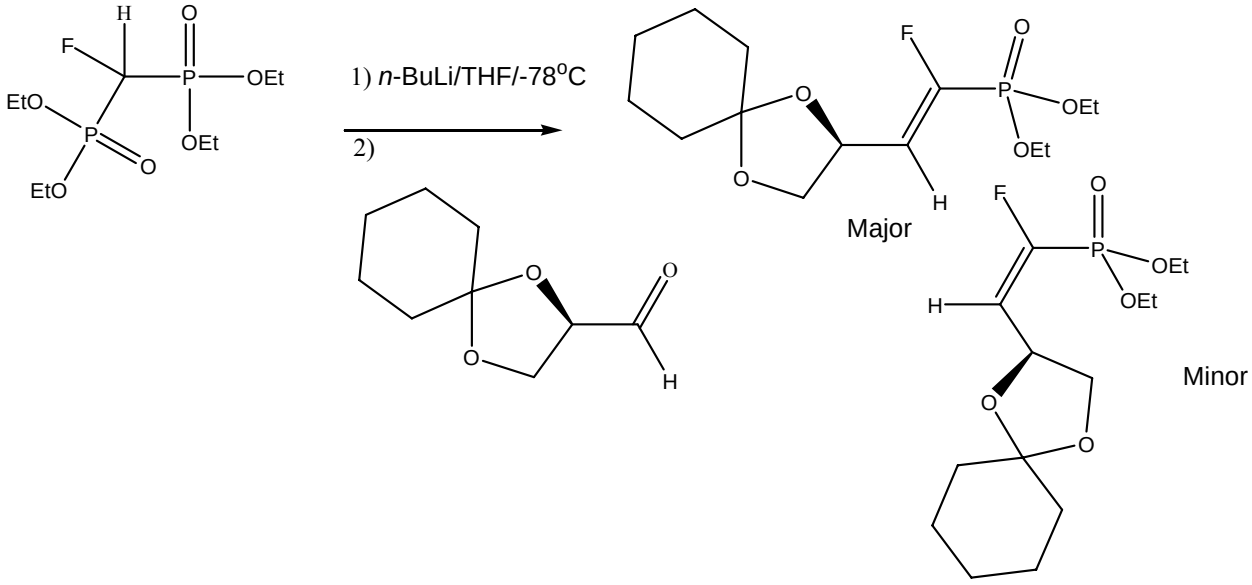


**Scheme 3-8**

Interestingly, as shown in the $^{1}H$ and $^{13}C$ NMR characteristics (Scheme 3-9) of the authentic α-fluorinated phosphonates prepared by the authors agree well with those of the impurity in the bromination reaction. It is however not clear how this vinylfluoride arises in the bromination reaction. One possibility is that it might arise from the impurity present in the starting allyl system as discussed previously, for which the structure is unknown.

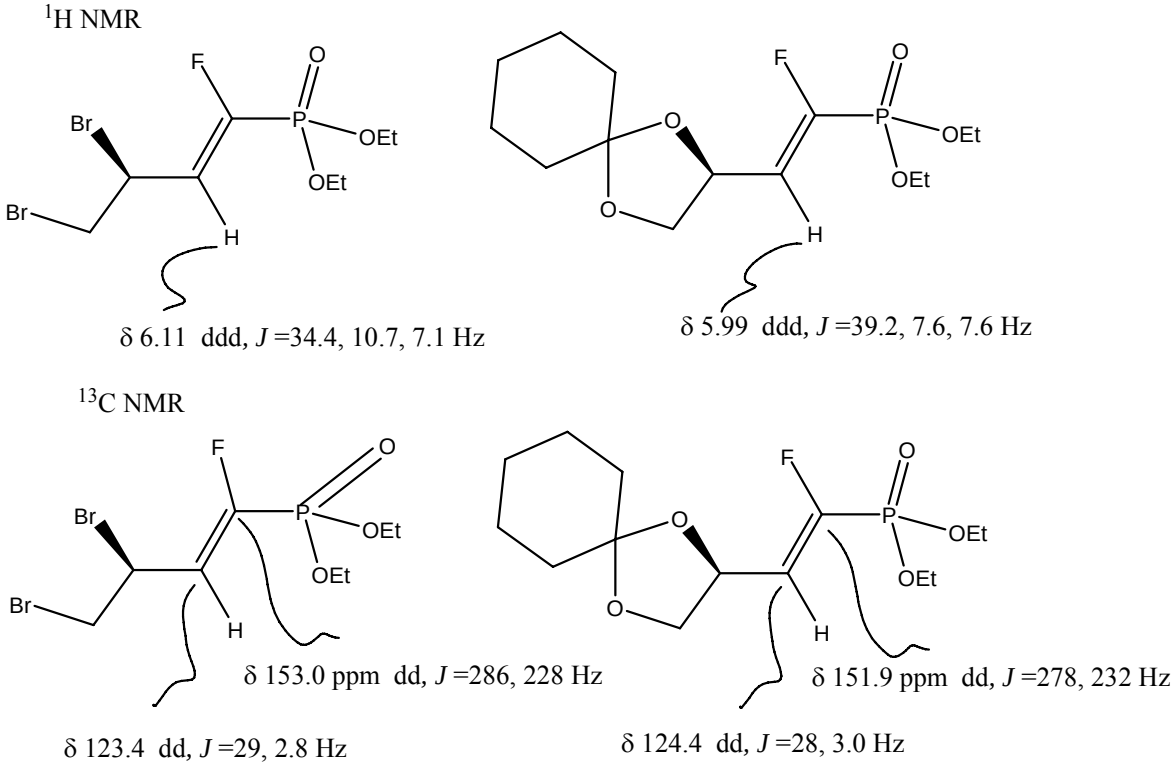


**Scheme 3-9**

The dibromide product **3-16** was not purified further but was used with the impurity present to be carried along in attempts of a double $S_N2$ displacement of the two bromides by conjugate base of thioacetic acid. This conjugate base was generated by reaction of thioacetic acid with diazabicyclo-undec-7-ene (DBU) in dimethyl formamide (DMF) as the solvent. Then **3-16** was

added slowly as a solution in DMF to the conjugate base solution and the reaction was allowed to proceed at room temperature overnight. After an aqueous work-up, TLC analysis of the crude product indicated that the starting material had been all consumed and three spots suggesting three new products were observed.

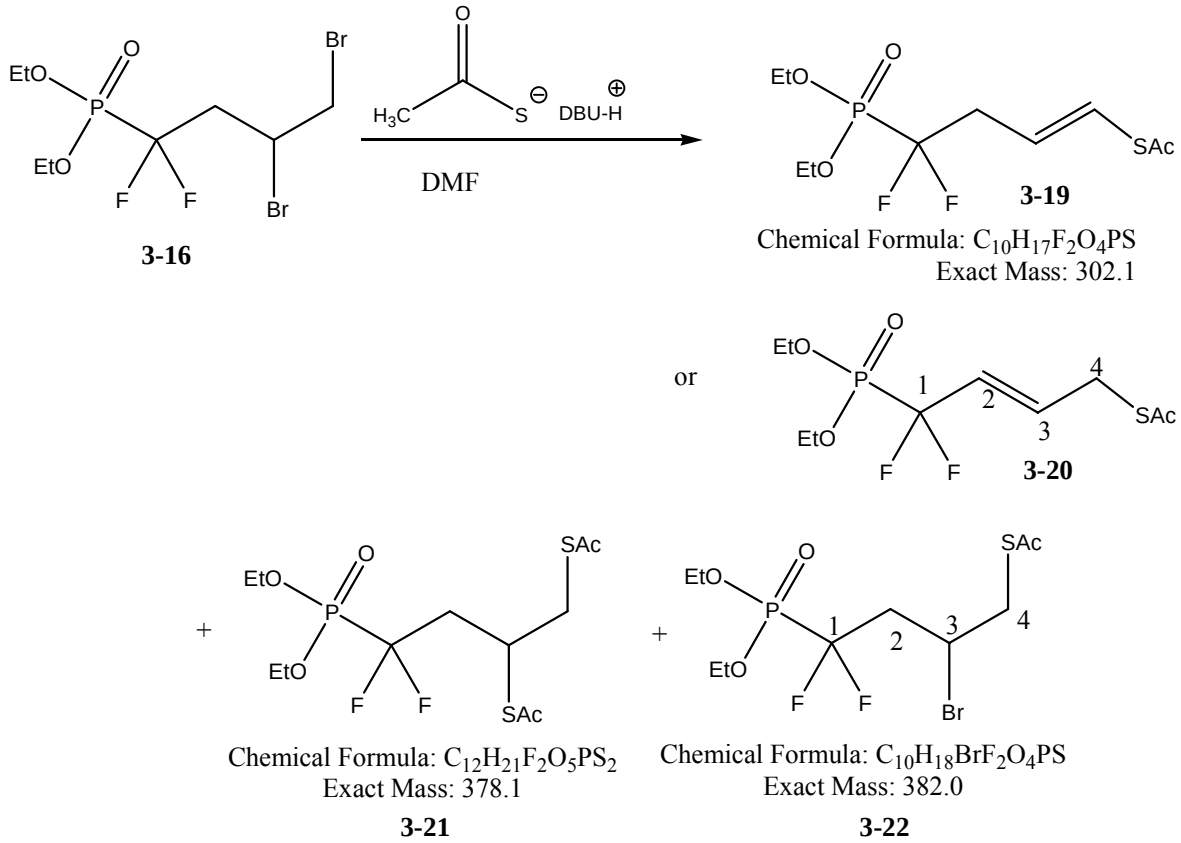


**Scheme 3-10**

Initial analysis of the $^{1}H$ NMR spectrum revealed the presence of vinyl proton signals as multiplets at $\delta$ = 6.21 and 5.85 ppm. This was suggestive of the major product to be the result of elimination (**3-19** or **3-20**, Scheme 3-10) rather than the desired double nucleophilic displacement reaction. In addition, signals found in the range of $\delta$ = 3.1 to 3.4 ppm were

compatible with the formation of some substitution product. Also, three singlets found in the range of 2.2 to 2.4 ppm might be indicative of incorporation of thioacetyl groups into some of the products.

Fortunately, results from mass spectrometry by examining the sample with chemical ionization and ammonia as the bath gas provided some insight into the possible composition of the crude product. The most intense peak was found at m/z = 320, corresponding to an $[M+18]^+$ fragment for the product of $S_N2$ displacement of one bromide by a thioacetyl nucleophile as well as E2 elimination of HBr. The second most intense peak found in the CI-MS is at m/z = 396, which could be attributed to the ideal situation that both bromides had been displaced by thioacetyl anion nucleophiles as desired. Furthermore, two peaks of equal intensity were observed at m/z = 400 and 402, which could correspond to the $[M+18]^+$ fragment for the two isotopomers of a product that only one bromide had been displaced through an $S_N2$ reaction.

The possible structure of the elimination product was then deduced to be **3-20** rather than **3-19** based on the multiplicities of the two vinyl hydrogen signals. It was observed that, one of the vinyl hydrogen signal at δ = 5.85 ppm exhibiting a quartet with a large coupling constant and some additional small coupling (Figure 3-7). The pattern might arise if it was the result of the vinyl hydrogen coupling to the two fluorine atoms as well as to the vicinal *trans* hydrogen with the H-F and H-H coupling constants being very similar (approximately 15 Hz). In addition, neither of the vinyl hydrogens in **3-19** was expected to possess such a large coupling to fluorine, however, it seemed reasonable to suggest that the vinyl hydrogen on C-2 in structure **3-20** might couple to the two fluorine atoms with a $^3J_{H\text{-}F}$ of approximately 15 Hz. Standard tabulations of

coupling constants of protons to heteroatoms suggest that, if the intervening carbon atom is $sp^3$ hybridized then the $^3J_{H\text{-}F}$ values are found in the fairly broad range of 3 to 24 Hz (*25*). However, the value of $^3J_{H\text{-}P}$ was found in the range of 15-20 Hz, thus not as small as suggested in the analysis above.

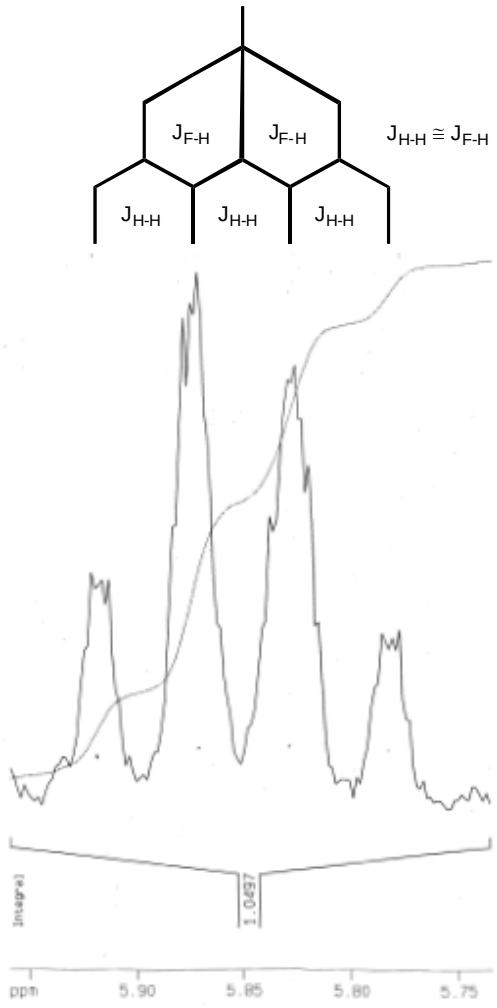


**Figure 3-7.** The apparent quartet and the splitting pattern of the C-2 hydrogen on 3-20 as seen on the $^1$H NMR spectrum.

A search of the literature was then performed in order to find structures that were similar to **3-20** with $^3J_{H\text{-}F}$ and $^3J_{H\text{-}P}$ values reported. One such example was found in the work of Percy and coworkers (*26*) who prepared ethyl (2*E*)-4-(diethoxyphosphoryl)-4,4-difluorobut-2-enoate **3-24**

by reaction of triethyl phosphonoacetate with the difluorophosphonate derivative **3-23** (Scheme 3-11). The *trans* H-H coupling for the hydrogen at C-2 was found to be 15.5 Hz, whereas the $^{3}J_{H\text{-}F}$ value was found to be 12.5 Hz. Also, the $^{3}J_{H\text{-}P}$ value was found to be merely 2.5 Hz. Therefore, $^{3}J_{H\text{-}P}$ values for hydrogen bound to an $sp^2$ hybridized carbon appear to be much smaller than those observed when the hydrogen is attached to an $sp^3$ centre. Thus, the interpretation of the NMR data in favour of the structure **3-20** rather than **3-19** seems valid. In addition, the other vinyl hydrogen on C-3 in **3-20** gives rise to a complex, but symmetrical, multiplet that includes coupling to the hydrogen on C-2, weaker long range coupling to the two fluorine atoms, to the phosphorus atom and to the hydrogens on C-4 (-$CH_2$-). The $CH_2$ group hydrogens give rise to a two proton mutiplet at $\delta$ = 3.59 ppm.

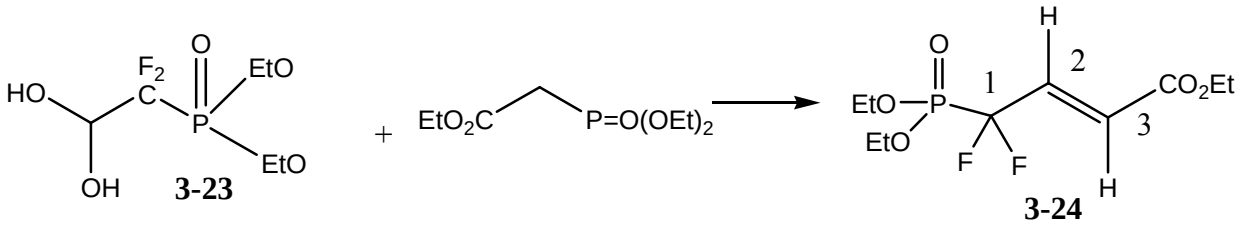


**Scheme 3-11**

The presence of four doublets of doublets in the range of 3.16 to 3.55 ppm observed on the $^{1}H$ NMR spectrum might be assigned to the two diastereotopic hydrogens on C-4 of products **3-21** and **3-22**. This is consistent with the mass spectrometric data which implicated the presence of these two compounds. These signals are of comparable intensity, suggesting that comparable amount of the monosubstitution (**3-22)** and disubstitution (**3-21)** products are present. The methylene hydrogens at C-2 which are coupled to the two fluorine atoms and phosphorus atom

were assigned to the multiplets in the range of 2.3 to 2.8 ppm. The remaining hydrogens from **3-21** and **3-22** were presumably hidden under the multiplets from the ethoxy group in the range of 4.0 to 4.3 ppm on the $^{1}$H NMR spectrum.

Since E2 elimination reactions tend to be favoured at high temperatures relative to $S_N2$ reactions, the reaction was repeated at lower temperature (i.e. –20 °C). It was possible to decrease the proportion of elimination product present as indicated by analysis of the proton NMR spectrum of the crude reaction product. However, both the monosubstitution and disubstitution products were found to be present. Due to the limits in time and the amounts of the dibromide **3-16** that were available, the study of this approach to the synthesis of the dithiol product **3-2** was terminated.

### 3.6 Future work

On top of the difficulty of the synthetic route of **3-2** with the method described, one potential drawback of this DMPS derivative inhibitor is that, the two thiol groups may undergo oxidation *in vivo* and form intermolecular disulfide bonds. This will render the inhibitor losing the capability to bind to the zinc ion before reaching the enzyme active site. It will be valuable that such a problematic circumstance can be minimized.

Interestingly, recent studies by Mobashery and coworkers have shown that gelatinase A, a zinc-dependent MMP can be irreversibly inhibited by rationally designed thioepoxide containing inhibitors (*27-29*). By mimicking the structure of the substrate of gelatinase A, the thioepoxide containing inhibitors bind to the zinc ion once in the active site through the thioepoxide moiety. The zinc acts as a Lewis acid in catalyzing the ring opening of the thioepoxide and this will lead to a nucleophilic attack by a carboxylate group of the glutamate which participates as a general base in the normal catalytic mechanism. The formation of the covalent bond between the inhibitor and the enzyme is irreversible and will render the enzyme inactivate as is typical of mechanism-based inhibitors. It is hoped that the related mechanism may apply to the active site of the Class II FBP aldolase such that a covalent bond formation would be achieved with the base involved in deprotonating DHAP between the potential inhibitors. It is reasoned that the proposed thioepoxide-based inhibitor **3-25** can be synthesized as shown in Scheme 3-12 also

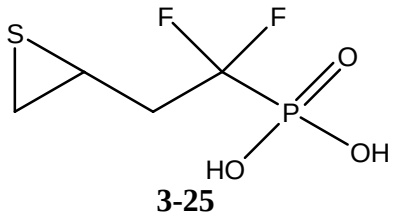


**3-25**

with the starting material **3-8**, followed by alkylation and epoxidation. After the conversion from epoxide to thioepoxide, **3-25** can be obtained though route A by hydrolysis. It is also analyzed that compound **3-2** can be obtained though route B by ring opening of the thiopoxide with thioacetic acid and a good base followed by hydrolysis, thus bypassing the original strategy to afford the desired inhibitor compound.

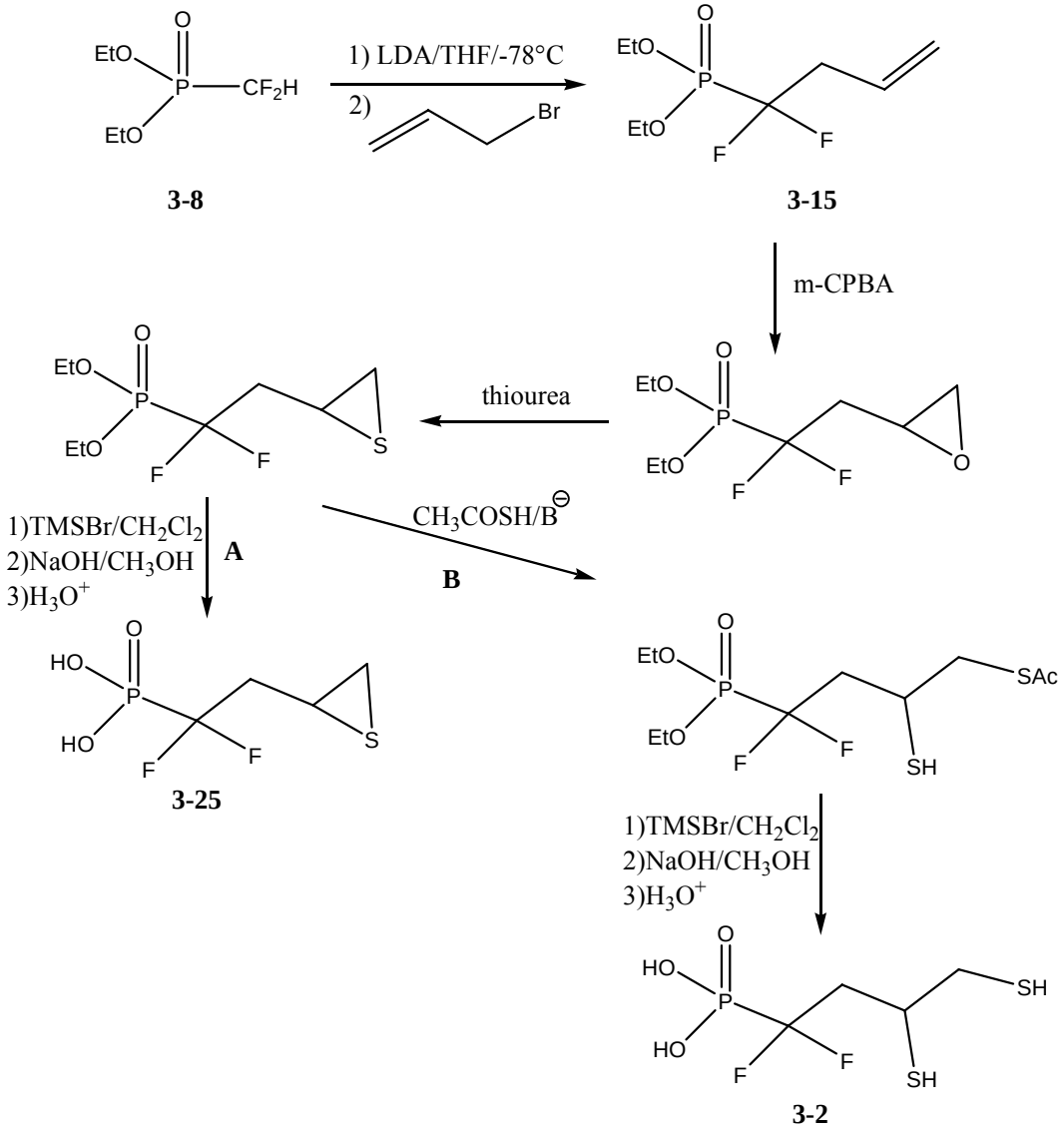


**Scheme 3-12**

## 3.7 Experimental

### General Experimental

All the reagents used were purchased from Sigma-Aldrich or from Lancaster Synthesis unless otherwise stated. All reactions were performed either under argon or nitrogen atmosphere and monitored by thin layer chromatography (TLC) using aluminum-backed sheets precoated with silica gel (0.2 mm) (EMD Chemical Inc.). TLC plates were analyzed by an ultraviolet lamp (254 nm). Anhydrous solvents were obtained from the Manual Solvent Purification System (M. Braun Inc.). Flash column chromatography was performed using silica gel (230-400 mesh).

The low resolution electron impact (EI), chemical ionization (CI) and electrospray (ESI) mass spectra were obtained by Dr. Richard Smith at University of Waterloo. $^{1}$H NMR and $^{13}$C NMR (J-MOD) spectra were obtained on a Bruker Avance-300 (300 MHz) or Avance-500 (500 MHz) NMR spectrometer with d-chloroform, $d_4$-methanol and $d_6$-dimethyl sulfoxide as the solvent attributed to specific compound. All the molecular modeling studies were performed using a computational modeling kit SYBYL 7.3 (Tripos) with the MMFF94 force field by Timothy Ramadhar and Geneviève Labbé in the Dr. Dmitrienko group.

### Diethyl Difluoromethylphosphonate (3-8)

This compound was prepared by Dr. Christopher Lanthier in this group. $^{1}$H NMR (300 MHz, $CDCl_3$) δ = 5.94 ppm (1H, td, $PCF_2\mathbf{H}$, $J_{H\text{-}F}$ = 48 Hz, $J_{P\text{-}H}$ = 27 Hz), 4.29 ppm (4H, symmetrical 8 line pattern, O-C$\mathbf{H}_2$-$CH_3$), 1.23 (6H, t, $J$ = 7.0 Hz) *(31)*.

**Diethyl -1,1-difluorobut-3-enylphosphonate (3-15)**

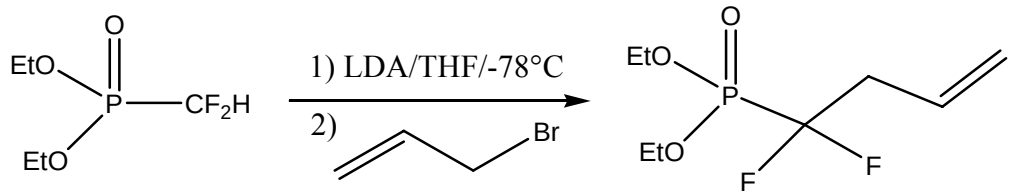


**3-8** **3-15**

The experimental procedure was adapted and modified from Durgam *et al.* (*30*) To a 100 mL, 2-neck round-bottomed flask, dry diisopropylamine (3.35 mmol, 0.47 mL, 1.1 equiv) was transferred by syringe into anhydrous THF (20 mL) which was being stirred at –78 °C (acetone/dry ice bath) under an argon atmosphere. Then a solution of 1.6 M n-butyllithium in hexane (3.29 mmol, 2.06 mL, 1.08 equiv) was delivered into the solution slowly, and the reaction flask was immediately transferred to a 0 °C bath to allow the reaction to go for 30 min under argon. The reaction flask was then transferred back to –78 °C bath and diethyl difluoromethylphosphonate (3.05 mmol in 2 mL dry THF, 1 equiv, prepared by Dr. Christopher Lanthier in this group) was added slowly to the reaction mixture. The reaction mixture was stirred for 30 min under argon and allyl bromide (3.66 mmol, 0.32 mL, 1.2 equiv) was added to the reaction mixture slowly. The reaction was then allowed to stir for 2 hours at 0 °C, brought up to room temperature and quenched by 150 mL saturated $NH_4Cl$ solution. The residual THF was removed in vacuo and the mixture was then extracted three times with 40 mL ethyl acetate. The organic layer was dried over anhydrous $Na_2SO_4$, filtered and concentrated in vacuo to afford the crude product (0.40 g). $^1$H NMR (300 MHz, $CDCl_3$) $\delta$ = 5.76-5.86 ppm (1H, m, overlapped with signal from CH of **3-8**, $CF_2CH_2C\mathbf{H}{=}CH_2$), 5.25-5.31 (2H, m, $C{=}C\mathbf{H}_2$), 4.21-4.34 (4H, m,

$OC\mathbf{H}_2CH_3$), 2.74-2.94 (2H, symmetrical m, $PCF_2C\mathbf{H}_2CH{=}CH_2$), 1.38 (6H, t, $OCH_2C\mathbf{H}_3$ overlapped with signals from **3-8** and other minor contaminants).

**Diethyl-3,4-dibromo-1,1-difluorobutylphosphonate (3-16)**

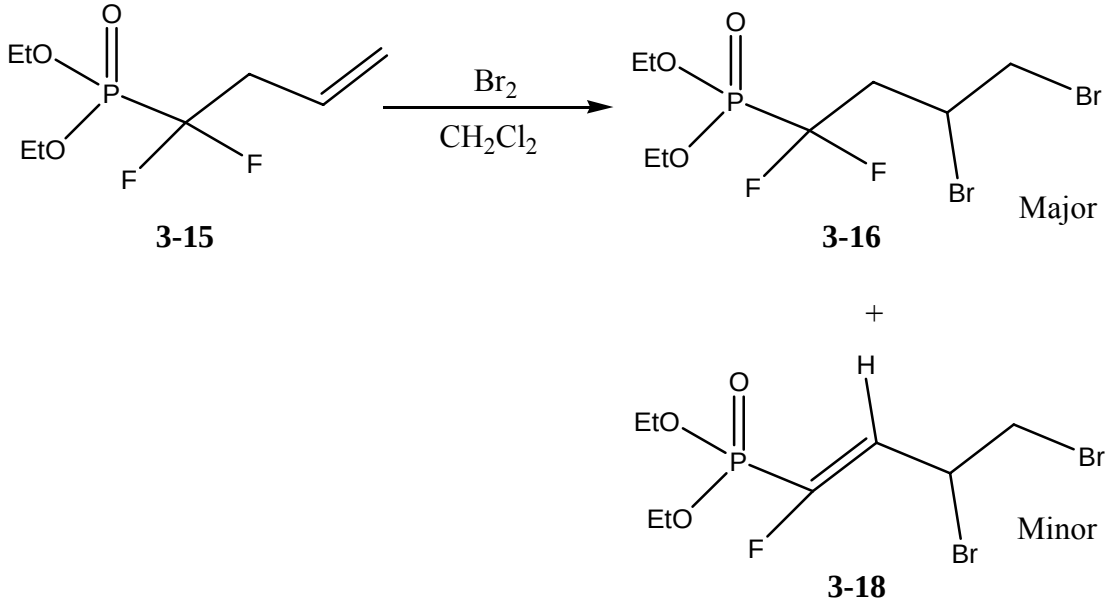


**3-15** **3-16** + **3-18**

Bromine solution (0.80 M) was prepared by adding 0.30 mL of $Br_2$ to a 10 mL volumetric flask and then adding dry $CH_2Cl_2$ to make up the rest of the volume. The crude mixture containing diethyl-1,1-difluorobut-3-enylphosphonate (0.40 g) was dissolved with 4 mL of dry $CH_2Cl_2$ in a 25 mL round-bottomed flask and stirred at room temperature under argon for 5 minutes. Then 1.5 mL of the $Br_2$ solution (1.2 mmol) was transferred into the reaction flask slowly via syringe. The reaction was allowed to proceed for 1 hr at room temperature and monitored by TLC (EtOAc:Hex = 3:7), then quenched by 50 mL of saturated sodium thiosulphate. The reaction mixture was then extracted three times with $CH_2Cl_2$. The organic layers were then combined and dried over anhydrous $Na_2SO_4$, and concentrated in vacuo to afford 0.41 g of crude product. The crude product was then purified through silica gel flash column chromatography (EtOAc:Hex = 1:4). The combined fractions with the desired compound were concentrated in vacuo to afford 0.20 g of a clear and colorless oily product that was mostly

diethyl-3,4-dibromo-1,1-difluorobutylphosphonate. $^{1}$H NMR (300 MHz, $CDCl_3$) δ = 4.53 ppm (1H, symmetrical m, C**H**Br), 4.35 (4H, symmetrical m, OC**H**$_2$CH$_3$), 3.90 (1H, dd, *J* = 10.9, 7.6 Hz), 3.72 (1H, dd, *J* = 10.9, 4.5 Hz), 2.96-3.19 (1H, m, PCF$_2$C**H**HCHBrC), 2.55-2.79 (1H, m, PCF$_2$CH**H**CHBrC), 1.39 (6H, t, *J* = 7.1 Hz). Proton NMR signals were also observed for an impurity identified as **3-18** (see page 86 for a discussion). $^{13}$C NMR J-MOD ($CDCl_3$) δ = 119.2 (up, dt), 64.5 (up), 42 (down, dt), 40.6 (up, dt), 37.2 (up), 17.1 (down). Signals were also observed for the impurity **3-18**, see page 87 for discussion. CI ($NH_3$)–MS: m/z = 404, 406, 408 (1:2:1 intensity ratio) ($M+NH_3^+$) for bromine isotopomers of $C_8H_{15}Br_2F_2O_3P$. Peaks at m/z δ = 384, 386, 388 (1:2:1 intensity ratio) ($M+NH_3^+$) for bromine isotopomers of $C_8H_{14}Br_2FO_3P$.

**Reaction of 3-16 with thioacetate anion**

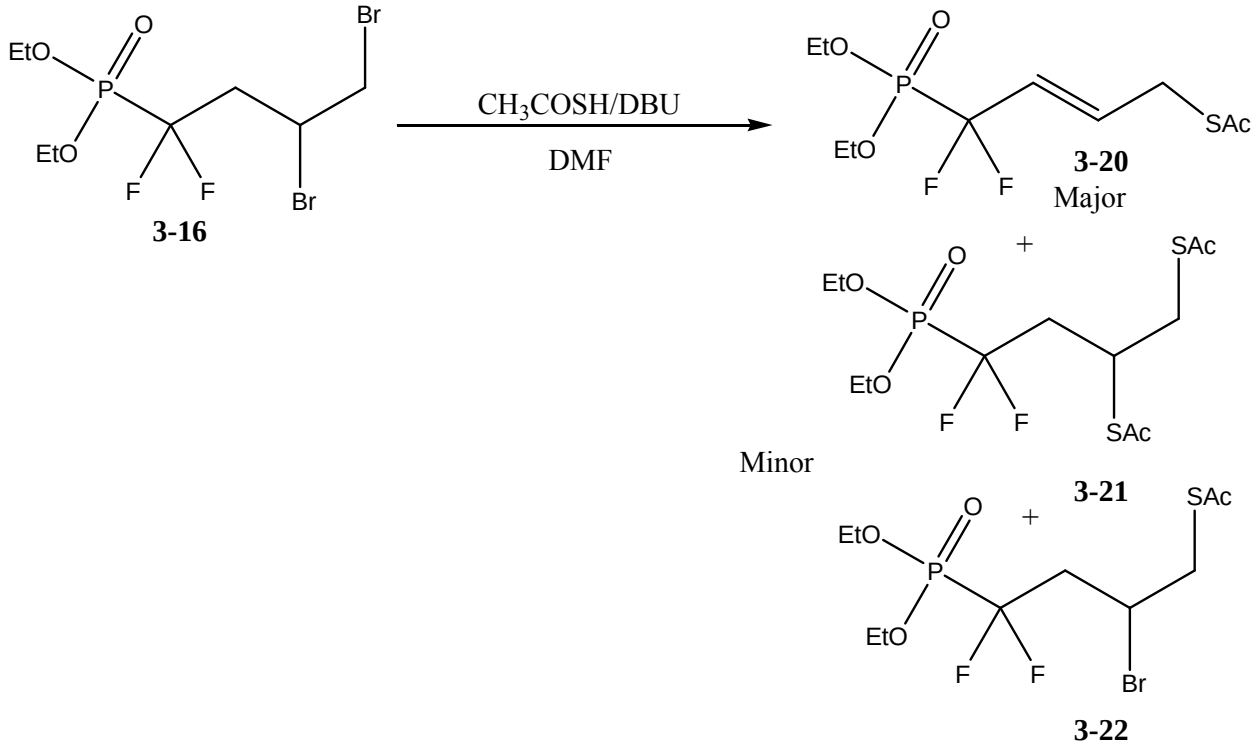

A stock solution of diazabicyclo-undec-7-ene (DBU) (0.25 M) was prepared in a 10 mL volumetric flask by dissolving 0.35 mL of 2.48 mmol DBU in DMF. A stock solution of thioacetic acid (0.20 M) was prepared in a 10 mL volumetric flask by dissolving 0.17 mL of 1.98 mmol thioacetic acid in DMF. An aliquot from the DBU stock solution (0.97 mL, 0.24 mmol, 3.05 equiv) and an aliquot from the thioacetic acid (1.22 mL, 0.24 mmol, 3.1 equiv) were both transferred into a 25 mL round-bottomed flask under $N_2$ and stirred at room temperature for 10 minutes. Diethyl-3,4-dibromo-1,1-difluorobutylphosphonate (30.6 mg, 0.079 mmol, 1 equiv) was then dissolved in 2.0 mL of DMF and transferred slowly into the reaction flask containing DBU and thioacetic acid. The reaction was allowed to proceed for overnight under $N_2$ at room temperature. To monitor the reaction by TLC, a mini work-up was applied due to DMF's high boiling point. In a small vial, 4 mL of distilled water and approximately 1.0 mL of ethyl acetate were added. Then 0.1 mL of the sample from the reaction was added to the vial and stirred vigorously to form an emulsion. The ethyl acetate layer was then sampled and analyzed by TLC (EtOAc:Hex = 3:7). Three spots rather than the spot of the starting material were observed, indicating a mixture of three compounds were present. The reaction was then allowed to continue overnight at room temperature. The reaction mixture was then diluted with 70 mL of brine and then exacted three times with 30 mL of ethyl acetate. The organic layers were combined, dried over anhydrous $Na_2SO_4$, and concentrated in vacuo to afford 12.9 mg of crude product including **3-20, 3-21 and 3-22**. Since E2 elimination reactions tend to be favoured at high temperatures relative to $S_N2$ reactions, the reaction was repeated at lower temperature. The NMR analysis of the mixture is described above on pages 90-94. CI ($NH_3$)-MS: m/z = 320 ($M+NH_3^+$) for $C_{10}H_{17}F_2O_4PS$; 396 ($M+NH_3^+$) for $C_{12}H_{21}F_2O_5PS_2$; 400 and 402 (equal intensity) ($M+NH_3^+$) for bromine isotopomers of $C_{10}H_{18}BrF_2O_4PS$.

The second trial of this reaction was performed under different experimental conditions. In a 25 mL round-bottomed flask, diethyl-3,4-dibromo-1,1-difluorobutylphosphonate (13.2 mg, 0.034 mmol, 1 equiv) was dissolved with 3.0 mL of DMF and then stirred at −20 °C acetone bath (temperature was maintained by cooling machine) under $N_2$. An aliquot from the DBU stock (0.41 mL, 0.10 mmol, 3 equiv) and an aliquot from the thioacetic acid stock (0.55 mL, 0.11 mmol, 3.2 equiv) were then transferred to another 25 mL round-bottomed flask and stirred for 20 min in an ice bath under $N_2$. The DBU and thioacetic acid mixture was then delivered into the first reaction flask slowly via syringe and the reaction was allowed to stir overnight at −20 °C under $N_2$. To monitor the reaction by TLC, a mini work-up was applied as in the first trial except that brine was used instead of distilled water. Observation by TLC indicated the presence of residual starting material. The reaction was allowed to continue overnight at −20 °C under $N_2$ and was then brought up to room temperature. The mixture was then diluted with 70 mL of brine, and extracted three times with 20 mL of ethyl acetate. The organic layers were combined, dried over anhydrous $Na_2SO_4$ and concentrated in vacuo to afford 12.9 mg of crude product including both **3-21 and 3-22**.

The third trial was performed under the same conditions as the first trial with a larger scale but shorter reaction time. In a 25 mL round-bottomed flask, diethyl-3,4-dibromo-1,1-difluorobutylphosphonate (69.1 mg, 0.18 mmol, 1 equiv) was dissolved in 2.0 mL of DMF. In another 25 mL round-bottomed flask, an aliquot from the DBU stock (2.15 mL, 0.53 mmol, 3 equiv) and an aliquot from the thioacetic acid stock (2.80 mL, 0.55 mmol, 3.1 equiv) were mixed and stirred for 10 min at room temperature under $N_2$. The mixture of DBU and thioacetic acid

was then transferred to the first reaction flask via syringe slowly and allowed to stir overnight at room temperature. To monitor the reaction by TLC, a mini work-up was applied in the same fashion as the second trial. The reaction mixture was then diluted with 80 mL of brine and extracted three times with 10 mL of ethyl acetate. The organic layers were combined, dried over anhydrous $Na_2SO_4$ and concentrated in vacuo to afford 38.1 mg of crude product.

# References

## References for chapter 1


(1) Meyerhof, O., and Lohmann, K. (1934) *Biochem. Z. 271*, 89.

(2) Toone, E. J., Simon, E. S., Bednarski, M. D., and Whitesides, G. M. (1989) Enzyme-catalyzed synthesis of carbohydrates. *Tetrahedron 45*, 5365-5422.

(3) Rutter, W. J. (1964) Evolution of aldolase. *Fed. Proc. 23*, 1248-1257.

(4) Plater, A. R., Zgiby, S. M., Thomson, G. J., Qamar, S., Wharton, C. W., and Berry, A. (1999) Conserved residues in the mechanism of the *E. coli* Class II FBP-aldolase. *J. Mol. Biol. 285*, 843-855.

(5) Takayama, S., McGarvey, G. J., and Wong, C. H. (1997) Microbial aldolases and transketolases: new biocatalytic approaches to simple and complex sugars. *Annu. Rev. Microbiol. 51*, 285-310.

(6) Osten, C. H. v. d., Sinskey, A. J., Barbas, C. F., Pederson, R. L., Wang, Y.-F., and Wong, C.-H. (1989) Use of a recombinant bacterial fructose-1,6-bisphosphate aldolase in aldol reactions: preparative syntheses of 1-deoxynojirimycin, 1-deoxymannojirimycin, 1,4-dideoxy-1,4-imino-D-arabinitol, and fagomine. *J. Am. Chem. Soc. 111*, 3924-3927.

(7) Bednarski, M. D., Simon, E. S., Bischofberger, N., Fessner, W.-D., Kim, M.-J., Lees, W., Saito, T., Waldmann, H., and Whitesides, G. M. (1989) Rabbit muscle aldolase as a catalyst in organic synthesis *J. Am. Chem. Soc. 111*, 627-635.

(8) Machajewski, T. D., and Wong, C.-H. (2000) The catalytic asymmetric aldol reaction. *Angew. Chem. Int. Ed. 39*, 1352-1374.

(9) Schoevaart, R., van Rantwijk, F., and Sheldon, R. A. (2000) Stereochemistry of nonnatural aldol reactions catalyzed by DHAP aldolases. *Biotechnol. Bioeng. 70*, 349-52.

(10) Horecker, B. L., Tsolas, O., and Lai, C. Y. (1972) *The Enzymes* Vol. 7, 3rd ed., Academic press, New York.

(11) Siebers B., Brinkmann H., Dorr C., Tjaden B., Lilie H., Van der O.J., and Verhees C.H. (2001) Archaeal fructose-1,6-bisphosphate aldolases constitute a new family of archaeal type Class I aldolase. *J. Biol. Chem. 276*, 28710-28718.

(12) Ramsaywak, P. C., Labbe, G., Siemann, S., Dmitrienko, G. I., and Guillemette, J. G. (2004) Molecular cloning, expression, purification, and characterization of fructose 1,6-bisphosphate aldolase from *Mycobacterium tuberculosis* - A novel Class II A tetramer. *Protein Expr. Purif. 37*, 220-228.

(13) Plaumann, M., Pelzer-Reith, B., Martin, W. F., and Schnarrenberger, C. (1997) Multiple recruitment of Class-I aldolase to chloroplasts and eubacterial origin of eukaryotic Class-II aldolases revealed by cDNAs from *Euglena gracilis*. *Curr. Genet. 31*, 430-438.

(14) Thomson, G. J., Howlett, G. J., Ashcroft, A. E., and Berry, A. (1998) The dhnA gene of *Escherichia coli* encodes a Class I fructose bisphosphate aldolase. *Biochem. J. 331*, 437-445.

(15) Sygusch J., Beaudry D., and Allaire M. (1987) Molecular architecture of rabbit skeletal muscle aldolase at 2.7 Å resolution. *Proc. Natl. Acad. Sci. USA 84*, 7846-7850.

(16) Hester G., Brenner-Holzach O., Rossi F.A., Struck-Donatz M., Winterhalter K.H., Smit J.D., and Piontek K. (1991) The crystal structure of fructose-1,6-bisphosphate aldolase from *Drosophila melanogaster* at 2.5 Å. *FEBS Lett. 292*, 237-242.
(17) Gambin S.J., Davies G.J., Grimes J.M., Jackson R.M., Littlechild J.A., and Watson H.C. (1991) Activity and specificity of human aldolases. *J. Mol. Biol. 219*, 573-576.
(18) Jia J., Huang W., Schörken U., Sahm H., Sprenger G.A., Lindqvist Y., and Schneider G. (1996) Crystal structure of transaldolase B from *Escherichia coli* suggests a circular permutation of the α/ß barrel within the Class I aldolase family. *Structure 4*, 715-724.
(19) Gefflaut, T., Blonski, C., Perie, J., and Willson, M. (1995) Class I aldolases: substrate specificity, mechanism, inhibitors and structural aspects. *Prog. Biophys. Mol. Biol. 63*, 301-340.
(20) Fonvielle, M., Weber, P., Dabkowska, K., and Therisod, M. (2004) New highly selective inhibitors of Class II fructose-1,6-bisphosphate aldolases. *Bioorg. Med. Chem. Lett. 14*, 2923-2926.
(21) Sanchez, L. B., Horner, D. S., Moore, D. V., Henze, K., Embley, T. M., and Muller, M. (2002) Fructose-1,6-bisphosphate aldolases in amitochondriate protists constitute a single protein subfamily with eubacterial relationships. *Gene 295*, 51-59.
(22) Kroth, P. G., Schroers Y., and Kilian O. (2005) The peculiar distribution of Class I and Class II aldolases in diatoms and in red algae. *Curr. Genet. 48*, 389-400.
(23) Sauve V., and Sygusch J. (2001) Molecular cloning, expression, purification, and characterization of fructose-1,6-bisphosphate aldolase from *Thermus aquaticus*. *Protein Expr. Purif. 21*, 293-302.
(24) Dreyer M.K., and Schulz G.E. (1993) The spatial structure of the Class II L-Fuculose-1-phosphate aldolase from *Escherichia coli*. *J. Mol. Biol. 231*, 549-553.
(25) Joerger A.C., Gosse C., Fessner W., and Schulz G.E. (2000) Catalytic action of fuculose 1-phosphate aldolase (Class II) as derived from structure-directed mutagenesis. *Biochemistry 39*, 6033-6041.
(26) Cooper, S. J., Leonard, G. A., McSweeney, S. M., Thompson, A. W., Naismith, J. H., Qamar, S., Plater, A., Berry, A., and Hunter, W. N. (1996) The crystal structure of a Class II fructose-1,6-bisphosphate aldolase shows a novel binuclear metal-minding active site embedded in a familiar fold. *Structure 4*, 1303-1315.
(27) Galkin, A., Kulakova, L., Melamud, E., Li, L., Wu, C., Mariano, P., Dunaway-Mariano, D., Nash, T. E., and Herzberg, O. (2007) Characterization, kinetics, and crystal structures of fructose-1,6-bisphosphate aldolase from the human parasite, *Giardia lamblia*. *J. Biol. Chem. 282*, 4859-4867.
(28) Izard, T., and Sygusch, J. (2004) Induced fit movements and metal cofactor selectivity of Class II aldolases: structure of *Thermus aquaticus* fructose-1,6-bisphosphate aldolase. *J. Biol. Chem. 279*, 11825-11833.
(29) Lee J.H., Bae J., Kim D., Choi Y., Im Y.J., Koh S., Kim J.S., Kim M., Kang G.B., Hong S., Lee D., and Eom S.H. (2006) Stereoselectivity of fructose-1,6-bisphosphate Aldolase in *Thermus caldophilus*. *Biochem. Biophys. Res. Commun. 347*, 616-625.
(30) Pegan, S. D., Rukseree, K., Franzblau, S. G., and Mesecar, A. D. (2009) Structural basis for catalysis of a tetrameric Class IIa fructose 1,6-bisphosphate aldolase from *Mycobacterium tuberculosis*. *J. Mol. Biol. 386*, 1038-1053.

(31) Naismith J.H., Ferrara J.D., Bailey S., Marshall K., Dauter Z., Wilson K.S., Habash J., Harrop S.J., Berry A.J., and Hunter W.N. (1992) Initiating a crystallographic study of a class II fructose-1,6-bisphosphate aldolase. . *J. Mol. Biol. 225*, 1137-1141.
(32) Blom, N. S., Tetreault, S., Coulombe, R., and Sygusch, J. (1996) Novel active site in *Escherichia coli* fructose 1,6-bisphosphate aldolase. *Nat. Struct. Biol. 3*, 856-862.
(33) Lorentzen E., Pohl E., Zwart P., Stark A., Russell R.B., Knura T., Hensel R., and Siebers B. (2003) Crystal structure of an archaeal class I aldolase and the evolution of $(\alpha/\beta)_8$ barrel proteins. *J. Biol. Chem. 278*, 47253-47260.
(34) Nagano N., Orengo C.A., and Thornton J.M. (2002) One fold with many functions: the evolutionary relationships between TIM barrel families based on their sequences, structures and functions. *J. Mol. Biol. 321*, 741-765.
(35) Hall, D. R., Leonard, G. A., Reed, C. D., Watt, C. I., Berry, A., and Hunter, W. N. (1999) The crystal structure of *Escherichia coli* Class II fructose-1,6-bisphosphate aldolase in complex with phosphoglycolohydroxamate reveals details of mechanism and specificity. *J. Mol. Biol. 287*, 383-394.
(36) Qamar, S., Marsh, K., and Berry, A. (1996) Identification of arginine 331 as an important active site residue in the Class II fructose-1,6-bisphosphate aldolase of *Escherichia coli*. *Protein Sci. 5*, 154-161.
(37) Vallee B.L., and Auld D.S. (1990) Active-site ligands and activated $H_2O$ of zinc enzymes. *Proc. Natl. Acad. Sci. USA 87*, 220-224.
(38) Christianson, D. W. (1991) Structural biology of zinc. *Adv. Protein Chem. 42*, 281-355.
(39) Vallee B.L., and Auld D.S. (1993) New perspective on zinc biochemistry: co-catalytic sites in multi-zinc enzymes. *Biochemistry 32*, 6493-6500.
(40) Lewis, D. J., and Lowe, G. (1973) Phosphoglycolohydroxamic acid: an inhibitor of class I and II aldolases and triosephosphate isomerase. A potential antibacterial and antifungal agent. *J.C.S. Chem. Commun.*, 713-715.
(41) WHO. (2008), World Health Organization.
(42) O'Brien R.J., and Nunn P.P. (2001) The need for new drugs against tuberculosis: obstacles, opportunities, and next steps. *Am. J. Respir. Crit. Care. Med. 162*, 1055-1058.
(43) Bai, N. J., Pai, M. R., Murthy, P. S., and Venkitasubramanian, T. A. (1974) Effect of oxygen tension on the aldolases of *Mycobacterium tuberculosis* H37Rv. *FEBS Lett. 45*, 68-70.
(44) Stribling, D., and Perham, R. N. (1973) Purification and characterization of two fructose diphosphate aldolases from *Escherichia coli* (Crookes' strain). *Biochem. J. 131*, 833-841.
(45) Marsh, J. J., and Lebherz, H. G. (1992) Fructose-bisphosphate aldolases: an evolutionary history. *Trends. Biochem. Sci. 17*, 110-113.
(46) Scamuffa, M. D., and Caprioli, R. M. (1980) Comparison of the mechanisms of two distinct aldolases from *Escherichia coli* grown on gluconeogenic substrates. *Biochim. Biophys. Acta. 614*, 583-590.
(47) Liebke H.H., and Speyer J.F. (1983) A new gene in *Escherichia coli* RNA synthesis. . *Mol. Gen. Genet. 189*, 314-320.
(48) Singer, M., Rossmiessl, P., Cali, B. M., Liebke, H., and Gross, C. A. (1991) The *Escherichia coli* ts8 mutation is an allele of fda, the gene encoding fructose-1,6-diphosphate aldolase. *J. Bacteriol. 173*, 6242-6248.
(49) Schneider, D. A., and Gourse, R. L. (2003) Changes in the concentrations of guanosine 5'-diphosphate 3'-diphosphate and the initiating nucleoside triphosphate account for

inhibition of rRNA transcription in fructose-1,6-diphosphate aldolase (fda) mutants. *J. Bacteriol. 185*, 6192-6194.
(50) Rosenkrands, I., Slayden, R. A., Crawford, J., Aagaard, C., Barry, C. E., 3rd, and Andersen, P. (2002) Hypoxic response of *Mycobacterium tuberculosis* studied by metabolic labelling and proteome analysis of cellular and extracellular proteins. *J. Bacteriol. 184*, 3485-3491.
(51) Gerdes, S. Y., Scholle, M. D., Campbell J.W., Balazsi, G., Ravasz, E., and Daugherty M.D. (2003) Experimental determination and system level analysis of essential genes in *Escherichia coli* MG 1655. *J. Bacteriol. 185*, 5673-5684.
(52) Baba, T., Ara, T., Hasegawa, M., Takai, Y., Okumura, Y., and Baba, M. (2006) Construction of *Escherichia coli* K-12 in-frame, single-gene knockout mutants: the Keio collection. *Mol. Syst. Biol. 2*, 2006-2008.
(53) Lyczak J.B., Cannon C.L., and Pier G.B. (2002) Lung infections associated with cystic fibrosis. *Clin. Microbiol. Rev. 15*, 194-222.
(54) Costerton J.W., Stewart P.S., and Greenberg E.P. (1999) Bacterial biofilms: a common cause of persistent infections. *Science 284*, 1318-1322.
(55) Banerjee P.C., Vanags R.I., Chakrabarty A.M., and Maitra P.K. (1985) Gluconeogenic mutations in *Pseudomonas aeruginosa*: genetic linkage between fructose-bisphosphate aldolase and phosphoglycerate kinase. *J. Gen. Microbiol. 133*, 1099-1107.
(56) Banerjee, P. C., Darzins, A., and Maitra, P. K. (1987) Gluconeogenic mutations in *Pseudomonas aeruginosa*: genetic linkage between fructose-bisphosphate aldolase and phosphoglycerate kinase. *J. Gen. Microbiol. 133*, 1099-1107.

## References for chapter 2

(1) Blostein, R., and Rutter, W. J. (1963) Comparative studies of liver and muscle aldolase. Ii. Immunochemical and chromatographic differentiation. *J. Biol. Chem. 238*, 3280-5.
(2) Labbe, G., Bezaire, J., Groot, S. d., How, C., Rasmusson, T., Yaeck, J., Jervis, E., Dmitrienko, G. I., and Guy Guillemette, J. (2007) High level production of the *Magnaporthe grisea* fructose 1,6-bisphosphate aldolase enzyme in *Escherichia coli* using a small volume bench-top fermentor. *Protein Expression and Purification 51*, 110-119.
(3) Dean, S. M., Greenberg, W. A., and Wong, C.-H. (2007) Recent advances in aldolase-catalyzed asymmetric synthesis *Adv. Synth. Catal. 349*, 1308-1320.
(4) Bednarski, M. D., Simon, E. S., Bischofberger, N., Fessner, W.-D., Kim, M.-J., Lees, W., Saito, T., Waldmann, H., and Whitesides, G. M. (1989) Rabbit muscle aldolase as a catalyst in organic synthesis *J. Am. Chem. Soc. 111*, 627-635.
(5) Osten, C. H. v. d., Sinskey, A. J., Barbas, C. F., Pederson, R. L., Wang, Y.-F., and Wong, C.-H. (1989) Use of a recombinant bacterial fructose-1,6-bisphosphate aldolase in aldol reactions: preparative syntheses of 1-deoxynojirimycin, 1-deoxymannojirimycin, 1,4-dideoxy-1,4-imino-D-arabinitol, and fagomine. *J. Am. Chem. Soc. 111*, 3924-3927.
(6) Machajewski, T. D., and Wong, C.-H. (2000) The catalytic asymmetric aldol reaction. *Angew. Chem. Int. Ed. 39*, 1352-1374.
(7) Christie, R. M. (2007) Why is indigo blue? *Biotech. Histochem. 82*, 51-56.

(8) Silverstein, R. M., Bassler, G. C., and Morrill, T. C. (1980) in *Spectrometric identification of organic compounds* pp 305-331, John Wiley & Sons, Inc., New York.
(9) Nakagawa, M., Nakao, H., and Watanabe, K. (1985) Steric effects of chiral ligands in a new type of aldol condensations catalyzed by zinc(II) complexes of α-amino acid esters. *Chem. Lett. 14*, 391-394.
(10) List, B., Lerner, R. A., and Barbas, C. F. (2000) Proline-catalyzed direct asymmetric aldol reactions. *J. Am. Chem. Soc. 122*, 2395-2396.
(11) Notz, W., and List, B. (2000) Catalytic asymmetric synthesis of *anti*-1,2-diols. *J. Am. Chem. Soc. 122*, 7386-7387.
(12) Sakthivel, K., Notz, W., Bui, T., and Barbas, C. F. (2001) Amino acid catalyzed direct asymmetric aldol reactions: a bioorganic approach to catalytic asymmetric carbon-Carbon bond-forming reactions. *J. Am. Chem. Soc. 123*, 5260-5267.
(13) Zimmerman, H. E., and Traxler, M. D. (1957) The stereochemistry of the Ivanov and Reformatsky Reactions. *J. Am. Chem. Soc. 79*, 1920–1923.
(14) Heathcock, C. H., Buse, C. T., Kleschick, W. A., Pirrung, M. C., Sohn, J. E., and Lampe, J. (1980) Acyclic stereoselection. 7. Stereoselective synthesis of 2-alkyl-3-hydroxy carbonyl compounds by aldol condensation. *J. Org. Chem. 45*, 1066-1081.
(15) Kano, T., Takai, J., Tokuda, O., and Maruoka, K. (2005) Design of an axially chiral amino acid with a binaphthyl backbone as an organocatalyst for a direct asymmetric aldol reaction. *Angew. Chem. Int. Ed. 44*, 3055-3057.
(16) Darbre, T., and Machuqueiro, M. (2003) Zn-proline catalyzed direct aldol reaction in aqueous media. *Chem. Comm.*, 1090-1091.
(17) Fernandez-Lopez, R., Kofoed, J., Machuqueiro, M., and Darbre, T. (2005) A selective direct aldol reaction in aqueous media catalyzed by zinc–proline. *Eur. J. Org. Chem.*, 5268-5276.
(18) Kofoed, J., Darbre, T., and Reymond, J.-L. (2006) Dual mechanism of zinc-proline catalyzed aldol reactions in water. *Chem. Comm.*, 1482-1484.
(19) List, B. (2004) Enamine catalysis is a powerful strategy for the catalytic generation and use of carbanion equivalents. *Acc. Chem. Res. 37*, 548-557.
(20) Cordova, A., Zou, W., Dziedzic, P., Ibrahem, I., Reyes, E., and Xu, Y. (2005) Direct asymmetric intermolecular aldol reactions catalyzed by amino acids and small peptides. *Eur. J. Chem. 12*, 5383-5397.
(21) Jiang, Z., Liang, Z., Wu, X., and Lu, Y. (2006) Asymmetric aldol reactions catalyzed by tryptophan in water. *Chem. Comm.*, 2801-2803.
(22) Ramasastry, S. S. V., Zhang, H., Tanaka, F., and Barbas, C. F. (2006) Direct catalytic asymmetric synthesis of *anti*-1,2-amino alcohols and *syn*-1,2-diols through organocatalytic *anti*-Mannich and *syn*-aldol reactions. *J. Am. Chem. Soc. 129*, 288-289.
(23) Ramasastry, S. S. V., Albertshofer, K., Utsumi, N., Tanaka, F., and Barbas, C. F. (2007) Mimicking fructose and rhamnulose aldolases: organocatalytic *syn*-aldol reactions with unprotected dihydroxyacetone. *Angew. Chem. Int. Ed. 46*, 5572-5575.
(24) Utsumi, N., Imai, M., Tanaka, F., Ramasastry, S. S. V., and Barbas, C. F. (2007) Mimicking aldolases through organocatalysis: *syn*-selective aldol reactions with protected dihydroxyacetone. *Org. Lett. 9*, 3445-3448.
(25) Markert, M., Mulzer, M., Schetter, B., and Mahrwald, R. (2007) Amine-catalyzed direct aldol addition. *J. Am. Chem. Soc. 129*, 7258-7259.

(26) Luo, S., Xu, H., Li, J., Zhang, L., and Cheng, J.-P. (2007) A simple primary-tertiary diamine-Brønsted acid catalyst for asymmetric direct aldol reactions of linear aliphatic ketones. *J. Am. Chem. Soc. 129*, 3074-3075.
(27) Luo, S., Xu, H., Zhang, L., Li, J., and Cheng, J.-P. (2008) Highly enantioselective direct *syn*- and *anti*-aldol reactions of dihydroxyacetones catalyzed by chiral primary amine catalysts. *Org. Lett. 10*, 653-656.
(28) Huang, H., and Jacobsen, E. N. (2006) Highly enantioselective direct conjugate addition of ketones to nitroalkenes promoted by a chiral primary amine-thiourea catalyst. *J. Am. Chem. Soc. 128*, 7170-7171.
(29) Sugiyama, M., Hong, Z., Whalen, L. J., Greenberg, W. A., and Wong, C.-H. (2006) Borate as a phosphate ester mimic in aldolase-catalyzed reactions: practical synthesis of L-fructose and L-iminocyclitols *Adv. Synth. Catal. 348*, 2555-2559.
(30) Ma, C., Kwok, W. M., Chan, W. S., Du, Y., Kan, J. T. W., Toy, P. H., and Philips, D. L. (2006) Ultrafast time-resolved transient absorption and resonance raman spectroscopy study of the photodetection and rearrangement reactions of *p*-hydroxyphenacyl caged phosphates. *J. Am. Chem. Soc. 128*, 2558-2570.
(31) Drueckhammer, D. G., Durrwachter, J. R., Pederson, R. L., Crans, D. C., Daniels, L., and Wong, C.-h. (1989) Reversible and *in situ* formation of organic arsenates and vanadate s as organic phosphate mimics in enzymatic reactions: mechanistic investigation of aldol reactions and synthetic applications *J. Org. Chem. 54*, 70-77.
(32) Schoevaart, R., Rantwijk, F. v., and Sheldon, R. A. (2001) Facile enzymatic aldol reactions with dihydroxyacetone in the presence of arsenate. *J. Org. Chem. 66*, 4559-4562.
(33) Dawson MC. (1987) *Data for biochemical research*, 3rd ed., Oxford scientific publications.
(34) Mitchell, J. M., and Finney, N. S. (2000) An efficient method for the preparation of *N,N*-disubstituted 1,2-diamines. *Tetrahedron Lett. 41*, 8431-8434.

## References for chapter 3

(1) Lewis, D. J., and Lowe, G. (1973) Phosphoglycolohydroxamic acid: an inhibitor of class I and II aldolases and triosephosphate isomerase. A potential antibacterial and antifungal agent. *J.C.S. Chem. Commun.*, 713-715.
(2) Naismith J.H., Ferrara J.D., Bailey S., Marshall K., Dauter Z., Wilson K.S., Habash J., Harrop S.J., Berry A.J., and Hunter W.N. (1992) Initiating a crystallographic study of a Class II fructose-1,6-bisphosphate aldolase. . *J. Mol. Biol. 225*, 1137-1141.
(3) Fonvielle, M., Weber, P., Dabkowska, K., and Therisod, M. (2004) New highly selective inhibitors of Class II fructose-1,6-bisphosphate aldolases. *Bioorg. Med. Chem. Lett. 14*, 2923-2926.
(4) Gavalda, S., Braga, R., Dax, C., Vigroux, A., and Blonski, C. (2005) N-sulfonyl hydroxamate derivatives as inhibitors of class II fructose-1,6-diphosphate aldolase. *Bioorg. Med. Chem. Lett. 15*, 5375-5377.
(5) Fonvielle, M., Coincon, M., Daher, R., Desbenoit, N., Kosieradzka, K., Barilone, N., Gicquel, B., Sygusch, J., Jackson, M., and Therisod, M. (2008) Synthesis and

biochemical evaluation of selective inhibitors of Class II fructose bisphosphate aldolases: towards new synthetic antibiotics. *Chem. Eur. J. 14*, 8521-8529.

(6) Park J.D., Kim D.H., Kim S.J., Woo J.R., and Ryu S.E. (2002) Sulfamide-based inhibitors for carboxypeptidase A. Novel type transition state analogue inhibitors for zinc proteases. *J. Med. Chem. 45*, 5295-5302.

(7) Lee H.S., and Kim D.H. (2003) Synthesis and evaluation of α,α-disubstituted-3-mercaptopropanoid acids as inhibitors for carboxypeptidase A and implications with respect to enzyme inhibitor design. *Bioorg. Med. Chem. 11*, 4685-4691.

(8) Park J.D., and Kim D.H. (2004) Sulfamide derivatives as transition state analogue inhibitors for carboxypeptidase A. *Bioorg. Med. Chem. 12*, 2349-2356.

(9) Kleifeld O., Kotra L.P., Gervasi D.C., Brown S., Bernardo M.M., Fridman R., Mobashery S., and Sagi I. (2001) X-ray absorption studies of human matrix metalloproteinase-2 (MMP-2) bound to a highly selective mechanism-based inhibitor. *J. Biol. Chem. 276*, 17125-17131.

(10) Campbell D.A., Xiao X.Y., Harris D., Ida S., Mortezaei R., Ngu K., Shi L., Tien D., Wang Y., Navre M., Patel D.V., Sharr M.A., DiJoseph J.F., Killar L.M., Leone C.L., Levin J.I., and Skotnicki J.S. (1998) Malonyl α-mercaptoketones and α-mercaptoalcohols, a new class of matrix metalloproteinase inhibitors. *Bioorg. Med. Chem. Lett. 8*, 1157-1162.

(11) Auge F., Hornebeck W., Decarme M., and Laronze J. (2003) Improved gelatinase and selectivity by novel zinc binding groups containing galardin derivatives. *Bioorg. Med. Chem. Lett. 13*, 1783-1786.

(12) Whittaker M., Floyd C.D., Brown P., and Gearing A.J.H. (1999) Design and therapeutic application of matrix metalloproteinase inhibitors. *Chem. Rev. 99*, 2735-2776.

(13) Giavazzi R., and Taraboletti G. (2001) Preclinical development of metalloproteases inhibitors in cancer therapy. *Crit. Rev. Onco. Hemato. 37*, 53-60.

(14) Leung D., Abbenante G., and Fairlie D.P. (2000) Protease inhibitors: current status and future prospects. *J. Med. Chem. 43*, 305-341.

(15) Ramsaywak, P. C., Labbe, G., Siemann, S., Dmitrienko, G. I., and Guillemette, J. G. (2004) Molecular cloning, expression, purification, and characterization of fructose 1,6-bisphosphate aldolase from *Mycobacterium tuberculosis* - A novel class II A tetramer. *Protein Expr. Purif. 37*, 220-228.

(16) Cooper, S. J., Leonard, G. A., McSweeney, S. M., Thompson, A. W., Naismith, J. H., Qamar, S., Plater, A., Berry, A., and Hunter, W. N. (1996) The crystal structure of a Class II fructose-1,6-bisphosphate aldolase shows a novel binuclear metal-binding active site embedded in a familiar fold. *Structure 4*, 1303-1315.

(17) Gefflaut, T., Blonski, C., Perie, J., and Willson, M. (1995) Class I aldolases: substrate specificity, mechanism, inhibitors and structural aspects. *Prog. Biophys. Mol. Biol. 63*, 301-340.

(18) Collins, K. D. (1974) An activated intermediate analogue. The use of phosphoglycolohydroxamate as a stable analogue of a transiently occurring dihydroxyacetone phosphate-derived enolate in enzymatic catalysis. *J. Biol. Chem. 249*, 136-142.

(19) Hall, D. R., Leonard, G. A., Reed, C. D., Watt, C. I., Berry, A., and Hunter, W. N. (1999) The crystal structure of *Escherichia coli* Class II fructose-1,6-bisphosphate aldolase in

complex with phosphoglycolohydroxamate reveals details of mechanism and specificity. *J. Mol. Biol. 287*, 383-394.
(20) Siemann, S., Clarke, A. J., Viswanatha, T., and Dmitrienko, G. I. (2003) Thiols as classical and slow-binding inhibitors of IMP-1 and other binuclear metallo-β-lactamases *Biochemistry 42*, 1673-1683.
(21) Burton, D. J., and Flynn, R. M. (1977) Michaelis-Arbuzov preparation of halo-F-methylphosphonates. *J. Fluorine Chem. 10*, 329-332.
(22) Rai, V., and Namboothiri, I. N. N. (2008) Enantioselective conjugate addition of dialkyl phosphites to nitroalkenes *Tetrahedron Asymm. 19*, 2335-2338.
(23) Obayashi, M., Ito, E., Matsui, K., and Kondo, K. (1982) (Diethylphosphinyl)-difluoromethyllithium. Preparation and synthetic application. *Tetrahedron Lett. 23*, 2323-2326.
(24) Xu, Y., Qian, L., and Prestwich, G. D. (2003) Synthesis of α-fluorinated phosphonates from α-fluorovinylphosphonates: a new route to analogues of lysophosphatidic acid. *Org. Lett. 5*, 2267-2270.
(25) Silverstein, R. M., Webster, F. X., and Kiemle, D. J. (2005) *Spectrometric identification of organic compounds*, Seventh ed., John Wiley & Sons, Inc. , New York.
(26) Blades, K., Butt, A. H., Cockerill, G. S., Easterfield, H. J., Lequeux, T. P., and Percy, J. M. (1999) Synthesis of activated alkenes bearing the difluoromethylenephosphonate group: a range of building blocks for the synthesis of secondary difluorophosphonates. *J. Chem. Soc., Perkin Trans. 1*, 3609–3614.
(27) Brown S., Bernardo M.M., Li Z., Kotra L.P., Tanaka Y., Fridman R., and Mobashery S. (2000) Potent and selective mechanism-based inhibition of gelatinases. *J. Am. Chem. Soc. 122*, 6799-6800.
(28) Lim I.T., Brown S., and S., M. (2004) A convenient synthesis of a selective gelatinase inhibitor as an antimetastatic agent. *J. Org. Chem. 69*, 3572-3573.
(29) Ikejiri M., Bernardo M.M., Meroueh S.O., Brown S., Chang M., Fridman R., and S., M. (2005) Design, synthesis, and evaluation of a mechanism-based inhibitor for Gelatinase A. *J. Org. Chem. 70*, 5709-5712.
(30) Durgam, G. G., Virag, T., Walker, M. D., Tsukahara, R., Yasuda, S., Liliom, K., van Meeteren, L. A., Moolenaar, W. H., Wilke, N., Siess, W., Tigyi, G., and Miller, D. D. (2005) Synthesis, structure-activity relationships, and biological evaluation of fatty alcohol phosphates as lysophosphatidic acid receptor ligands, activators of PPAR gamma, and inhibitors of autotoxin. *J. Med. Chem. 48*, 4919-30.
(31) Bergstrom D. E., Shum P. W. (1988) Synthesis and characterization of new fluorine substituted nonionic dinucleoside phosphonate analogue, *p*-deoxy-*p*-(difluoromethyl)-thymidylyl(3'-5')thymidine. *J. Org. Chem. 53*, 3953-3958.

**Appendix A**
**$^{1}$H NMR spectrum (300 MHz) of racemic *N*, *N*-dipropylcyclohexane-1,2-diamine**